IMPROVED UNDERSTANDING OF SUBSURFACE HYDROLOGY IN VARIABLE SOURCE AREAS AND ITS IMPLICATIONS FOR WATER QUALITY

A Dissertation

Presented to the Faculty of the Graduate School

of Cornell University

In Partial Fulfillment of the Requirements for the Degree of

Doctor of Philosophy

by

Helen Elisabeth Dahlke

January 2011

IMPROVED UNDERSTANDING OF SUBSURFACE HYDROLOGY IN VARIABLE SOURCE AREAS AND ITS IMPLICATIONS FOR WATER QUALITY

Helen Elisabeth Dahlke, Ph. D.

Cornell University 2011

Variable source areas (VSAs) are hot spots of hydrological (saturation-excess runoff) and biogeochemical processes (e.g. nitrogen, phosphorus, organic carbon cycling) in the landscapes of the northeastern U.S. Despite the substantial research conducted in the past 50 years, there is still process understanding to be gained on how VSA connect with the surrounding area, how this interaction influences surface and subsurface runoff generation and chemical transport and how these processes can be captured in ungaged basins using watershed models. To determine the controls on VSA formation and connectivity, a 0.5 ha hillslope was instrumented (trenched) in the southern tier of New York, U.S. Water flux from different soil layers in the trench and upslope water table dynamics were recorded for 16 events and isotopic and geochemical tracers were measured during five events. In conjunction with the surface and bedrock topography these measurements allowed detailed characterization of the subsurface storm flow response within the VSA. Analysis revealed that the most important control on storm flow response was antecedent moisture. During events with dry antecedent conditions subsurface flow was dominated by percolation through the fragipan (i.e. cracks and macropores). Flow from below the fragipan showed a constant flow rate (0.8 mm/h), which was independent of storm size and antecedent moisture. Under wet antecedent conditions hydrological connectivity increased and

subsurface flow is dominated by lateral flow through the soil atop the fragipan. During these events flow contributing slope length to the trench was five to tenfold increased. Thus, pollutant and nutrient transport from a greater distance has to be considered in water management during events with wet antecedent conditions. Application of the empirical Soil Conservation Service Curve Number method showed that discharge volumes were generally well predicted but revealed that for continuous predictions of VSA dynamics more conceptually coherent solutions need to be developed that consider the effect of antecedent moisture on runoff generation. This research shows that indirect indicators such as the average water table depth, the base flow rate prior to events or water balance estimates of the soil water content can be incorporated into watershed models to improve predictions.

BIOGRAPHICAL SKETCH

Helen Elisabeth Dahlke was born in Leipzig, Germany, in 1978. After she graduated from Alexander-von-Humboldt-Gymnasium in Leipzig in 1997, she enrolled at the Friedrich-Schiller-University in Jena, Germany and received in 2004 a M.Sc. in Geography (Diplom-Geograph), with minors in Geology and Ecology. During her time at Friedrich-Schiller-University in Jena she worked and traveled in South Africa, and became interested in catchment hydrology and hydrological systems that are impacted by environmental changes across spatial and temporal scales. After finishing her M.Sc. in Germany she continued working in catchment hydrology projects in Eastern Europe and Sweden and gained experience in geostatistical, field measurement, and geophysical methods, as well as GIS and modeling. In January 2007, Helen joined Cornell University to start her Ph.D. program at the Department of Biological and Environmental Engineering.

This dissertation is dedicated to my parents Johanna and Ulrich Dahlke, my sister Franka, my grandparents Elfriede and Heinz Weinhold, to my partner Anthony and my closest friend Verónica, who have encouraged me, loved and believed in me during the many years leading to this dissertation.

ACKNOWLEDGMENTS

This work would not have been possible without the dedication and support of numerous people and funding sources. First of all I would like to thank my advisor Tammo Steenhuis and my committee members Larry Brown and Jery Stedinger for their steady support, patience, constructive critique and the many hours of help and discussion they offered during the last four years. I especially want to thank Tammo Steenhuis for giving me the opportunity to join the graduate program at Cornell University and to become a member of his diverse and multi-national research lab.

This research was mainly funded through the U.S. Department of Agriculture and the Cooperative State Research, Education and Extension Service (CSREES) by the grant "Improving the Transport Component of the P-Index for Nutrient Management Plans in the Northeast ". Beyond this, I gratefully acknowledge the B.K. Krenzer and N.G. Kaul scholars for their financial support of this research.

This field research would not have been a success without the help of my many colleagues and friends who volunteered unconditionally for many times. I especially would like to acknowledge Zachary Easton who spent many hours planning, digging and discussing site instrumentation, data analysis and data interpretation. Beside him I owe special thanks to Steve Lyon who suggested to come to Cornell University as well as Chris Berry, Brian Buchanan, Carla Ferreira, Joshua Faulkner, Daniel Fuka, Christian Guzman, Ri Young Ko, Becky Marjerison, Veronica Morales, Sheila Saia, Anthony Salvucci, Eric White, and Wei Zhang. I am also grateful to M. Todd Walter, Larry Goehring and Brian Richards from the Soil and Water Lab for advising me and discussing the many technical and instrumental challenges faced during my PhD.

Finally, I want to cordially thank my family, especially my mother Johanna and my partner Anthony, for their support, love and encouragement over years.

TABLE OF CONTENTS

LIST OF FIGURES

LIST OF TABLES

LIST OF ABBREVIATIONS

AGNPS	AGricultural Non-Point Source Pollution Model.
ArcIMS	Arc Image Mapping Service software.
BMP	Best Management Practices.
CMP	Common Mid Point.
CN	Curve Number.
CREAMS	Chemicals, Runoff and Erosion from Agricultural Management Systems model.
DEM	Digital Elevation Model.
DSS	Decision Support System.
EPIC	Erosion Productivity Impact Calculator.
FO	Fixed-offset.
FOM	Fixed-Offset Method.
GFS	Global Forecast System.
GHz	Giga Hertz.
GIS	Geographical Information System.
GPR	Ground Penetrating Radar
GWLF	General Watershed Loading Function.
HAT	Hydrologic Assessment Tool.
HSA	Hydrologically Sensitive Areas.
HSA-DSS	Hydrologically Sensitive Area Decision Support System.
I/O	Input/Output.
KITH	GFS MOS station code for the Ithaca airport station.
L-THIA	Long-Term Hydrologic Impact Assessment model.
Lidar	Light Detection And Ranging.

MHz	Mega Hertz.
MOS	Model Output Statistic.
MRF	Medium Range Forecast.
MTA	Multiple trace analysis.
NMPs	Nutrient Management Plans.
NOAA	National Oceanic and Atmospheric Administration.
NPS	Nonpoint source pollution
NRCC	Northeastern Regional Climate Center.
NRCS	Natural Resources Conservation Service.
NY	New York State.
NYS	New York State.
P	Phosphorus.
P-Index	Phosphorus Runoff Index.
P24	24-hr probability of precipitation.
Q24	24-hr quantitative precipitation forecast.
RMSE	Root-mean-squared error.
SCS-CN	Soil Conservation Service curve number.
SMDR	Soil Moisture Distribution and Routing model.
SSURGO	Soil Survey Geographic Database.
STA	Single trace analysis.
STI	Soil Topographic Index.
SWAT	Soil & Water Assessment Tool.
SWMM	Storm Water Management Model.
TDR	Time-domain reflectometry.
TI	Topographic Index.
TOPMODEL	Rainfall-runoff model based on topography.

USDA	United States Department of Agriculture.
USGS	United States Geological Service.
VSAs	Variable Source Areas.
WARR	Wide-angle reflection and refraction.
X/N	Predicted maximum daytime and minimum nighttime temperature.
STI	soil topographic index.

LIST OF SYMBOLS

a	Calibration parameter.
A_f	Fraction of the watershed that contributes runoff.
A_s	Fraction of a wetness class.
$A_{s,j}$	Percent of the watershed area that has a local effective soil water storage less than or equal to $\sigma_{e,j}$.
a_{summer}, a_{winter}	baseflow recession coefficients (d^{-1}).
c	Free space electromagnetic propagation velocity (3×10^8 m/s).
D	Local soil depth (m).
E	Nash-Sutcliffe efficiency.
E_a	Actual evapotranspiration (mm).
E_p	Potential evapotranspiration (mm).
f	Frequency (MHz or GHz).
I_a	Initial abstraction (mm).
$\hat{K}_s$	Saturated hydraulic conductivity (m/d).
P	Precipitation (mm/d)
P_e	Effective precipitation (mm).
$Perc$	Percolation rate to the subsoil (mm/d).
Q_p	Percolation fraction (mm).
r	Pearson product-moment correlation coefficient.
R	Saturation-excess runoff (mm/d).
r^2	Coefficient of determination.
$\sqrt{\varepsilon_b}$	Refractive index.
S	Depth of the watershed-wide water storage in the soil profile (mm).
$S_{t-\Delta t}$	Moisture storage on the previous day (mm)

t	Time step (d^{-1})
t_{AW}	Air wave arrival time (s).
t_{GW}	Ground wave arrival time (s).
t_{RW}	Two-way arrival time of the reflected wave (s).
v	Radar velocity or propagation velocity (m/ns).
v_{AW}	Air wave velocity (m/ns).
v_{GW}	Ground wave velocity (m/ns).
x	Antenna separation (m).
α	upslope contributing area (m^2).
β	Local, surface topographic slope (radians).
ΔP	Depth of precipitation (mm).
ΔQ	Runoff depth (mm).
Δt	Difference in the picked arrival times of air wave and ground wave (ns).
ε	Apparent permittivity (F/m).
ε_r, ε'	Relative dielectric permittivity (F/m).
θ_v	Volumetric soil water content (m^3/m^3).
λ	Wave length (m).
μ_r	Relative magnetic permeability (H/m).
$\sigma_{e,j}$	Maximum effective storage for each wetness class j (mm).
σ_m	Maximum available soil water storage of a fraction of the watershed (mm).

CHAPTER 1

INTRODUCTION

Nonpoint source pollution (NPS) from agricultural activity has the potential to contribute to surface water quality degradation in the United States (Puckett, 1995; Ekholm et al., 2000; Sharpley et al., 2001; Andraski and Bundy, 2003). During the last 30 years various environmental standards (e.g. NRCS 590 standard, Phosphorus Index) and watershed management practices have been implemented in an attempt to reduce NPS of surface water bodies but, in practice, are highly variable in their effectiveness (Brannan et al.; 2000, Lee et al.; 2000, Gitau et al., 2006). This variable effectiveness often arises due to the complexity of the underlying hydrological transport processes, which is difficult to quantify with simple guidelines. Incorporation of process understanding in water quality models, which are widely used to predict pollutant loads and source locations, remains one of the greatest challenges the scientific and regulatory community needs to overcome to better manage agricultural landscapes (i.e. Phosphorus Index, Generalized Watershed Loading Function) Scientific approaches developed from experimental hillslope or plot studies (Easton et al., 2007) are critical to furthering our understanding of how areas of a landscape respond.

Many water quality models use some form of the Natural Resources Conservation Services (formerly Soil Conservation Service) curve number (CN) equation (USDA-SCS, 1972) to predict storm runoff and pollutant loads from watersheds. However, the way the CN is applied in these models implicitly assumes an infiltration excess response to rainfall. Storm runoff generation based on the infiltration-excess, or the

"Hortonian flow", concept occurs when rainfall intensity exceeds the rate at which water can infiltrate the soil (e.g., Horton, 1933, 1940). In contrast, saturation-excess occurs when rain (or snowmelt) encounters soils that are nearly or fully saturated, often due to a perched water table that forms when the infiltration front reaches a zone of low permeability, thus precluding infiltration (e.g., Dunne and Black, 1970; Hewlett and Nutter, 1970). In the northeastern U.S. high infiltration capacities make infiltration-excess runoff unlikely during storm events (Walter et al., 2002). The predominance of shallow, high-transmissive soils in steep topography and the presence of impeding sub-soil layers (i.e. hardpans, fragipans, bedrock) cause the development of perched water tables where shallow surface and lateral subsurface flow accumulates in the landscape. Saturated areas, also called variable source areas (VSAs), develop within hours or days and expand and contract spatially depending on the rainfall depth (Dunne and Black, 1970; Hewlett and Nutter, 1970), thus, providing rapid hydrological transport pathways for potential pollutants (Gburek et al, 2000, 2002).

Water quality risks arise in these landscapes where pollutant sources coincide with areas that are prone to generate runoff during storm events (Walter et al., 2000). These areas are often referred to as hydrologically sensitive areas (HSAs) (Walter et al., 2000; Gburek and Sharpley, 1998; Walter et al., 2001; Gburek et al., 2002). To reduce the contribution of NPS to water bodies, managing and protecting HSAs is critical and knowledge of the location of areas generating saturation-excess runoff is paramount in order to effectively place best management practices (BMPs) (Rao et al., 2008). Although many CN-based water quality models such as the Generalized Watershed Loading Function (GWLF) model (Haith and Shoemaker, 1987), the Soil Water Assessment Tool (SWAT) model (Arnold et al., 1998), the Storm Water Management

Model (SWMM) (Krysanova et al., 1998), the Erosion Productivity Impact Calculator (EPIC) model (Williams et al., 1984), and the Long-Term Hydrologic Impact Assessment (L-THIA) model (Bhaduri et al., 2000) can correctly predict stream discharge or chemical/sediment loads at the catchment outlet they insufficiently represent intra-catchment processes important for the identification of runoff and pollutant source locations (Srinivasan et al., 2005). Recent studies by Lyon et al. (2004), Schneiderman et al. (2007) and Easton et al. (2007), which largely build on a VSA interpretation of the SCS-CN method developed by Steenhuis et al. (1995), have shown how CN-based models that consider VSA hydrology can be used to accurately predict runoff generation and VSA locations in catchments. VSA locations can be generally well predicted using variants of the topographic index (TI), i.e. TOPMODEL (Beven and Kirkby, 1979), or the soil topographic index (STI) (Ambroise et al., 1996), which integrates the soil transmissivity and soil depth in addition to topographic controls such as local slope and upslope contributing area. Lyon et al. (2004) showed that the STI in combination with the SCS-CN method provided an accurate method to describe the evolution of the shallow water table in a small catchment in the Catskill Mountains, NY and that this shallow water table was the primary control on the spatiotemporal development of VSAs. Based on this proof of concept, Agnew et al. (2006) showed how the STI can be integrated in water quality management to improve the prediction of runoff risk and potential pollutants sources in the agricultural watersheds. They showed that the risk or probability of saturation excess runoff generation could be more accurately predicted with the soil topographic index (monthly $r^2 = 0.86 – 0.95$) than the distance from stream (i.e. fixed-width stream buffers) (monthly $r^2 = 0.55 – 0.66$) (Agnew et al., 2006).

However, the applicability of the STI to locate VSAs remains of variable success and depends strongly on seasonality (Lyon et al., 2006), scale (de Alwis et al., 2007; Dahlke et al., 2009) and the lateral redistribution of water (Harpold et al., 2010) but appears to result in better predictability under wet antecedent conditions and on the basis of accurate topography and soils information. Since the STI is just a surrogate to distribute VSAs in the landscape based on predictions commonly made with CN-based models, the variable success of the STI method can be largely attributed to the lack of flexibility in the SCS-CN method for use in continuous watershed models (Dahlke et al., 2009; Shaw and Walter et al., 2009). Although more sophisticated methods are available the SCS-CN method shows continued popularity, particularly among practicing water resources engineers due to its simplicity, ease of use, and dependence on readily available catchment properties (Ponce and Hawkins, 1996; Garen and Moore, 2005). However, its limitation stems from the hydrological reality that the catchment specific parameter S in the SCS-CN equation, which defines the catchment's water storage capacity and the precipitation threshold above which runoff is generated, should vary with antecedent moisture conditions (Michel et al., 2005; Shaw and Walter, 2009). Thus, recent work has focused on refining the SCS-CN method for more conceptually coherent use in continuous watershed models. Approaches of consideration of antecedent moisture conditions in the SCS-CN method range from introduction of a local effective available storage, σ_e, (Schneiderman et al., 2007), which determines that runoff generation is initiated from areas in the landscape as soon as the local storage is less than the effective precipitation (P_e), incorporation of rainfall return periods and the frequency of different soil moisture states based on antecedent base flow (Shaw and Walter, 2009), to consideration of the antecedent rainfall surplus (i.e. rain on the previous day) or deficit (i.e. antecedent actual evapotranspiration) in the determination of P_e (Dahlke et al., 2009).

The variable success of accurate prediction of VSA runoff and locations is also to a great extent influenced by the fact that subsurface stormflow processes in VSA are still poorly understood. The classical VSA hydrology concept, which is based on Betson's (1964) partial area hydrology concept, states that surface runoff is produced only from limited areas of the catchment in any given storm event (Dunne et al., 1975). Gburek and Sharpley (1998) further defined that VSA occur primarily in the near-stream zones in response to the close proximity of the water table to the land surface, which causes seep zones and high antecedent soil water content contents. Accordingly, water quality management in VSA dominated catchments has mainly focused on near-stream areas and surface topographic and soil storage controls to predict VSA runoff locations (Sharpley et al., 1994; Pionke et al., 1996; Gburek and Sharpley et al., 1998; Pionke et al., 1999; Sharpley et al., 2001; Gburek et al., 2002; Easton et al., 2007, 2008). However, much of the work has largely neglected the role of hillslope subsurface stormflow to streams and the role of subsurface heterogeneities such as cracks, macropores and transmissivity gradients in soils as well as the role of infiltration into fragipan soil layers on runoff generation. Although it is clear that the majority of runoff generated during storm events originates from VSAs, it is also likely that other processes contribute to the response as well. For instance, Parlange et al. (1989), Steenhuis et al. (1988), Hinton et al. (1993), Day et al. (1998), and McHale et al. (2002) have hypothesized that deep percolation through the impeding fragipan horizon and infiltration-excess overland flow during high-intensity summer thunderstorms (Walter et al., 2003; Needleman et al., 2004; Buda et al., 2009) also produce a response.

To improve process understanding and simulation of watershed processes, hillslope experiments are considered one of the most important building blocks (Hewlett and

Hibbert, 1963; Kirkby, 1978; Weyman, 1970; Freer et al., 2002; Tromp-van Meerveld and Weiler, 2008). Trenches, in particular, have proven to be a very helpful "tool" to advance the hydrological understanding of surface and subsurface hydrological processes (Hewlett and Hibbert; 1963, Dunne and Black 1970; McDonnell, 1990; Bonell, 1993; Woods and Rowe, 1996; Freer et al., 2002). Perhaps the greatest achievement of trenched hillslope studies is the greater understanding of the variety of subsurface flow paths important in controlling hillslope contributions to streams (Freer et al., 2002). Studies that combined measurements of subsurface flow in a trench face with upslope water table or soil moisture dynamics have advanced our understanding of the role of bedrock and surface topography (Freer et al., 2002; Tromp-van Meerveld and McDonnell, 2006b), subsurface flow sources (Burns et al., 2002, 2003), stream water chemistry (Hooper et al., 1998), groundwater-stream water relations (McGlynn et al., 2004), subsurface controls on rainfall-runoff thresholds (Tromp-van Meerveld and McDonnell, 2006a) and the role of macropores and preferential flow (Weiler and McDonnell, 2007) on subsurface stormflow generation.

Many of these studies assume impermeable bedrock and hence a no-flow boundary at the soil-bedrock interface. However, recent experiments have shown considerable flow through the soil-bedrock interface (Anderson et al., 1997; Scherrer et al., 2007; Tromp-van Meerveld et al., 2007; Uchida et al., 2002). However, there is a need to conduct rigorous long-term water balance studies to determine how these processes control the hydrologic response (Tromp-van Meerveld and Weiler, 2008; Weiler and McDonnell, 2007). Some hillslope studies, mostly restricted to the Panola Mountain Research Watershed in Georgia (U.S.) and the Maimai catchment in New Zealand, have clearly shown the effects of bedrock topography (the soil surface interface and soil-bedrock interface differ due to variability in soil depth) on subsurface stormflow

initiation and local flow concentration (Freer et al., 1997, 2002; Tromp-van Meerveld and McDonnell, 2006b; Woods and Rowe, 1996), and spatial variability in water quality (Brammer et al., 1995; Burns et al., 1998, 2001). Yet, simulation of the effect of soil depth variability and bedrock topography (defined as the soil-fragipan interface) on subsurface stormflow response in VSA hydrology dominated catchments remains largely unknown. Until now, simple topographic index models provide the only method to simulate the effect of soil depth variability and bedrock topography on subsurface flow response (Freer et al., 2002). However, topographic indices do not describe the spatiotemporal dynamics of subsurface stormflow during differently sized storm events. Thus, in addition to long-term streamflow monitoring additional data or other diagnostic tools such as geophysical methods (Weiler et al., 1998; Huisman et al., 2001, 2003; Sherlock and McDonnell, 2003; Tromp-van Meerveld and McDonnell, 2009) are required to define intra-catchment and hillslope processes and model complexity.

1.1 Objectives

Based on the above literature review the main hypothesis for this dissertation research is that subsurface stormflow response in variable source areas is threshold based and largely controlled by physical parameters such as bedrock topography and hydraulic soils properties as well as antecedent moisture conditions. It is assumed that these factors determine what processes and surface/sub-surface flow pathways will dominate the flow response at different moisture conditions.

The main goal of this study is to improve upon the partial process understanding that currently exists on subsurface stormflow processes in VSAs. Specifically, that the hillslope subsurface stormflow contributions to the VSAs depend on characteristics of

the bedrock topography and fragipan properties, which determine the development of preferential flow paths and the connectivity of hillslopes to VSAs and streams. VSA serve as a nexus for flow pathways (both spatially and temporally) and biogeochemical processes. Based on the improved knowledge gained with this research on flow pathways more accurate determination of the role of VSA as hot spots/hot moments for biogeochemical reactions and their accurate consideration in water quality management will be possible.

The key objectives of this dissertation research are:

1. Improve understanding of subsurface hydrology in VSAs by measuring the variability of flow components (surface runoff, interflow, groundwater) in a trenched hillslope (0.5 ha) using geophysical, hydrometric, geochemical and isotopic measurements.
2. Translate this knowledge into a simple hydrologic model that explains flow mechanisms in VSAs and runoff generation based on topography and soil characteristics.
3. Integrate the hydrologic model into an on-line available decision support system that identifies locations in the landscape based on their quantifiable risk of generating runoff and transporting nutrients to streams.

REFERENCES

Agnew, L.J., Lyon, S., Gérard-Marchant, P., Collins, V.B., Lembo, A.J., Steenhuis, T.S., and M.T. Walter. 2006. Identifying hydrologically sensitive areas: Bridging science and application. Journal of Environmental Management 78: 64-76.

Ambroise, B., Beven, K., and J. Freer. 1996. Toward a generalization of the TOPMODEL concepts: topographic indices of hydrological similarity. Water Resour. Res. 32 (7): 2135–2145.

Anderson, S.P., Dietrich, W.E., Torres, R., Montgomery, D.R., and K. Loague. 1997. Concentration-discharge relationships in runoff from a steep, unchanneled catchment. Water Resources Research 33(1): 211–225.

Andraski, T.W., and L.G. Bundy. 2003. Relationship between phosphorus levels in soil and in runoff from corn production systems. J. Environ. Qual. 32: 310–316.

Arnold, J.G., Srinivasan, R., Muttiah, R.S., and J.R. Williams. 1998. Large Area Hydrologic Modeling and Assessment – Part I: Model Development. Journal of the American Water Resources Association (JAWRA) 34(1): 73-89.

Betson, R.P. 1964. What is watershed runoff? Journal of Geophysical Research 69: 1541–1542.

Beven, K.J., and M.J. Kirkby. 1979. A physically-based, variable contributing area model of basin hydrology. Hydrol. Sci. Bull. 24: 43-69.

Bhaduri, B., Harbor, J., Engel, B., and M. Grove. 2000. Assessing watershed-scale, long-term hydrologic impacts of land-use change using a GIS-NPS model. Environ. Manag. 26: 643–658.

Bonell, M. 1993. Progress in the understanding of runoff generation dynamics in forests. J. Hydrol. 150: 217–275.

Brammer, D.D., McDonnell, J.J., Kendall, C., and L.K. Rowe. 1995: Controls on the downslope evolution of water, solutes and isotopes in a steep forested hillslope. EOS, Transactions of the American Geophysical Union 76(46): 268.

Brannan, K.M., Mostaghimi, S., McClellan, P.W., and S. Inamdar. 2000. Animal waste BMP impacts on sediment and nutrient losses in runoff from the Owl Run watershed. Trans. ASAE 43(5): 1155-1166.

Buda, A.R., Kleinman, P.J.A., Srinivasan, M.S., Bryant, R.B., and G.W. Feyereisen. 2009. Factors influencing surface runoff generation from two agricultural hillslopes in central Pennsylvania. Hydrological Processes 23: 1295-1312.

Burns, D.A., Murdoch, P.S., Lawrence, G.B., and R.L. Michel. 1998. Effect of groundwater springs on NO3 concentrations during summer in Catskill mountain streams. Water Resources Research 34(8): 1987–1996.

Burns, D.A., McDonnell, J.J., Hooper, R.P., Peters, N.E., Freer, J.E., Kendall, C., and K. Beven. 2001. Quantifying contributions to storm runoff through end-member mixing analysis and hydrologic measurements at the Panola Mountain Research Watershed (Georgia, USA). Hydrological Processes 15: 1903–24.

Burns, D.A. 2002. Stormflow hydrograph separation based on isotopes: the thrill is gone – what's next? Hydrological Processes, 16: 1515–1517.

Burns, D.A., Plummer, L.N., McDonnell, J.J., Busenberg, E., Casile, G.C., Kendall, C., Hooper, R.P., Freer, J.E., Peters, N.E., Beven, K., and P. Schlosser. 2003. The geochemical evolution of riparian groundwater in a forested Piedmont catchment. Groundwater 41(7): 913–925.

Dahlke, H.E., Easton, Z.M., Fuka, D.R., Lyon, S.W., and T.S. Steenhuis. 2009. Modeling Variable Source Area Dynamics in a CEAP Watershed. Ecohydrology 2: 337-349.

Day, R.L., Calmon, M.A., Stiteler, J.M., Jabro, J.D., and R.L. Cunningham. 1998. Water balance and flow patterns in a fragipan using in situ soil soil block. Soil Science 163(7): 517-528.

de Alwis, D.A., Easton, Z.M., Dahlke, H.E., Philpot, W.D., and T.S. Steenhuis. 2007. Unsupervised classification of saturated areas using a time series of remotely sensed images. Hydrol. Earth Syst. Sci. 11: 1609–1620.

Dunne, T., Black, R.D.. 1970. Partial area contributions to storm runoff in a small New England watershed. Water Resources Research 6: 1296–1311.

Dunne, T., Moore, T.R., and C.H. Taylor. 1975. Recognition and prediction of runoff-producing zones in humid regions. Hydrol Sci Bull, 20(3): 305–327.

Easton, Z.M., Gerard-Marchant, P., Walter, M.T., Petrovic, A.M., and T.S. Steenhuis. 2007. Hydrologic assessment of an urban variable source watershed in the Northeast US. Water Resources Research 43, W03413, :10.1029/2006WR005076, 2007.

Easton, Z.M., Fuka, D.R., Walter, M.T., Cowan, D.M., Schneiderman, E.M., and T.S. Steenhuis. 2008. Re-conceptualizing the Soil and Water Assessment Tool (SWAT) model to predict runoff from variable source areas. Journal of Hydrology 348: 279–291.

Ekholm, P., Kallio, K., Salo, S., Pietilainen, O.P., Rekolainen, S., Laine, Y., and Joukola. 2000. Relationship between catchment characteristics and nutrient concentrations in an agricultural river system. Water Res., 34: 3709-3716.

Freer, J., McDonnell, J., Beven, K.J., Brammer, D., Burns, D., Hooper, R.P., and C. Kendal. 1997. Topographic controls on subsurface storm flow at the hillslope scale for two hydrolog- ically distinct small catchments. Hydrological Processes 11(9): 1347–1352.

Freer, J., McDonnell, J., Beven, K.J., Peters, N.E., Burns, D.A., Hooper, R.P., Aulenbach, B., and C. Kendall. 2002. The role of bedrock topography on subsurface storm flow. Water Resour. Res. 38:1269 :10.1029/2001WR000872.

Garen, D.C., and D.S. Moore. 2005. Curve number hydrology in water quality modeling: Uses, abuses, and future directions. J. Am. Water Resour. Assoc. 41: 377–388.

Gburek, W.D., and A.N. Sharpley. 1998. Hydrologic controls on phosphorus loss from upland agricultural watersheds. Journal of Environmental Quality 27: 267–277.

Gburek, W.J., Sharpley, A.N., Heathwaite, L., and G.J. Folmar. 2000. Phosphorus management at the watershed scale: a modification of the phosphorus index. Journal of Environmental Quality 29: 130–144.

Gburek, W.J., Drungil, C.C., Srinivasan, M.S., Needelman, B.A., and D.E. Woodward. 2002. Variable-source area controls on phosphorus transport: Bridging the gap between research and design. Journal of Soil and Water Conservation 57(6): 534–543.

Gitau, M.W., Veith, T.L., Gburek, W.J., and A.R. Jarrett. 2006. Watershed-level BMP selection and placement in the Town Brook watershed, NY. J. Am. Water Resour. As. 42 (6): 1565-1581.

Haith, D.A., and L.L. Shoemaker. 1987. Generalized watershed loading functions for stremflow nutrients. Water Resources Research 23(3): 471–478.

Harpold, A.A., Lyon, S.W., Troch, P.A., and T.S. Steenhuis. 2010. The Hydrological Effects of Lateral Preferential Flow Paths in a Glaciated Watershed in the Northeastern USA. Vadose Zone Journal, 9: 397–414.

Hewlett, J.D., and A.R. Hibbert. 1963. Moisture and energy conditions within a sloping soil mass during drainage. Journal of Geophysical Research 68(4): 1081–1087.

Hewlett, J.D., and W.L. Nutter. 1970. The varying source area of streamflow from upland basins, Proceedings of the Symposium on Interdisciplinary Aspects of Watershed Management. Bozeman, MT. ASCE, New York, pp. 65–83.

Hinton, M.J., Schiff, S.L., and M.C. English. 1993. Physical properties governing groundwater flow in a glacial till catchment. Journal of Hydrology, 142: 229-249.

Hooper, R.P., Aulenbach, B.T., Burns, D.A., McDonnell, J., Freer, J., Kendall, C., and K. Beven. 1998. Riparian control of stream-water chemistry: implications for hydrochemical basin models. IAHS Publications-Series of Proceedings and Reports-Intern Assoc Hydrological Sciences, 248: 451–458.

Horton, R.E. 1933. The role of infiltration in the hydrologic cycle. Transactions American Geophysical Union 14: 446–460.

Horton, R.E. 1940. An approach toward a physical interpretation of infiltration capacity. Soil Science Society of America Proceedings 4: 399–417.

Huisman, J.A., Sperl, C., Bouten, W., and J.M. Verstraten. 2001. Soil water content measurements at different scales: Accuracy of time domain reflectometry and ground-penetrating radar. J. Hydrol. 245: 48–58.

Huisman, J.A., Hubbard, S.S., Redman, J.D., and A.P. Annan. 2003. Measuring soil water content with ground penetrating radar: a review. Vadose Zone Journal 2: 476-491.

Kirkby, M.J. 1978: Hillslope hydrology. Chichester, Wiley.

Krysanova, V., Muller-Wohlfeil, D.I., and A. Becker. 1998. Development and test of a spatially distributed hydrological water quality model for mesoscale watersheds. Ecol. Model. 106: 261–289.

Lee, K., Isenhart, T.M., Schultz, R.C., and S.K. Mickelson. 2000. Multispecies riparian buffers trap sediment and nutrients during rainfall simulations. J. Environ. Qual. 29(4): 1200-1205.

Lyon, S.W., Gérard-Marchant, P., Walter, M.T., and T.S. Steenhuis. 2004. Using a topographic index to distribute variable source area runoff predicted with the SCS-Curve Number equation. Hydrological Processes 18(15): 2757–2771.

Lyon, S.W., Seibert, J., Lembo, A.J., Walter, M.T., and T.S. Steenhuis. 2006. Geostatistical investigation into the temporal evolution of spatial structure in a shallow water table. Hydrology and Earth System Sciences 10: 113–125.

McDonnell, J.J. 1990. A rationale for old water discharge through macropores in a steep, humid catchment. Water Resources Research 26: 2821–32.

McGlynn, B.L., McDonnell, J.J., Seibert, J., and C. Kendall. 2004. Scale effects on headwater catchment runoff timing, flow sources, and groundwater-streamflow relations, Water Resour. Res., 40, W07504,DOI:10.1029/2003WR002494.

McHale, M., McDonnell, J.J., Mitchell, M.J., and C.P. Cirmo. 2002. A field based study of soil- and groundwater nitrate release in an Adirondack forested watershed. Water Resources Research 38(4): 1029/2000WR000102.

Michel, C., Andreassian, V., and C. Perrin. 2005. Soil Conservation Service curve number method: How to mend a wrong soil moisture accounting procedure? Water Resour. Res., 41, W02011, DOI:10.1029/ 2004WR003191.

Needelman, B.A., Gburek, W.J., Petersen, G.W., Sharpley, A.N., and P.J. Kleinman. 2004. Surface runoff along two agricultural hillslopes with contrasting soils. Soil Sci. Soc. Am. J. 68: 914-923.

Parlange, M.B., Steenhuis, T.S., Timlin, D.J., Stagnitti, F., and R.B. Bryant. 1989. Subsurface Flow Above a Fragipan Horizon. Soil Sciences 148: 77-86.

Pionke, H.B., Gburek, W.J, Sharpley, A.N., and R.R. Schnabel. 1996. Flow and nutrient export patterns for an agricultural hill-land watershed. Water Resour. Res. 32: 1795-1804.

Pionke, H.B., Gburek, W.J., Schnabel, R.R., Sharpley, A.N., and G.F. Elwinger. 1999. Seasonal flow, nutrient concentrations and loading patterns in stream flow draining an agricultural hill-land watershed. J. Hydrol. 220: 62–73.

Ponce, V.M., and R.H. Hawkins. 1996. Runoff curve number: Has it reached maturity? J. Hydrol. Eng., 1: 11 –19, DOI:10.1061/(ASCE)1084-0699(1996)1:1(11).

Puckett, L.J. 1995. Identifying the major sources of nutrient water-pollution. Environ. Sci. Tech. 29: A408-A414.

Rao, N.S., Easton, Z.M., Schneiderman, E.M., Zion, M.S., Lee, D.R., and T.S. Steenhuis. 2009. Modeling Watershed-Scale Effectiveness of Agricultural Best Management Practices to Reduce Phosphorus Loading. Journal of Environmental Management 90: 1385-1395.

Sharpley, A.N., Chapra, S.C., Wedepohl, R., Sims, J.T., Daniel, T.C., and K.R. Reddy. 1994. Managing agricultural phosphorus for protection of surface waters: issues and options. Journal of Environmental Quality 23: 437–451.

Sharpley, A.N., McDowell, R.W., Weld, J.L., and P.J.A. Kleinman. 2001. Assessing site vulnerability to phosphorus loss in an agricultural watershed. J. Eviron. Qual. 30: 2026-357.

Shaw, S.B., and M.T. Walter. 2009. Formulating storm runoff risk using bivariate frequency analyses of rainfall and antecedent watershed wetness. Water Resour. Res. 45: W03404 : 10.1029/2008WR006900.

Scherrer, S., Naef, F., Faeh, A.O., and I. Cordery. 2007. Formation of runoff at the hillslope scale during intense precipitation. Hydrology and Earth System Sciences 11: 907–922.

Schneiderman, E.M., Steenhuis, T.S., Thongs, D.J., Easton, Z.M., Zion, M.S., Mendoza, G.F., Walter, M.T., and A.L. Neal. 2007. Incorporating variable source area hydrology into the curve number based Generalized

Watershed Loading Function model. Hydrological Processes 21: 3420–3430, : 10.1002/hyp6556.

Sherlock, M.D., and J.J. McDonnell. 2003. A new tool for hillslope hydrologists: spatially distributed groundwater level and soilwater content measured using electromagnetic induction. Hydrol. Proces. 17: 1965-1977.

Srinivasan, M.S., Gerard-Marchant, P., Veith, T.L., Gburek, W.J., and T.S. Steenhuis. 2005. Watershed scale modeling of critical source areas of runoff generation and phosphorus transport. J. Am. Water Resour. Assoc. 41: 361–375.

Steenhuis, T.S., Richard, T.L., Parlange, M.B., Aburime, S.O., Geohring, L.D., and J.Y. Parlange. 1988. Preferential flow influences on drainage of shallow sloping soils. Agricultural Water Management, 14: 137-151.

Steenhuis, T.S., Winchell, M., Rossing, J., Zollweg, J.A., and M.F. Walter. 1995. SCS Runoff Equation Revisited for Variable-Source Runoff Areas. ASCE Journal of Irrigation and Drainage 121: 234–238.

Tromp-van Meerveld, H.J., and J.J. McDonnell. 2006a. Threshold relations in subsurface stormflow: A 147-storm analysis of the Panola hillslope. Water Resources Research, 42: W02410.

Tromp-van Meerveld, H.J., and J.J. McDonnell. 2006b. Threshold relations in subsurface stormflow: 2. The fill and spill hypothesis. Water Resources Research 42: W02411, Doi:10·1029/2004WR003800.

Tromp-van Meerveld, I., and J.J. McDonnell. 2009. Assessment of multi-frequency electromagnetic induction for determining soil moisture patterns at the hillslope scale. Journal of Hydrology, 368: 56-67.

Tromp-van Meerveld, I., and M. Weiler. 2008. Hillslope dynamics modeled with increasing complexity. Journal of Hydrology 361: 24–40.

Tromp-van Meerveld, H.J., Peters, N.E., and J.J. McDonnell. 2007. Effect of bedrock permeability on subsurface stormflow and the water balance of a trenched hillslope at the Panola Mountain Research Watershed, Georgia, USA. Hydrological Processes 21: 750–769.

Uchida, T., Kosugi, K.I., and T. Mizuyama. 2002. Effects of pipe flow and bedrock groundwater on runoff generation in a steep headwater catchment in Ashiu, central Japan. Water Resources Research 38(7). DOI:10.1029/2001WR00026.

USDA-SCS (Soil Conservation Service). 1972. National Engineering Handbook, Part 630 Hydrology, Section 4, Chapter 10.

Walter, M.T., Walter, M.F., Brooks, E.S., Steenhuis, T.S., Boll, J., and K.R. Weiler. 2000. Hydrologically sensitive areas: Variable Source Area hydrology

implications for water quality risk assessment. Journal of Soil and Water Conservation 55(3): 277–284.

Walter, M.T., Brooks, E.S., Walter, M.F., Steenhuis, T.S., Scott, C.A., and J.Boll. 2001. Evaluation of soluble phosphorus transport from manure-applied fields under various spreading strategies. Journal of Soil and Water Conservation 56(4): 329–336.

Walter, M.T., Steenhuis, T.S., Mehta, V.K., Thongs, D., Zion, M., and E. Schneiderman. 2002. Refined conceptualization of TOPMODEL for shallow subsurface flows. Hydrolog. Process. 16(10): 2041– 2046.

Walter, M.T., Mehta, V.K., Marrone, A.M., Boll, J., Steenhuis, T.S., and M.F. Walter. 2003. Simple estimation of prevalence of Hortonian flow in New York City watersheds. ASCE Journal of Hydrology and Engineering. 8(4): 214–218.

Weiler, K.W., Steenhuis, T.S., Boll, J., K-J.S. Kung. 1998. Comparison of ground penetrating radar and time domain reflectometry as soil water sensors. Soil Sci. Soc. of Am. J. 62: 1237–1239.

Weiler, M., and J.J. McDonnell. 2007. Conceptualizing lateral preferential flow and flow networks and simulating the effects on gauged and ungauged hillslopes. Water Resources Research 43. DOI:10.1029/2006WR00486.

Weyman, D.R. 1970. Throughflow on hillslopes and its relation to the stream hydrograph. Bulletin of the International Association of Scientific Hydrology 15(2): 25–33.

Williams, J.R., Jones, C.A., and P.T. Dyke. 1984. The EPIC model and its applications. Proc. ICRISAT–IBSNAT–SYSS Symposium on Minimum Data Sets for Agrotechnology Transfer.

Woods, R., and L. Rowe. 1996. The changing spatial variability of subsurface flow across a hillside. Journal of Hydrology (NZ) 35(1): 51–86.

CHAPTER 2

DISSECTING THE VARIABLE SOURCE AREA CONCEPT – FLOW PATHS AND WATER MIXING PROCESSES

Abstract

Variable source areas (VSAs) are hot spots of hydrological (saturation excess runoff) and biogeochemical processes (e.g. nitrogen, phosphorus, organic carbon cycling) in the landscapes of the northeastern U.S. The prevalence of shallow, highly transmissive soils, steep topography, and impeding clay layers in the soil (i.e. fragipan) have long been recognized as first-order controls on VSA formation. Nevertheless, there is still process understanding to be gained on how VSA connect with the surrounding area and how this interaction influences surface and subsurface runoff generation. To determine the controls on VSA formation and connectivity we instrumented (trenched) a 0.5 ha hillslope in the southern tier of New York State, U.S.A.. Measurements of water flux in the trench, upslope water table dynamics, surface and bedrock topography in conjunction with isotopic and geochemical tracers allowed a four-dimensional characterization (XYZ and Time) of the subsurface storm flow response within the VSA. Here we focus on the use of tracer-based hydrograph separation models and physically measured flow components to separate temporally (i.e. event and pre-event) and quantify (by difference) shallow water from above the fragipan layer (including both surface runoff and shallow interflow) and deeper water from below the fragipan layer. With increasing antecedent moisture conditions we observed a switch from predominately vertical to lateral flow in the hillslope. During events with dry antecedent conditions infiltrating rainwater is percolating through the fragipan layer to deeper soil layers. Thus, during these conditions the majority of total

discharge is comprised of deeper water (33 – 71 %) contributed from below the fragipan. During storm events with wet antecedent conditions and large rainfall amounts (> 15 mm) shallow water (event and pre-event) contributions were one magnitude greater than deeper water flow when soils above the fragipan were saturated and lateral subsurface flow above the fragipan dominated runoff generation. Deeper water contributions to total trench discharge were constant (0.08 mm/h) and independent of total rainfall amounts, rainfall intensities, and water table dynamics. Observed saturated area extends and similarity of water chemistry in the total discharge and water sampled from upslope piezometer wells indicate that water from a distance of up to 56 m was contributing runoff during storm events. Our results have important implication for the protection of streams from dissolved pollutant transport and recommend that preference be given to variable-width buffers over fixed-width stream buffers.

2.1 Introduction

Our understanding of runoff processes has come a long way since the seminal work of Horton (1933, 1940) on infiltration-excess runoff. This includes development of theories of saturation-excess surface runoff (Dunne and Leopold, 1978) with its corollary variable source area (VSA) concept (Hewlett and Hibbert, 1967; Dunne and Black, 1970) and rapid subsurface storm flow (Dunne and Leopold, 1978; McDonnell, 1990). Recently, Troch et al. (2009) revisited the work of Horton (1933) to gain insight on the connections between hydrologic partitioning and vegetation water-use efficiency. Taking inspiration from this work, it appears that catchments can be considered, to some extent, as analogous to living organisms in their ability to evolve over time in response to water availability and climate. Based on such an analogy, perhaps hydrological sciences can learn something by taking a page from biology. For

example, Wagner et al. (2007) identify the potential benefits of developing classification schemes and consistent taxonomy akin to the nomenclature of biology to aid in advancing hydrologic theory. Along these lines, we consider borrowing another common biology technique to advance our understanding of hydrological processes: dissection.

Any dissection requires some sort of scalpel or knife for cutting. For the experimental hydrologist, this comes in the form of the trench. Trenches (and excavations in general) on experimental hillslopes (e.g., Hewlett and Hibbert; 1967, Dunne and Black 1970; McDonnell, 1990; Bonell, 1993; Woods and Rowe, 1996; Freer et al., 2002) are commonly used to quantify subsurface storm flow and water mixing in response to storm rainfall and snowmelt (Tromp-van Meerveld and McDonnell, 2007). In experimental hydrology, much advancement has been made at the hillslope scale through the use of trenches with a focus (primarily) on subsurface storm flow (Bonell, 1993; 1998). For example, recent studies by Tromp-van Meerveld and McDonnell (2007) from a trenched hillslope in the Panola Mountain Research Watershed (2006 a,b,c) have presented a benchmark concept of nonlinear behavior of hillslope subsurface storm flow generation into a threshold-driven response (the fill-and-spill hypothesis). Other studies have looked at subsurface flow at the trench face to identify subsurface flow sources (Burns et al., 2002, 2003), groundwater-streamwater relations (McGlynn et al., 2004), and the role of macropores and preferential flow (Weiler and McDonnell, 2007) for subsurface storm flow generation. This focus on subsurface storm flow results in many trench experiments being designed to measure hillslope response at the trench wall and as a result they often neglect where the water is originating from in the contributing area of the trench. By dissection, we propose using the common trench to slice across the hydrologically active area of the

landscape in order to gain knowledge of its internal workings particularly with respect to runoff generation processes.

Since trenching has shown that there are a variety of subsurface flow paths that are important in controlling and transporting hillslope contributions to streams (Freer et al., 2002), trenching could be potentially helpful in improving process understanding of subsurface flow processes in VSA. In the northeastern U.S. the predominance of shallow, highly transmissive soils, steep topography and the presence of impeding sub-soil layers (i.e. hardpans, fragipans, bedrock) often lead to the development of saturation-excess runoff and VSAs that expand and contract spatially and temporally depending on the rainfall depth (Dunne and Black, 1970; Hewlett and Nutter, 1970). The high infiltration capacities make infiltration-excess runoff unlikely during storm events (Walter et al., 2002). Thus, risk of pollutant transport is elevated where VSA overlap with potentially contaminant containing source areas.

Thus, several water quality studies have focused on determining VSA runoff and protecting receiving streams from nutrient or pollutant flux with fixed-width stream buffers based on the assumption that a small portion of the landscape, typically the near stream areas, produces the majority of runoff (Sharpley et al., 1994;Gburek and Sharpley et al., 1998; Sharpley et al., 2002; Gburek et al., 2002; Easton et al., 2007, 2008b, Dahlke et al., 2009). However, two recent VSA dynamic studies from Lyon et al. (2006b) and Harpold et al. (2010) both pointed out that VSAs can occur in every landscape position and are not restricted to near-stream areas. Further these VSA locations can be generally well predicted using the topographic index (Beven and Kirkby, 1979) or soil topographic index (Ambroise et al., 1996) concept to distribute saturated areas in space and to predict runoff volumes generated during storm events

(e.g., Lyon et al., 2004; Gérard-Marchant et al., 2006, Easton et al. 2008a,b; Dahlke et al. 2009).

However, the applicability of the topographic index to locate VSAs remains of variable success and depends strongly on seasonality (Lyon et al., 2006b), scale (deAlwis et al., 2007; Dahlke et al., 2009) and the lateral redistribution of water (Harpold et al., 2010) but appears to result in better predictability under wet antecedent conditions and on the basis of accurate topography and soils information. Although the dominant VSA hydrology concept may hold for the majority of runoff generated during storm events in the northeastern U.S. (Walter et al., 2003), water balance studies from Parlange et al. (1989), Steenhuis et al. (1988), Day et al. (1998), and Buda et al. (2009) have hypothesized deep percolation through the impeding fragipan horizon and infiltration excess overland flow during high-intensity summer thunderstorms as alternative runoff mechanisms in conjunction with VSAs. Clearly, there is more process understanding to be gained with regards to how VSAs form and connect various sources of water within the landscape.

To investigate these hypothesized alternatives and better understand the flow pathways of water through a VSA, we present the results of a VSA dissection. This allows for documenting the complexity of a VSA to improve upon the partial process understanding that currently exists. We installed a trench in a VSA with the goal of understanding its spatial and temporal dynamics under different antecedent moisture conditions. In this study we present the subsurface stormflow response of the VSA and its internal and spatial, isotopic and chemical mixing processes observed during five events using a network of direct hydrometric and water table measurements and analytical techniques such as chemical hydrograph separation techniques.

2.2 Study Site

This study was conducted on a 0.5 ha, N-NE facing hillslope located in a spring area of a headwater catchment near Ithaca, central New York State, USA (76°14'48.44" W, 42°24'56.86" N). The study hillslope length is short (< 125 m), moderately steep (average 7°) in an elevation ranging from 482 to 499 m (Fig. 2.1). Annual precipitation averages 930 mm with an annual mean temperature of 7.8 °C. Physiographic settings of the instrumented hillslope are typical for the fragipan-soil-dominated landscapes of the humid northeastern US. The vegetation in the study site is mixed grassland that is cut biannually for hay production (typically in June and September). Hardwood deciduous forest with American beech, oaks, and sugar maples bound the study site towards the western, steeper shoulder.

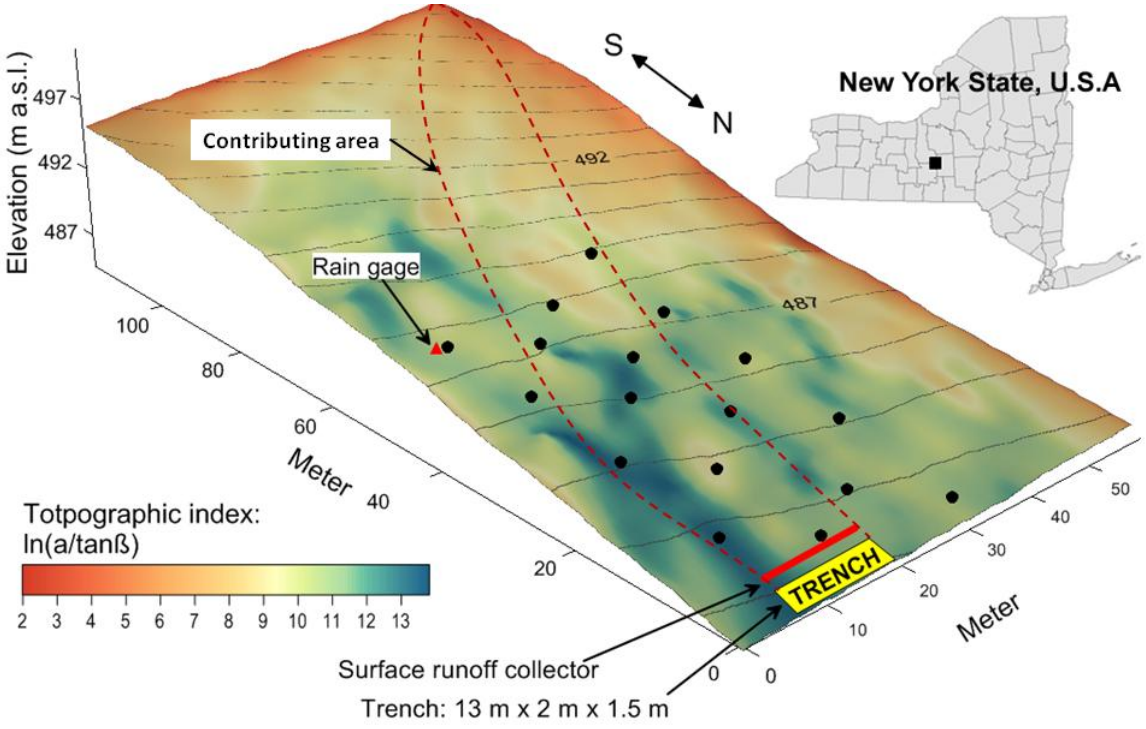

Figure 2.1: Location of study hillslope in central New York State, U.S.A.. Black dots indicate locations of water level loggers. The red dashed line is indicating the watershed boundary for the trench contributing area as derived from surface topography.

The bedrock material consists of glacial till on middle Devonian shales and siltstones (Miller, 1993). The depth to the bedrock is locally variable and ranges between 1.5 m on the hilltops and several meters (> 25 m) in the valley bottoms (Miller, 1993). The dominant soil type at the site is a Mardin channery silt loam, which is classified as coarse-loamy, mixed, active, mesic typic Fragiudepts (parent material is glacial till) (Soil Survey Geographic Database, NRCS-USDA). The Mardin channery silt loam is a moderately acid soil with a high content of rock fragments. A description of the soil profile in the trench showed a Mardin silt loam consisting of a dark brown channery silt loam (Ap, 0-10 cm) overlaying a yellowish brown, friable, channery silt loam Bw horizon with 15 percent rock fragments (10- 30 cm), followed by a pale brown channery silt loam (E horizon, 30-45 cm) showing signs of redoximorphic depletion and a clear boundary to the next layer. The fragipan horizon was found in the trench soil profile at a depth ranging from 45 to 105 cm as yellowish brown to light olive brown Bx horizon showing redoximorphic depletion and clear pale brown prism faces that are wider at the top becoming narrower with increasing depth. The Bx horizon was underlain by a light olive brown, massive, firm, very channery silt loam with 45% rock fragments (C horizon, 105-140 cm).

Depth to the fragipan and the subsurface topography upslope of the trench was estimated using multiple ground penetrating radar (GPR) scans over the entire hillslope and ranged between 0.43 and 1.20 m with an average of 0.66 m (Fig. 2.2). These GPR scans also indicated that a sand lens was covering part of the contributing trench area approximately 25 m upslope of the trench face (red dashed line, Fig. 2.3). This area is characterized by a very low clay content (μ = 1%) compared to the surrounding soils (average clay content μ = 13.3%).

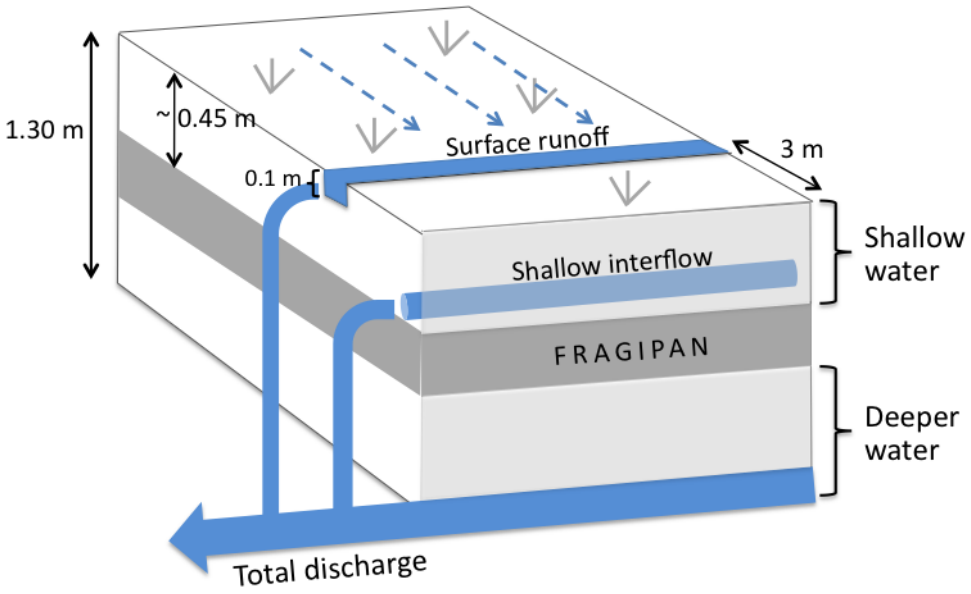

Figure 2.2: Schematic layout of the trench instrumentation and collectors of different flow components (surface runoff, shallow interflow, total discharge). For the chemical hydrograph separation water coming to the trench is separated into shallow water from top the fragipan and deeper water from below the fragipan.

2.3 Methodology

The hillslope-trench site was monitored from October 2009 through May 2010 (excluding the winter period). During this period 16 individual storm events were automatically measured on the hillslope study site with tipping buckets and flow gages. During five of the sixteen storms isotopic and chemical measurements ($\delta^{18}O$, Si, and DOC) of the water flowing to the trench were made. The data were analyzed using different analytical techniques as well as a network of direct measurements, which are described in more detail in the following sections.

2.3.1 Hydrometric measurements

A 13 m long by 2 m wide trench was excavated in a VSA located at the bottom of the 100 m long hillslope (Fig. 2.1). The hillslope trench was sited to span across a known saturated area at the base of this hillslope. The trench face was constructed orthogonal

to flowlines derived from surface topography. The trench was dug to a depth of approximately 1.5 m to intersect the fragipan horizon, which is located at a depth of 0.45 – 1.05 m in the trench face. Both the flux and composition of the water draining through the trench were monitored with pressure transducers and tipping bucket data loggers. Water level and chemistry observations were made within the drainage area of the trench face.

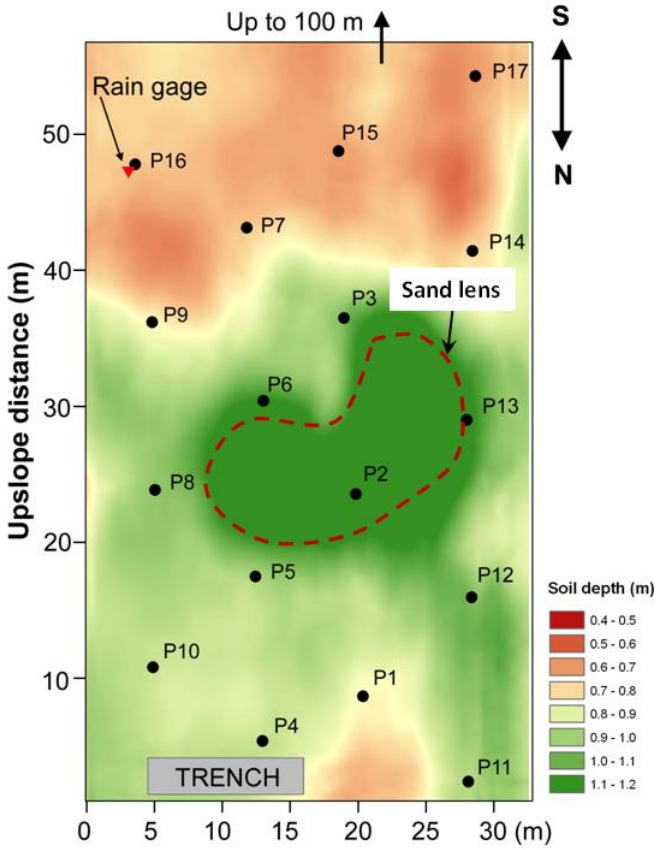

Figure 2.3: Hillslope instrumentation and depth to fragipan survey. Locations of water level loggers are indicated by black dots. A sand lens (red dashed line) was detected with ground penetrating radar and confirmed with particle distribution data of soil samples.

2.3.1.1 Trench instrumentation

Three main sources of water were monitored in the trench: surface runoff, shallow interflow, and total discharge. A surface runoff collector was installed 3 m upslope of

the trench wall to collect flow from the upper 10 cm of the soil (Fig. 2.2). This water is defined as "surface runoff" (SR). 2 m upslope of the trench wall a perforated drain tile with a 10 cm diameter was installed at the soil-fragipan interface in a ditch approximately 45 cm depth. When refilling the ditch, clay was used to seal the downslope face to intercept and collect shallow subsurface flow above the fragipan. This water is defined as "shallow interflow" (SI). Surface runoff and shallow interflow water were routed with pipes to the center of the trench, where tipping buckets, each connected to a HOBO pendant event data logger (Onset Computer Corporation, Pocasset, MA, USA) measured the flow rates. The tipping buckets were leveled and fixed to a solid wood structure to minimize changes in calibration with increasing tipping frequency. Surface runoff rate was measured with a tipping bucket that captured 4 L per tip while shallow interflow was measured with a bucket capacity of 430 mL per tip.

A third perforated drain tile with a diameter of 10 cm was installed at the bottom of the trench (1.5 m). This drain tile collected surface runoff, shallow interflow as well as deeper subsurface flow from underneath the fragipan. As this integrates across the entire soil profile, this water is defined as "total discharge" (TD). This total discharge was measured at a 5-min interval using a compound weir equipped with a Telog Inc. (Victor, NY, USA) pressure transducer (1 psi). As the trench was left uncovered, except for the section where tipping buckets were installed, total discharge was corrected for rainfall inputs into the trench by simply subtracting rainfall amounts times uncovered trench area (~ 26 m^2).

2.3.1.2 Hillslope instrumentation

A grid of 17 piezometers wells were installed in the lower half of the contributing area of the trench (Fig. 2.1). Water levels were measured at 5-min intervals using 500 mm and 1000 mm long capacitance probes (TruTrack Inc., New Zealand). The loggers were installed in four transects with a distance of 8 m across the slope and 14 m upslope between the loggers. This logger network covered 60 % of the total hillslope area. All capacitance probes were completely embedded in the soil inside 5 cm-PVC tubes, resulting in installation depths of 0.83 m for the WT-HR500 probes (wells P1 – P17, except well P3) and 1.30 m for one WT-HR1000 probe (well P3) respectively. The PVC tubing was screened over the lower 25 cm and served as ground water wells for water grab sampling used in the chemical analysis described below.

A tipping bucket rain gauge (Spectrum Technologies Inc., Plainfield, IL, USA) was installed on site that recorded rainfall amounts over 5-min intervals. Meteorological data (temperature, precipitation, wind, solar radiation) were concurrently available from a climate reference network station in Harford, NY, (347 m a.s.l.) approximately 2.3 km north of the site.

2.3.2 Water sampling and laboratory analysis

In addition to the automatically logged hydrometric sampling, grab water samples of each flow component (surface runoff, shallow interflow) and of the integrated signal (total discharge) were manually collected bi-weekly during site visits and at shorter time intervals (20 min to 1 hour) during five storm events for isotopic and chemical analysis. During the five storm events, multiple precipitation samples were collected over the duration of each event using a funnel collector positioned adjacent to the rain gage. Water samples from the wells (P1 – P17) were taken weekly if water was

present, using a peristaltic pump. For some of the storm events grab samples were taken from all wells before and after the storm, if water was present. All samples were collected using 125-mL high-density polyethylene bottles and were refrigerated until laboratory analysis. Once analyzed, these samples provided the basis for chemical hydrograph separations for five events.

All samples were analyzed for major cations and anions, as well as dissolved organic carbon (DOC), within 48 hours of sample collection. Samples were passed through 0.45-μm membrane filters prior to chemical analysis. DOC concentrations were estimated using the heated persulfate oxidation method with an OI Analytical 1010 TOC analyzer. Cation concentrations (Ca^{2+}, Mg^{2+}, Na^{+}, K^{+}, Si^{+}) were analyzed using an inductively coupled plasma analyzer. Samples were analyzed for $\delta^{18}O$ at the Cornell Stable Isotope Laboratory in Ithaca, New York, by mass spectrometer and reported in ‰ relative to Vienna standard mean ocean water (VSMOW) with 0.15 ‰ precision.

2.3.3 Hydrograph separation

2.3.3.1 Measured and calculated flow components

Measured flow of surface runoff, shallow interflow and total discharge were used to estimate the flux of deeper water and chemical mixing processes of the flow components during storm events. Using a simple water balance the deeper water fraction, which could not be directly measured in the trench, was calculated as the difference of total discharge to the sum of surface runoff and shallow interflow. As the trench was left uncovered flow volumes were also corrected for rain falling into the trench. Thus, for each storm we subtracted the total rainfall amount, P (mm), times the

trench area, A_{trench} (m^2), from the total discharge and calculated the deeper water fraction using the following mass balance:

$$Q_{TD} - (P * A_{trench}) = Q_{SR} + Q_{SI} + Q_{DW} - (P * A_{trench}) \quad (2.1)$$

where Q_{TD} (L/s) is the total discharge or the volume of water draining into the trench containing flow contributions of surface runoff, shallow interflow, and deeper water, Q_{SR}, Q_{SI}, and Q_{DW} (L/s) respectively. Losses related to interception storage were ignored for the presented study period as the grassland was cut at the end of September 2009 and the storm events of interest occurred outside the growing season.

2.3.3.2 Chemical-based hydrograph separation

A two-component (one tracer) hydrograph separation approach was used to temporally separate each flow component (surface runoff, shallow interflow) and total discharge into pre-event and event water based on measured $\delta^{18}O$ ratios in the precipitation and total discharge (Sklash and Farvolden, 1979, Kendall and McDonnell, 1998, Buttle and McDonald, 2002):

$$Q_t C_t = Q_p C_p + Q_e C_e \quad (2.2)$$

where Q is the measured discharge of the respective flow component, C is the concentration of the isotopic tracer $\delta^{18}O$, and the subscripts t, p, and e refer to total, pre-event, and event water, respectively.

Since this two-component separation technique was applied to each flow component coming to the trench and to the total discharge, it was also possible to temporally (i.e., pre-event and event) separate the shallow water from above the fragipan layer (including both surface runoff and shallow interflow) and deeper water from below the fragipan layer. Since it was not possible to sample deeper water directly, temporal characterization of deeper water was done by combining the measured flow volumes with the tracer-based separation of event and pre-event water fractions of surface runoff, shallow interflow and total discharge. Assuming that rainwater falling into the trench contributes only to the new water fraction, the temporal components (i.e. event and pre-event water) of deeper water from below the fragipan could be calculated using the following mass balance equations:

$$Q_{DWe} = Q_{TDe} - \left[(P * A_{trench}) + Q_{SRe} + Q_{SIe}\right] \tag{2.3}$$

$$Q_{DWpe} = Q_{TDpe} - \left(Q_{SRpe} + Q_{SIpe}\right) \tag{2.4}$$

where Q_{DW} (L/s) is the calculated fraction of deeper water and $Q_{TD,}$ Q_{SR}, and Q_{SI}, (L/s) are observed total discharge, surface runoff and shallow interflow volumes respectively. Subscripts *p* and *e* refer to pre-event and event water, respectively and (P^* A_{trench}) (L) is the amount of rainwater falling into the trench. The two-component hydrograph separation assumes unique source signatures for valid isotopic separations. In this study the event water fraction was estimated based on average δ^{18}O values of bulk rain samples collected at irregular increments during the storm events. Pre-event water was the base flow chemistry of each flow component and total discharge at the beginning of each rain event.

To explore subsurface flow paths in more detail we generated DOC vs. Si mixing diagrams for each event showing observed tracer signals in each flow component, the total discharge and the piezometer wells.

2.3.3.3 Uncertainty estimation

Uncertainty associated with the calculated mixing fractions in the isotopic hydrograph separations was estimated using the technique of Genereux (1998), in the following displayed for the two-component hydrograph separation:

$$W_{f_p} = \left\{ \left\lfloor \frac{C_e - C_t}{\left(C_e - C_p\right)^2} W_{c_p} \right\rfloor + \left\lfloor \frac{C_t - C_p}{\left(C_e - C_p\right)^2} W_{c_e} \right\rfloor + \left\lfloor \frac{1}{C_e - C_p} W_{c_t} \right\rfloor \right\} \tag{2.5}$$

where W_{fp} is the uncertainty of the pre-event mixing fraction, and W_{Cp} and W_{Ce} are the uncertainties associated with the isotopic or chemical tracer of the pre-event and event water respectively, and C_t, C_e and C_p are the δ^{18}O values in the total discharge, event and pre-event component respectively. We used a constant 10% to account for potential flow measurement errors and an absolute error of double the analytical precision for Si (2.16 µeq/l) and δ^{18}O (0.3 ‰) to estimate uncertainty in the two-component and three-component hydrograph separation.

2.3.4 Observation of the saturated hillslope area

The fractional saturated area (A_f) in the hillslope observed during storm events was determined using hourly averages of measured water table depths. To obtain A_f we first interpolated water table depths using ordinary kriging (Ripley, 1981; Goovaerts, 1999) and then estimated A_f as the ratio of the area with water tables above a specified threshold to the total contributing area (2575 m^2). Lyon et al. (2006a, b) found that the generation of saturation excess overland flow rapidly increased when the median

water table was within the top 10 cm of the soil. Following the findings of Lyon et al. (2006b) and Dahlke et al. (2010, submitted) we similarly applied a water table threshold of 10 cm to derive the fractional saturated area in the hillslope.

In addition we calculated the flow contributing slope length for the trench for each storm event based on observed volumes of shallow water (surface runoff and shallow interflow) and the drainable porosity of the soils. The drainable porosity was calculated from recession flows and known saturated area extend in the hillslope.

2.4 Results

2.4.1 Event characteristics

The five storm events presented in this study (Table 2.1 and Fig. 2.4) occurred on 24 October, 28 October, and 2 December 2009 and on 17 April and 26 April 2010. These events showed rainfall and total discharge depths ranging from 9.9 mm to 46 mm, and from 1 to 8.9 mm, respectively (Table 2.1). Rainfall events lasted from 12 to 33 hours and had low intensities (0.4 to 1.9 mm/5-mins), common to rainfall in the northeast US (Buda et al., 2009). At no time during the study was the infiltration capacity of the soil exceeded by the rainfall intensity, as supported by field observed infiltration rates of 148 to 334 mm/hr, measured using the sprinkler infiltrometer method of Ogden et al. (1997).

The antecedent precipitation index (API), calculated as the sum of rainfall over a defined period of days, showed 7-day (API_7) and 30-day (API_{30}) antecedent rainfall ranging from 1 to 26 mm and from 60 to 144 mm, respectively. Base flow, defined here as the minimum total discharge within the 24-hours prior to a storm event, ranged from 2 to 60 L/hr and reflected a wide range of antecedent moisture conditions prior to

storm events. The average water table depth (average of 17 water level loggers) ranged from 780 mm (26 April 2010) to 320 mm (2 December 2009) and the saturated fractional area of the hillslope ranged between zero and 13 percent prior to storm events and reached a maximum extent of 5 to 38% during storm events. Three of the five storms (24 October 2004, 17 and 26 April 2010) had no saturated area present before the storm.

Table 2.1: Hydrometric characteristics for the five storm events presented in this study.

	24-Oct	**28-Oct**	**2-Dec**	**17-Apr**	**26-Apr**
API-30 (mm)	144.2	98.1	59.7	89.1	82.0
API-14 (mm)	20.7	35.1	53.9	8.6	37.5
API-7 (mm)	2.8	26.1	26.2	0.9	15.0
Event magnitude (mm)	26.1	45.5	9.9	16.5	37.3
Duration (hrs)	30	12	14	18	22
Max rain intensity (5-min)	0.7	1.9	0.7	1.2	0.4
Base flow (Q_{base}) prior to event (L/h)	2.0	5.2	59.6	6.6	9.3
Total discharge (mm)	1.04	8.87	2.07	0.68	1.05
Water table depth prior to event (mm)	684	474	320	706	780
Max. water table depth (mm)	338	75	215	632	367
Saturated fractional area prior to event ($A_{f\text{-}ini}$)	0.0	0.05	0.13	0.0	0.0
Max. saturated fractional area ($A_{f\text{-}max}$)	0.07	0.38	0.2	0.05	0.09
Avg. saturated fractional area ($A_{f\text{-}avg}$)	0.04	0.29	0.17	0.02	0.02
Shallow flow contributing slope length (m)[a]	8.9	55.6	14.3	1.6	7.4
Surface runoff contributing slope length (m)[b]	13.6	120.1	27.02	4.1	18.6

[a] Assuming an estimated drainable porosity of 4.4% and an average saturated thickness of 0.5 m.
[b] Assuming an estimated drainable porosity of 4.4% and an average saturated thickness of 0.15 m.

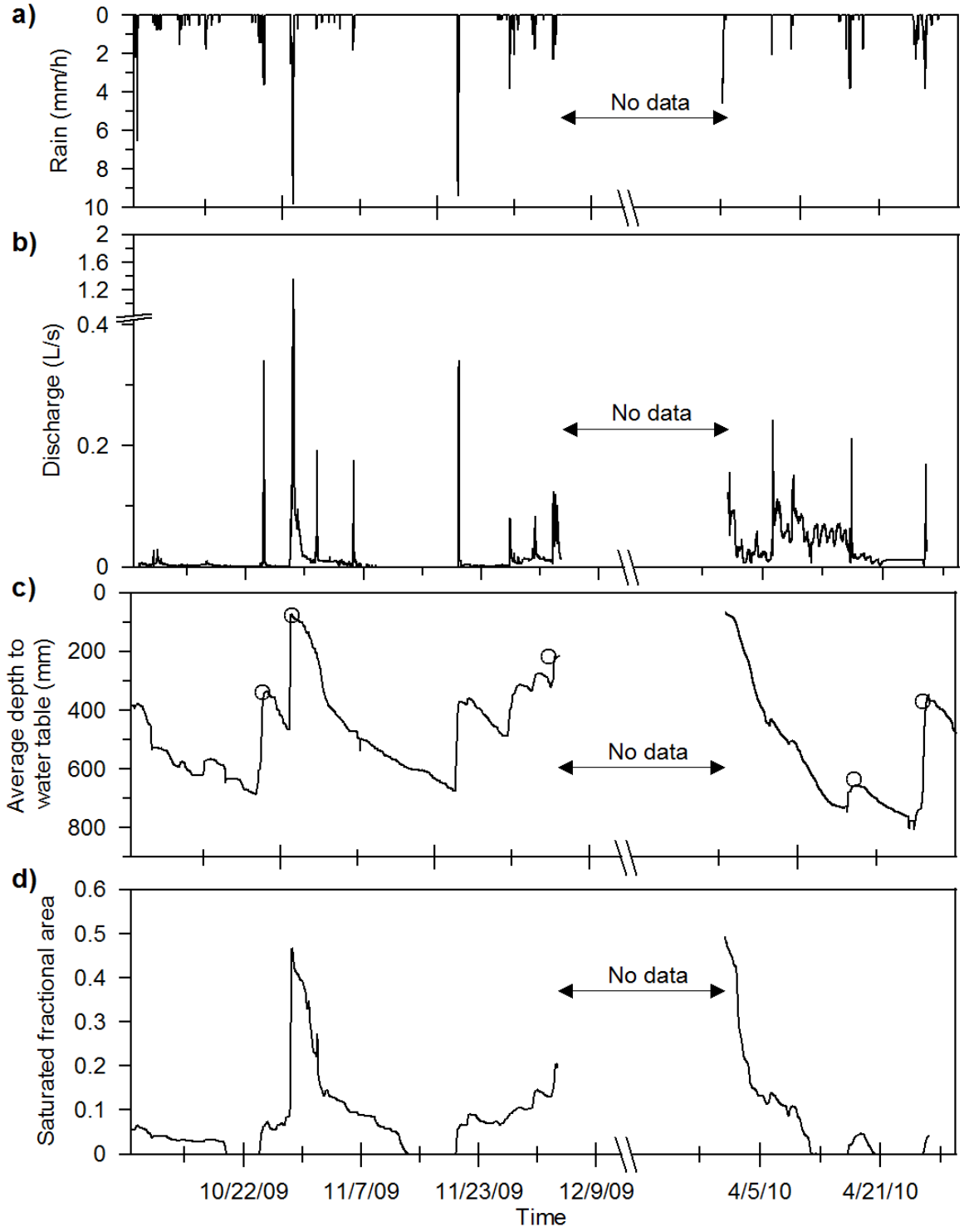

Figure 2.4: (a) Rainfall hyetograph and cumulative rain for the study period from October 2009 until May 2010 (excluding the frost period). (b)Total discharge (L/s) measured in the trenched hillslope. (c) Time series of the average depth to the water table in the hillslope, and (d) of the saturated hillslope fraction, derived when the water table was 10 cm below the soil surface.

The antecedent precipitation index (API), calculated as the sum of rainfall over a defined period of days, showed 7-day (API_7) and 30-day (API_{30}) antecedent rainfall ranging from 1 to 26 mm and from 60 to 144 mm, respectively. Base flow, defined here as the minimum total discharge within the 24-hours prior to a storm event, ranged from 2 to 60 L/hr and reflected a wide range of antecedent moisture conditions prior to storm events. The average water table depth (average of 17 water level loggers) ranged from 780 mm (26 April 2010) to 320 mm (2 December 2009) and the saturated fractional area of the hillslope ranged between zero and 13 percent prior to storm events and reached a maximum extent of 5 to 38% during storm events. Three of the five storms (24 October 2004, 17 and 26 April 2010) had no saturated area present before the storm.

2.4.2 Observed chemistry signals

Table 2.2 summarizes the solute concentrations and isotopic values for each end-member, the flow components and the integrated total discharge signal used in the chemical hydrograph separations. Precipitation isotopes ranged from -3.1 to -16.9‰ for the five storms but were generally more depleted in heavy isotopes during four out of the five storms than the discharge in the trench. Only during the 17 April 2010 event precipitation was more enriched in heavy isotopes (-3.1 to -6.3‰) than the $\delta^{18}O$ measured in the flow components.

In response to rainfall inputs the $\delta^{18}O$ ratios observed for surface runoff, shallow interflow and total discharge showed a high variability for the five storm events. Total discharge during base flow conditions was more enriched in heavy isotopes (μ = -9.49‰ ± 0.76) than the shallow water (μ = -9.65‰ ± 0.89) from above the fragipan. Total discharge showed a greater variability (μ = -10.13‰ ± 1.47) in observed isotope

ratios during storm events due to varying inputs of shallow, deeper, and rainwater. Surface runoff at base flow conditions showed depleted $\delta^{18}O$ values and the highest variability during storm events (μ = -10.46‰ ± 1.99) due to larger dilution effects in response to rainfall. Shallow interflow from the soil-fragipan interface showed the lowest variability in isotope ratios (μ = -10.08‰ ± 1.28) as shown in Figure 2.5.

Table 2.2: Solute concentrations and isotopic values for the end-members used in the two-component hydrograph separation model. End-members are averaged from multiple measurements taken during base flow conditions prior to storm events. Statistical moments of tracer signals summarized for each flow-component are calculated based on all samples taken during the storm events. μ is the average value, $\mu_{1/2}$ is the median, σ is the standard deviation, *CV* is the coefficient of variation, and *n* is the sample size.

	Tracers								
	Si					**$\delta^{18}O$**			
	n	***μ***	***$\mu_{1/2}$***	***σ***	***CV***	***μ***	***$\mu_{1/2}$***	***σ***	***CV***
End-members		μeq/l	μeq/l	μeq/l		μeq/l	μeq/l	μeq/l	
Precipitation	7	1	0.0	1.5	1.91	-11.3	-12.4	3.9	-0.37
Shallow water	29	153	141	31.3	0.20	-9.7	-10.2	0.9	-0.09
Deeper water	14	367	378	75.6	0.22	-9.5	-9.4	0.8	-0.08
Flow-components									
Surface runoff	51	89	113	58.2	0.65	-10.5	-10.8	2.0	-0.19
Shallow interflow	52	189	172	47.9	0.25	-10.1	-10.4	1.3	-0.12
Shallow water	146	134	133	63.0	0.47	-10.1	-10.4	1.7	-0.16
Total discharge	117	277	290	113.7	0.41	-10.1	-10.4	1.5	-0.14

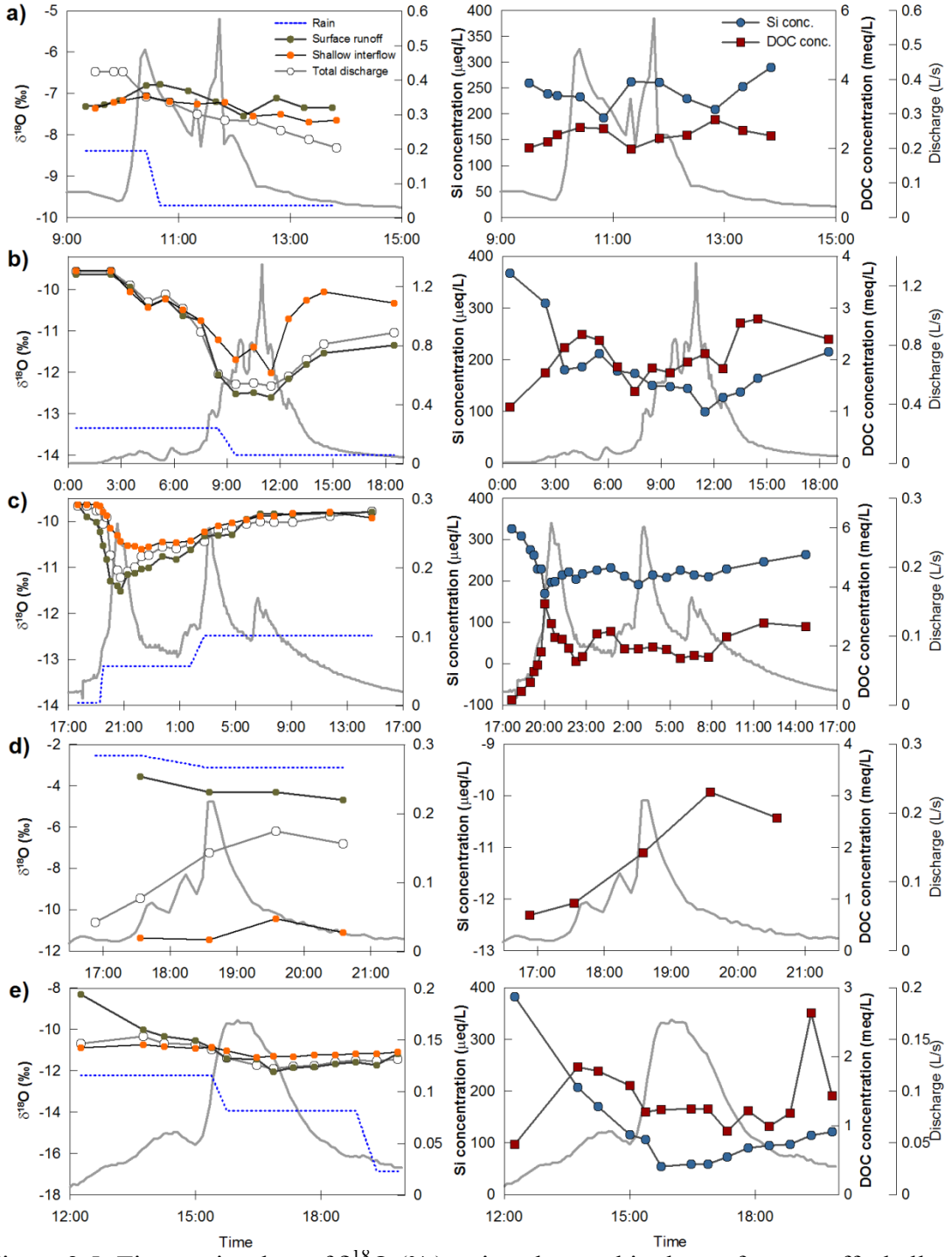

Figure 2.5: Time series data of $\delta^{18}O$ (‰) ratios observed in the surface runoff, shallow interflow and total discharge (left graphs), and Si (µeq/L) and DOC (meq/L) concentrations measured in the total discharge (right graphs) for the events on 24 October 2009 (a), 28 October 2009 (b), 2 December 2009 (c), 17 April 2010 (d), and 26 April 2010 (e). Bulk sample rain $\delta^{18}O$ data are indicated by blue dotted lines. For the five storms a two-component (one tracer) hydrograph separation was performed.

Mean Si concentrations in the precipitation averaged μ = 1 μeq/l (Table 2.2). Mean Si concentrations were significantly ($p \leq 0.0001$) greater in the total discharge during baseflow conditions (μ = 377.8 μeq/l ± 32.1) than in the shallow water from above the fragipan (μ = 152.9 μeq/l ± 31.3). Thus, Si concentrations allowed separation of spatial sources such as shallow water and deeper water. Surface runoff showed more diluted (μ = 89.4 μeq/l ± 58.2) Si concentrations than shallow interflow (μ = 188.9 μeq/l ± 47.9) and was most diluted during peak flows due to greater rainwater inputs. Water samples taken from the piezometer wells showed a large variation in observed Si concentrations and $\delta^{18}O$ ratios depending on the distance of each well to the trench and moisture conditions in the hillslope at the time of sampling.

DOC concentrations in the total discharge, surface runoff and interflow varied from 0.2 - 3.4, 0.9 – 4.6, and 0.5 – 3.4 meq/l, respectively. The DOC concentrations in the surface runoff and shallow interflow were highest early in the events and showed subsequent dilution with increasing rainfall. In contrast, DOC in the total discharge showed consistently lowest concentrations before the storm events and two DOC peaks during the storm events, one on the rising limb and one on the falling limb of the hydrograph (Fig. 2.5). The DOC concentrations in the piezometer wells showed the highest variability and ranged from 0 to 2.4 meq/l (coefficient of variation, CV = 0.54). The DOC and Si data from the piezometer wells were available for the storm events on 24 October, 2 December 2009 and 26 April 2010.

2.4.3 Hydrograph separations

2.4.3.1 Observed flow contributions

During the five storm events 28 to 85% of the total discharges were generated by shallow water (surface runoff and shallow interflow) atop the fragipan (Table 2.3).

Surface runoff contributed 57 to 79% to shallow water and between 22 to 64% to total discharge. Surface runoff contributions increased with effective precipitation (P_e) (rain falling after soils reached saturation) during storm events (the Pearson product-moment correlation coefficient, reported as r value, was $r = 0.87$) and the greater the saturated fractional area ($r = 0.90$) in the hillslope (Table 2.1, Table 2.3).

Table 2.3: Summary of measured and isotopically separated flow components. Observed flow components show percentages of observed surface runoff, shallow interflow and deeper water contributions to total discharge. The two-component hydrograph separation shows temporal sources (event, pre-event) of total discharge. Q denotes the total storm discharge and P_e the effective precipitation (total precipitation minus the rainfall amount needed to initiate runoff).

			Observed flow components			Two-component separation	
	Q	P_e	SR	IF	DW	Event	Pre-event
	mm	mm	%	%	%	%	%
24-Oct	1.04	20.3	38	29	33	15	85
28-Oct	8.87	43.3	62	28	10	55	45
2-Dec	2.07	9.9	37	18	45	23	77
17-Apr	0.68	5.3	22	6	71	25	75
26-Apr	1.05	11.9	43	13	45	30	70

Shallow interflow contributions to shallow water from above the fragipan ranged from 21 to 43% and from 6 to 29% to total discharge. Shallow interflow contributions were on average higher during storm events with wet antecedent conditions and large event rainfall (e.g. 28 % on 28 October 2009) than during storms with dry antecedent conditions and small event rainfall (6 % on 17 April 2010) (Table 2.1, Table 2.3). Shallow interflow (see Fig. 2.6 for time series data) showed a more dampened response to rainfall inputs than surface runoff. Deeper water contributions to total discharge varied between 15 and 71% for the five storm events and were greater during events with small rainfall amounts and dry antecedent moisture conditions

when shallow water contributions to total discharge were small (e.g. 71% on 17 April 2010) (Tables 2.1 and 2.3, Fig. 2.6). However, comparison of flow rates of each runoff component between events showed that deeper water contributed at a constant rate of 0.08 mm/h to total discharge and was independent of antecedent moisture conditions and total storm precipitation. Thus, deeper water contributions to total discharge were of greater importance during storm events with dry antecedent conditions when the total storm discharge was relatively small. In contrast, with wetter antecedent moisture conditions shallow water from atop the fragipan and especially surface runoff were contributing the majority of water total discharge.

2.4.3.2 Event and Pre-event water contributions

The two-component hydrograph separation of total discharge into event and pre-event components resulted in estimated storm averages of 45 to 85% of pre-event water and 15 to 55% of event water during the five storm events (Table 2.3 and 2.4). These storm averages show a dominance of pre-event water in the hillslope subsurface flow during most events except during the high magnitude event on 28 October 2009. However, the estimated fractions of event and pre-event water receive a greater meaning when comparing storm events with dry antecedent conditions (24 October 2009, 17 and 26 April 2010) to events with wet antecedent conditions (28 October and 2 December 2009). Uncertainty for the calculated event and pre-event water fractions varied between 0.3 and 14% for the five storm events.

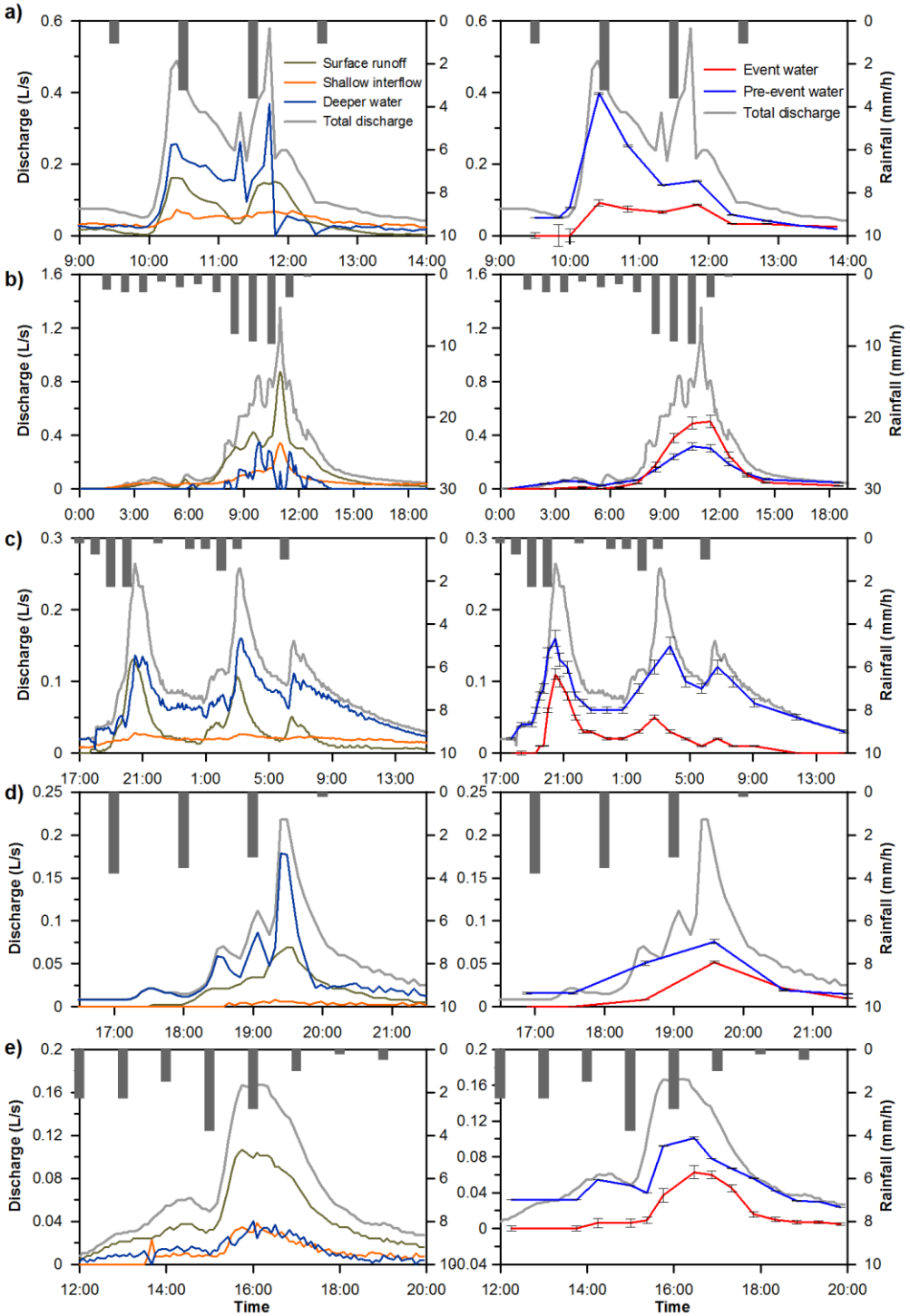

Figure 2.6: Time series of measured surface runoff, shallow interflow, total discharge, and hourly rainfall (left graphs), and the two-component, one-tracer ($\delta^{18}O$) hydrograph separation into event and pre-event water (right graphs) for the events on 24 October 2009(a), 28 October 2009 (b), 2 December 2009 (c), 17 April 2010 (d), and 26 April 2010 (e). Uncertainty bars represent the propagation of a 10% flow error and the double analytical precision of end-member tracers.

Table 2.4: Spatial sources of event and pre-event water in the total hillslope discharge. Separation is based on measured flow components and event and pre-event fractions calculated with the two-tracer hydrograph separation model. Corrected values indicate mass balance corrected fractions for direct rainwater inputs in the trench. Total flow volumes for each storm are listed as depth (mm) and rate (L/m^2 of saturated area).

Antece-dent moisture	Storm event	Q	P_e	Components: Event water SR	Event water IF	Event water DW	Pre-event water SR	Pre-event water IF	Pre-event water DW	Total Discharge: Event	Total Discharge: Pre-event
		mm	mm	%	%	%	%	%	%	%	%
D	24-Oct	1.04	20.3	8	4	3	30	24	31	15	85
W	28-Oct	8.87	43.3	37	10	8	25	17	3	55	45
W	2-Dec	2.07	9.9	13	3	8	23	15	38	24	76
D	17-Apr	0.68	5.3	24	1	0	4	6	65	25	75
D	26-Apr	1.05	11.9	28	2	0	39	16	15	30	70

D = events with dry antecedent conditions
W = events with wet antecedent conditions

During events with wet antecedent conditions shallow water was contributing the majority of event water (55% on 28 October 2009) to total discharge than during events with dry antecedent conditions (25% on 17 April 2010). In contrast, pre-event water contributions from deeper water were on average smaller during events with wet antecedent conditions (45% on 28 October 2009) than during events with dry antecedent conditions (75% on 17 April 2010) (Table 2.4).

Contribution of pre-event shallow water to total discharge was similar for events under dry or wet antecedent conditions and averaged approximately 40% for the five events. However, during events with wet antecedent conditions shallow water contributed proportionally more to total pre-event water (42% on 28 October 2009) than during events with dry antecedent conditions (10% on 17 April 2010). Thus, contribution of pre-event water by deeper water was greatest during events with dry antecedent conditions (65% on 17 April 2010), when total storm precipitation and the maximum saturated area extend in the hillslope were small. In contrast, with increasing moisture

conditions pre-event water contributed by shallow water increased, indicating the growing role of the soil layer atop the fragipan for runoff generation during large events or wet antecedent conditions. For all events the ratio of pre-vent surface runoff to pre-event shallow interflow was 3:2.

Event water fractions in the total discharge were greater, the greater the saturated area extend in the hillslope (A_f) (r=0.87) and the total rainfall (r=0.72). Event water contributed only by shallow water from above the fragipan was correlated to total rainfall (r = 0.78) and average rainfall intensity (r = 0.85), both of which affected the volume of runoff generated during storm events. Event water from surface runoff was mainly controlled by total rainfall onto saturated soils (r=0.77). In contrast, the amount of event water contributed by shallow interflow was generally negligible, but increased with storm duration (r=0.85), effective precipitation (r=0.98), and A_f (r=0.90) (Fig. 2.7). Contributions of pre-event deeper water showed poor correlation to parameters such as rainfall intensity (r=-0.35), storm duration (r=-0.51), the maximum fractional saturated area (r=-0.44), water table depth in the hillslope prior to storm events (r=0.06), but a negative correlation to total rainfall (r= -0.79) for all events.

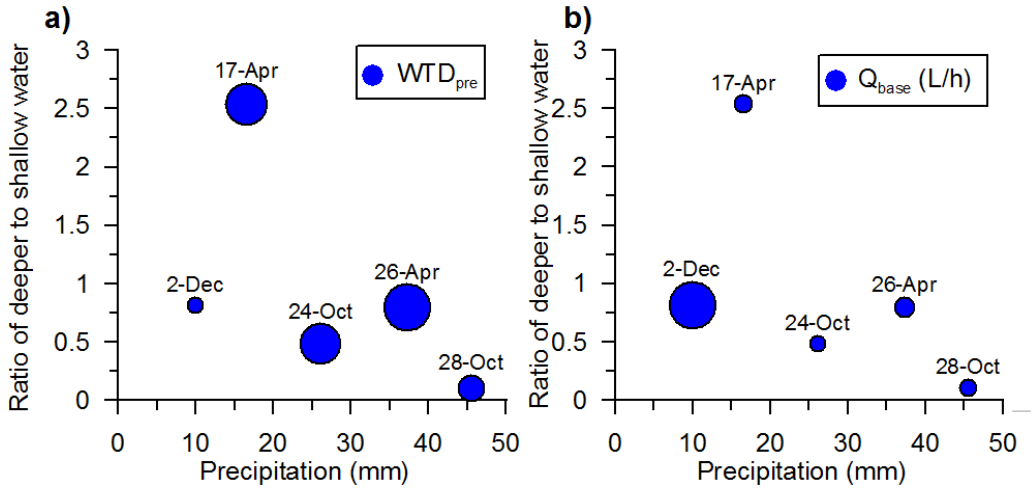

Figure 2.7: (a) Influence of total precipitation and depth to the water table prior to storm events (WTD_{pre}) on the ratio of deeper water to shallow water, and (b) influence of total precipitation and the base flow rate prior to storm events (Q_{base}) on the ratio of deeper water to shallow water for the five storm events. Bigger bubbles indicate higher values.

2.4.4 VSA runoff and flow contributing distance

We calculated the saturated slope length for the five events based on observed volume of shallow water (surface runoff and shallow interflow) from above the fragipan (Table 2.1). First an average drainable porosity of 4.4% was estimated from recession flows using the maximum A_f observed during storm events (Brutsaert and Nieber, 1977). Assuming that the shallow water is perched on top of the impeding fragipan layer, which is located at an average soil depth of 0.5 m in the hillslope, the saturated slope length ranged from 1 m during the smallest event on 17 April 2010 to 42 m during largest event on 28 October 2009. The saturated slope length considering only surface runoff contributing water in the top 15 cm of the soil ranged between 4 m (17 April 2010) and 120 m (28 October 2009). The calculated saturated slope length for both surface runoff and shallow interflow are indicated in Fig. 2.9 for the 24 October and 2 December event.

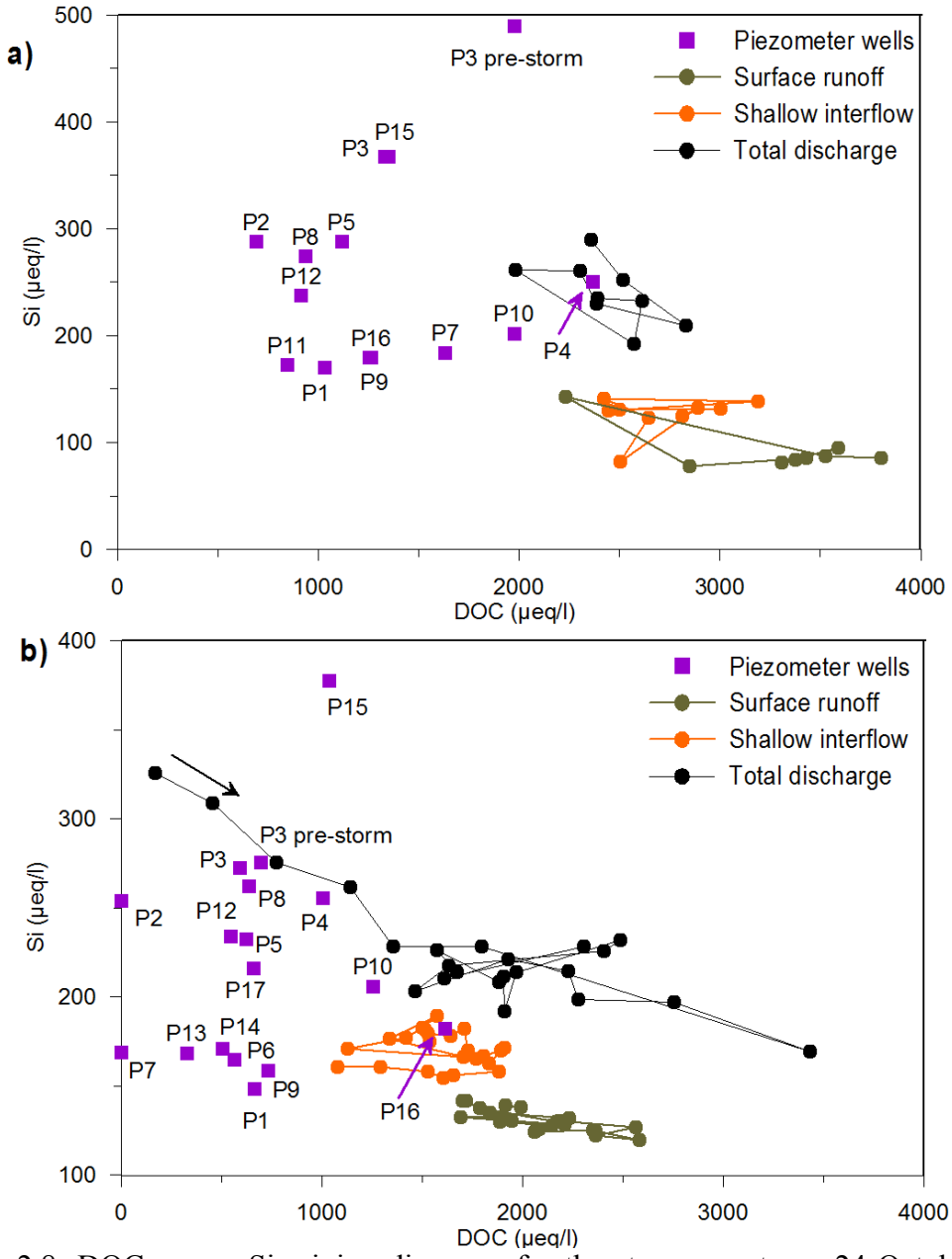

Figure 2.8: DOC versus Si mixing diagrams for the storm events on 24 October (a) and 2 December 2009 (b). Concentrations in the total discharge, surface runoff and shallow interflow are shown as black, green and orange solid circles respectively. Purple squares indicate the chemistry of free water purged from piezometer wells before (if water was present) and after each storm event. See Figure 2 and 9 for the location of piezometers in relation to the trench and saturated area in the hillslope.

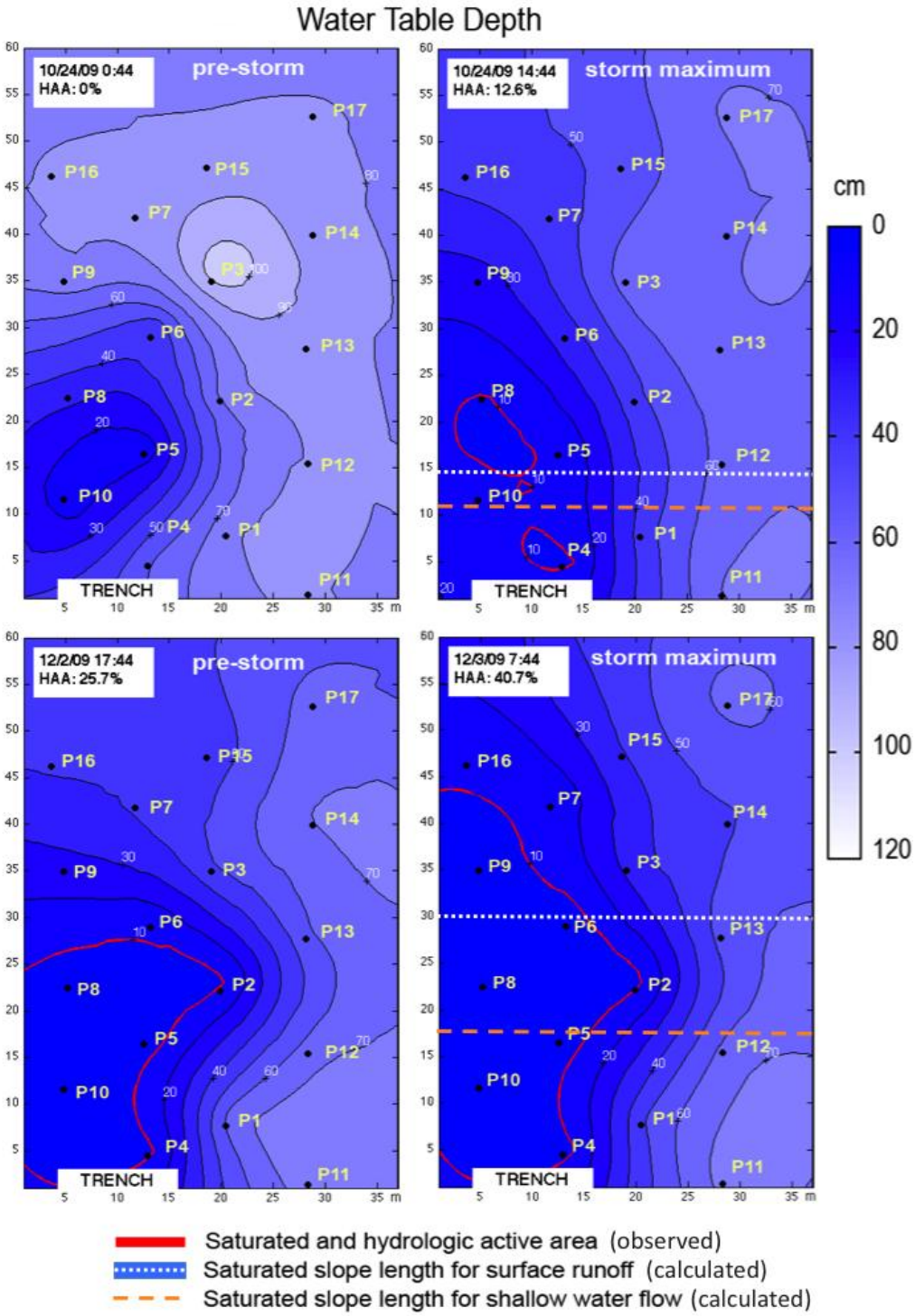

Figure 2.9: Pre-storm and maximum saturated area extend (highlighted with the red solid line) observed during the 24 October (top) and 2 December (bottom) storm event. Saturated and runoff generating areas were derived when the water table was above 10 cm below the soil surface. The white dotted and orange dashed line indicate the flow contributing, saturated slope length for each event, which was calculated based on observed surface runoff and shallow interflow volumes respectively.

To explore surface and subsurface flow paths, source areas and source distances of water coming to the trench in more detail we plotted DOC versus Si concentrations measured in each flow component, the total discharge and the free water in the piezometer wells. The DOC vs. Si mixing diagrams are shown in Fig. 2.8 for two of the five storm events, for which chemistry data from the piezometer wells were available. DOC and Si in total discharge, surface runoff and shallow interflow showed low variability during the 24 October storm but greater variability during the 2 December storm, especially for the total discharge. Shallow interflow and surface runoff showed generally little chemical overlap with the concentrations measured in the total discharge. However, the chemistry measured in some piezometer wells was similar to the one observed in the total discharge. This suggests that water from these well locations contributed to total discharge during the duration of these storm events. For example, the DOC vs. Si mixing diagram from 24 October shows the wells P4 and P10 with concentrations similar to shallow interflow and total discharge. In the mixing diagram of the 2 December event wells P3, P4, P8, and P10 showed DOC and Si concentrations similar to total discharge. When comparing the well locations with maps of the pre-storm, and maximum saturated area extends in the hillslope (Fig. 2.9) observed during these events it is evident that these wells are located within the saturated area and in close proximity to the trench.

2.5 Discussion

2.5.1 VSA evolution in four dimensions

By dissecting the VSA for the hillslope site using at trench, it was possible to map out the main flow pathways of water traversing the VSA. Clearly, VSAs are spatiotemporally complex. These VSAs serve as a nexus for flow pathways (both spatially and temporal) allowing for the rapid movement of water emanating from

different sources in the landscapes with different ages of residence. This has major implications for the hot spot/hot moment interpretation of biogeochemical transport from the landscape to the stream (e.g., McClain et al., 2003). Variable source areas provide hot spots/hot moments for biogeochemical reactions, such as denitrification, or dissolved and particulate phosphorus transport (e.g., Vidon et al., 2010). These processes are enhanced during times when convergence of hydrological flowpaths in VSA is the greatest.

Using dissection to improve upon the partial understanding of hydrological process interaction within VSAs is more than just an academic exercise. For example, in the past two decades much debate has evolved around implementing stream buffers of pre-defined size or vegetative filter strips to avoid chemical (Peterjohn and Correll, 1984; Lowrance et al. 1997; USEPA 2005, Walter et al. 2009) and particulate transport from hillslopes to streams (Broadmeadow and Nisbet 2004; Hawes and Smith 2005). The effectiveness of stream buffers on dissolved pollutant transport is particularly inconclusive (Howarth et al., 2000; Novotny, 2003; Sheppard et al., 2006) indicating that there is poor understanding of the relevant processes associated with chemical or dissolved pollutant transport. Dissection of a VSA helps fill in these knowledge gaps.

During the presented five storm events the VSA reached maximum extends of 5 to 38% of the total hillslope area depending on antecedent moisture conditions and storm magnitude. Considering that the majority of runoff is contributed by shallow water above the fragipan (22 – 62%) the observed VSA extends translated into a flow contributing, saturated slope length of 1.6 to 56 m. DOC and Si concentrations in the total discharge and piezometer wells showed that water free available water in the soil

matrix and macropores was mobilized within this distance and subsequently transported to the trench within the time period of the observed storm events (i.e. 24 October and 2 December DOC vs. Si mixing diagrams) (Fig. 2.9). The contributing saturated slope length is changing from event to event depending on antecedent moisture conditions and total rainfall. This highlights the impracticability of implementing fixed-width stream buffers. In addition, when considering the typical U.S./Canadian average buffer widths of 10-30 m, runoff generation will exceed these distances during high magnitude storm events facilitating dissolved, non-point source transport of pollutants.

The observed flow paths and mixing processes in the trenched VSA showed that both solutes available in the free water and in the soil matrix can be mobilized during storm events, however, the runoff generating area does not necessarily have to be surface saturated to contribute runoff, especially during events with dry antecedent conditions. Initiation of subsurface storm flow was observed as soon as the water table rose locally to a depth of 10 to 15 cm below soil surface causing preferential flow and mobilization of solutes and nutrients stored in macropores and the soil matrix (Lin et al. 2008). Thus, injection, knifing or immediate incorporation of manure will not reduce dissolved phosphorus export from areas that contribute runoff during storm events. Therefore it is recommended to give preference to variable-width buffers over fixed-width buffers, which can be delineated for example using the soil topographic index method (Agnew et al., 2006; Walter et al., 2009).

2.5.2 Effect of antecedent moisture on VSA runoff

During storm events with dry antecedent conditions, a larger fraction of the rainfall is used to fill up soil storage before storm runoff is initiated. This is exemplified by the

difference in total discharge observed for similar rainfall amounts. On 26 April 2010 when the hillslope received 38 mm of rainfall the total discharge for the event reached only 1 mm, which was approximately nine-fold smaller than observed during 28 October 2009, when 46 mm of rain fell. During the event with driest antecedent conditions (17 April 2010) total discharge was dominated by pre-event water contributed by deeper water from below the fragipan (65%). However, with increasingly wetter antecedent conditions shallow water (38 - 54%) was contributing gradually more pre-event water to total discharge. Surface runoff contributed as much as 39% of pre-event water (26 April 2010) and 38% of event-water (28 October 2009) to total discharge, depending on the maximum fractional saturated area reached during the storm event. In contrast, pre-event water contributions from deeper water decreased under wetter conditions.

The observed dynamics in flow components suggest the following flow mechanisms. During driest conditions, infiltrating rainwater percolates slowly through cracks in the fragipan, which have been frequently reported for fragipan soils by Parlange et al. (1989), Day et al. (1989) and Nieber et al. (2006), to sub-fragipan soil layers showing pre-event signatures due to longer flow paths and residence times in the subsoil. The flow rate of water percolating through the fragipan showed little variation (approximate flow rate of 0.08 mm/h) for the different antecedent moisture conditions or storm magnitudes. Thus, during small events (i.e. 17 April 2010) with dry antecedent moisture conditions vertical flow processes such as percolation through the fragipan played a greater role in the generation of subsurface storm flow. However, as soon as the soils and the fragipan layer were wetting up, shallow water (both event and pre-event) flow above the fragipan was increasing suggesting that subsurface saturation caused closure of macropores and cracks in the clay-rich fragipan layer,

preventing deeper percolation. Similar mechanisms were hypothesized by Steenhuis et al. (1990) and modeled by Nieber and Sidle (2010).

2.6 Conclusion

A variable source area was trenched at the base of a 100 m long hillslope in the southern tier of New York State. The site is characterized by shallow soils that show a clay-rich fragipan horizon in moderate depth (50 – 100 cm). Water flux and isotopic and geochemical composition of water draining from the soil surface (top 10 cm of the soil), the soil-fragipan interface (approx. 0.5 m depth) and the entire trench face, defined as total discharge, were monitored in conjunction with water table dynamics upslope of the trench during five storm events (10 - 46 mm). In addition application of tracer-based hydrograph separation models allowed a detailed four-dimensional characterization (XYZ and Time) of subsurface storm flow response within the variable source area. Based on this analysis, measured flow components were separated temporally (i.e. event and pre-event) and spatially into shallow water from above the fragipan (including both surface runoff and flow from the soil-fragipan interface) and deeper water from below the fragipan.

Surface runoff in the form of saturation excess overland flow contributed the majority of event and pre-event water (37 – 62%) during storm events with wet antecedent conditions and large rainfall amounts. During events with dry antecedent conditions deeper water from below the fragipan contributed 33 – 71% to total discharge and likely infiltrated through open cracks in the fragipan. Thus, with increasing subsurface saturation there occurred a switch from a vertical flow system, dominated by percolation of water through the fragipan, to a lateral flow system dominated by shallow lateral subsurface flow on top of the the fragipan layer. Mobilization of pre-

event water, either from below or above the fragipan, was greatest during storms with dry antecedent conditions while during high magnitude events with wet antecedent conditions total discharge was dominated by event water (i.e. rainwater) transported in the high transmissive topsoil (< 15 cm). Observed saturated area extends and similarity of water chemistry in the total discharge and water sampled from upslope piezometer wells indicate that water from a distance of up to 56 m was contributing runoff during storm events. These results have important implication for the protection of streams from dissolved pollutant transport and recommend that preference be given to variable-width buffers over fixed-width stream buffers.

REFERENCES

Agnew, L.J., Lyon, S., Gérard-Marchant, P., Collins, V.B., Lembo, A.J., Steenhuis, T.S., and M.T. Walter. 2006. Identifying hydrologically sensitive areas: Bridging science and application. Journal of Environmental Management 78: 64-76.

Ambroise, B., Beven, K., and J. Freer. 1996. Toward a generalization of the TOPMODEL concepts: topographic indices of hydrological similarity. Water Resour. Res. 32 (7): 2135–2145.

Beven, K.J., and M.J. Kirkby. 1979. A physically-based, variable contributing area model of basin hydrology. Hydrol. Sci. Bull. 24: 43-69.

Bonell, M. 1993. Progress in the understanding of runoff generation dynamics in forests. J. Hydrol. 150: 217–275.

Bonell, M. 1998. Selected challenges in runoff generation research in forests from the hillslope to headwater drainage basin scale, J. Am. Water Resour. Assoc., 34: 765–786.

Broadmeadow, S., and T.R. Nisbet. 2004. The effects of riparian forest management on the freshwater environment: a literature review of best management practices. Hydrology and Earth System Sciences 8(3): 286-305.

Brutsaert, W., and J.L. Nieber. 1977. Regionalized Drought Flow Hydrographs From a Mature Glaciated Plateau. Water Resources Research, 13(3): 637-643.

Buda, A.R., Kleinman, P.J.A., Srinivasan, M.S., Bryant, R.B., and G.W. Feyereisen. 2009. Factors influencing surface runoff generation from two agricultural hillslopes in central Pennsylvania. Hydrological Processes 23: 1295-1312.

Burns, D.A. 2002. Stormflow hydrograph separation based on isotopes: the thrill is gone – what's next? Hydrological Processes, 16: 1515–1517.

Burns, D.A., Plummer, L.N., McDonnell, J.J., Busenberg, E., Casile, G.C., Kendall, C., Hooper, R.P., Freer, J.E., Peters, N.E., Beven, K., and P. Schlosser. 2003. The geochemical evolution of riparian groundwater in a forested Piedmont catchment. Groundwater 41(7): 913–925.

Buttle, J.M., and D.J. McDonald. 2002. Coupled vertical and lateral preferential flow on a forested slope. Water Resources Research 38(5): 1060–1076.

Christophersen, N., and R.P. Hooper. 1992. Multivariate analysis of stream water chemical data: The use of Principal Components Analysis for the End-Member Mixing Problem. Water Resources Research, 28(1): 99-107.

Dahlke, H.E., Easton, Z.M., Fuka, D.R., Lyon, S.W., and T.S. Steenhuis. 2009. Modeling Variable Source Area Dynamics in a CEAP Watershed. Ecohydrology 2: 337-349.

Day, R.L., Calmon, M.A., Stiteler, J.M., Jabro, J.D., and R.L. Cunningham. 1998. Water balance and flow patterns in a fragipan using in situ soil soil block. Soil Science 163(7): 517-528.

de Alwis, D.A., Easton, Z.M., Dahlke, H.E., Philpot, W.D., and T.S. Steenhuis. 2007. Unsupervised classification of saturated areas using a time series of remotely sensed images. Hydrol. Earth Syst. Sci. 11: 1609–1620.

Dunne, T., Black, R.D.. 1970. Partial area contributions to storm runoff in a small New England watershed. Water Resources Research 6: 1296–1311.

Dunne, T., Moore, T.R., and C.H. Taylor. 1975. Recognition and prediction of runoff-producing zones in humid regions. Hydrol Sci Bull, 20(3): 305–327.

Easton, Z.M., Gerard-Marchant, P., Walter, M.T., Petrovic, A.M., and T.S. Steenhuis. 2007. Hydrologic assessment of an urban variable source watershed in the Northeast US. Water Resources Research 43, W03413, :10.1029/2006WR005076, 2007.

Easton, Z.M., Fuka, D.R., Walter, M.T., Cowan, D.M., Schneiderman, E.M., and T.S. Steenhuis. 2008. Re-conceptualizing the Soil and Water Assessment Tool (SWAT) model to predict runoff from variable source areas. Journal of Hydrology 348: 279–291.

Freer, J., McDonnell, J., Beven, K.J., Peters, N.E., Burns, D.A., Hooper, R.P., Aulenbach, B., and C. Kendall. 2002. The role of bedrock topography on subsurface storm flow. Water Resour. Res. 38:1269 :10.1029/2001WR000872.

Genereux, D.P. 1998. Quantifying uncertainty in tracer-based hydrograph separations. Water Resour. Res. 34:915–919.

Gburek, W.D., and A.N. Sharpley. 1998. Hydrologic controls on phosphorus loss from upland agricultural watersheds. Journal of Environmental Quality 27: 267–277.

Gburek, W.J., Drungil, C.C., Srinivasan, M.S., Needelman, B.A., and D.E. Woodward. 2002. Variable-source area controls on phosphorus transport: Bridging the gap between research and design. Journal of Soil and Water Conservation 57(6): 534–543.

Gérard-Marchant, P., Hively, W.D., and T.S. Steenhuis. 2006. Distributed hydrological modelling of total dissolved phosphorus transport in an agricultural landscape, part I: distributed runoff generation. Hydrology and Earth System Sciences 10: 245–261.

Goovaerts, P. 1999. Geostatistics in soil science: state-of-the-art and perspectives. Geoderma 89: 1-45.

Harpold, A.A., Lyon, S.W., Troch, P.A., and T.S. Steenhuis. 2010. The Hydrological Effects of Lateral Preferential Flow Paths in a Glaciated Watershed in the Northeastern USA. Vadose Zone Journal, 9: 397–414.

Hawes, E., and M. Smith. 2005. Riparian buffer zones: Functions and recommended widths. Rep. to the Eightmile River Wild and Scenic Study Committee,

http://www.eightmileriver.org/resources/digital_library/appendicies/09c3_Riparian%20Buffer%20Science_YALE.pdf Feb. 28, 2008.

Hewlett, J.D., and A.R. Hibbert. 1967. Factors affecting the response of small watersheds to precipitation in humid regions. In: Forest Hydrology (Sopper WE, Lull HW, eds.). Pergamon Press, Oxford.

Hewlett, J.D., and W.L. Nutter. 1970. The varying source area of streamflow from upland basins, Proceedings of the Symposium on Interdisciplinary Aspects of Watershed Management. Bozeman, MT. ASCE, New York, pp. 65–83.

Horton, R.E. 1933. The role of infiltration in the hydrologic cycle. Transactions American Geophysical Union 14: 446–460.

Horton, R.E. 1940. An approach toward a physical interpretation of infiltration capacity. Soil Science Society of America Proceedings 4: 399–417.

Howarth R, Anderson D, Cloern J, Elfring C, Hopkinson C, Lapointe B, Malone T, Marcus N, McGlathery K, Sharpley A, Walker D 2000. Nutrient pollution of coastal rivers, bays, and seas. Issues in Ecol., 7: 1–15.

Kendall, C., and J.J. McDonnell (Eds.). 1998. Isotope Tracers in Catchment Hydrology. Elsevier Science B.V., Amsterdam, 839 p.

Lowrance, R., Altier, L.S., Newbold, J.D., Schnabel, R.R., Groffman, P.M., Denver, J.M., Correll, D.L., Gilliam, J.W., Robinson, J.L., and R.B. Brinsfield. 1997. Water quality functions of riparian forest buffers in Chesapeake Bay Watersheds. Environ. Manage. (N.Y.), 21(5): 687–712.

Lin, H., Brooks, E., McDaniel, P., and J. Boll. 2008. Hydropedology and surface/subsurface runoff processes. Encyclopedia of Hydrological Sciences, Anderson MG (ed.) John Wiley & Sons, Ltd.: 25 pp.

Lyon, S.W., Gérard-Marchant, P., Walter, M.T., and T.S. Steenhuis. 2004. Using a topographic index to distribute variable source area runoff predicted with the SCS-Curve Number equation. Hydrological Processes 18(15): 2757–2771.

Lyon, S.W., Lembo, A.J., Walter, M.T., and T.S. Steenhuis. 2006a. Defining probability of saturation with indicator kriging on hard and soft data. Advances in Water Resources 29: 181–193.

Lyon, S.W., Seibert, J., Lembo, A.J., Walter, M.T., and T.S. Steenhuis. 2006b. Geostatistical investigation into the temporal evolution of spatial structure in a shallow water table. Hydrology and Earth System Sciences 10: 113–125.

McDonnell, J.J. 1990. A rationale for old water discharge through macropores in a steep, humid catchment. Water Resources Research 26(11): 2821–2832.

McGlynn, B.L., McDonnell, J.J., Seibert, J., and C. Kendall. 2004. Scale effects on headwater catchment runoff timing, flow sources, and groundwater-streamflow relations, Water Resour. Res., 40, W07504,DOI:10.1029/2003WR002494.

Miller, T.S. 1993. Glacial geology and the origin and distribution of aquifers at the Valley Heads moraine in the Virgil Creek and Dryden Lake-Harford valleys, Tompkins and Cortland counties, New York. U.S. Geological Service Water-resources investigations report, 90-4168.

Nieber, J.L., and R.C. Sidle. 2010. How do disconnected macropores in sloping soils facilitate preferential flow? Hydrological Processes, 24: 1582-1594.

Nieber, J.L., Steenhuis, T.S., Walter, T., and M. Bakker. 2006. Enhancement of seepage and lateral preferential flow by biopores on hillslopes. Biologia, 61/Suppl. 19: S225-S228.

Novotny, V. 2003. Water Quality: Diffuse Pollution and Watershed Management, 2nd ed. John Wiley and Sons, Inc., New York, NY.

Ogden, C.B., van Es, H.M., and R.R. Schindelbeck. 1997. Miniature rain simulator for measurement of infiltration and runoff. Soil Sci. Soc. Am. J. 61: 1041-1043.

Ogunkoya, O.O., and A. Jenkins. 1993. Analysis of storm hydrograph and flow pathways using a three component mixing hydrograph separation model. J. Hydrol. 142: 71–88.

Parlange, M.B., Steenhuis, T.S., Timlin, D.J., Stagnitti, F., and R.B. Bryant. 1989. Subsurface Flow Above a Fragipan Horizon. Soil Sciences 148: 77-86.

Peterjohn, W.T., and D.L. Correll. 1984. Nutrient dynamics in an agricultural watershed: Observation on the role of a riparian forest. Ecology, 65(5): 1466–1475.

Ripley, B.D. 1981. Spatial Statistics Wiley, New York.

Sharpley, A.N., Chapra, S.C., Wedepohl, R., Sims, J.T., Daniel, T.C., and K.R. Reddy. 1994. Managing agricultural phosphorus for protection of surface waters: issues and options. Journal of Environmental Quality 23: 437–451.

Sharpley, A.N., Kleinman, P.J.A., McDowell, R.W., Gitau, M., and R.B. Bryant. 2002. Modeling Phosphorus transport in agricultural watersheds: Processes and possibilities. Journal of Soil and Water Conservation, 57(6): 425-439.

Sheppard, S.C., Sheppard, M.I., Long, J., Sanipelli, B., and J. Tait. 2006. Runoff phosphorus retention in vegetated field margins on flat landscapes. Can. J. Soil Sci., 85(5): 871–884.

Sklash, M.G., R.N. Farvolden. 1979. The role of groundwater in storm runoff. J. Hydrol. 43: 4565.

Steenhuis, T.S., Richard, T.L., Parlange, M.B., Aburime, S.O., Geohring, L.D., and J.Y. Parlange. 1988. Preferential flow influences on drainage of shallow sloping soils. Agricultural Water Management, 14: 137-151.

Steenhuis, T.S., Parlange, J.Y., and M. Andreini. 1990. A Numerical Model for Preferential Solute Movement in Structured Soils. Geoderma 46:193-208.

Troch, P.A., Martinez, G.F., Pauwels, V.R.N., Durcik, M., Sivapalan, M., Harman, C., Brooks, P.D., Gupta, H., and T. Huxman. 2009. Climate and vegetation water use efficiency at catchment scales. Hydrological Processes, 23: 2409-2414.

Tromp-van Meerveld, H.J., and J.J. McDonnell. 2006a. Threshold relations in subsurface stormflow: A 147-storm analysis of the Panola hillslope. Water Resources Research, 42: W02410.

Tromp-van Meerveld, H.J., and J.J. McDonnell. 2006b. Threshold relations in subsurface stormflow: 2. The fill and spill hypothesis. Water Resources Research 42: W02411, Doi:10·1029/2004WR003800.

Tromp-van Meerveld, H.J., and J.J. McDonnell. 2006c. On the interrelations between topography, soil depth, soil moisture, transpiration rates and species distribution at the hillslope scale. Advances in Water Resources, 29: 293-310.

Tromp-van Meerveld, H.J., Peters, N.E., and J.J. McDonnell. 2007. Effect of bedrock permeability on subsurface stormflow and the water balance of a trenched hillslope at the Panola Mountain Research Watershed, Georgia, USA. Hydrological Processes, 21: 750–769.

USEPA. 2005. Riparian buffer width, vegetative cover, and nitrogen removal effectiveness: A review of current science and regulations. EPA/600/R-05/118, Office of Research and Development, Washington, D.C.

Wagner, T., Sivapalan, M., Troch, P., and R. Woods. 2007. Catchment classification and hydrologic similarity. Geography Compass 1(4): 901-931.

Walter, M.T., Archibald, J.A., Buchanan, B., Dahlke, H., Easton, Z.M., Marjerison, R.D., Sharma, A.N., and S.B. Shaw. 2009. A new paradigm for sizing riparian buffers to reduce risks of polluted storm water: A practical synthesis. ASCE Journal of Irrigation and Drainage Engineering 135(2): 200-209.

Walter, M.T., Mehta, V.K., Marrone, A.M., Boll, J., Steenhuis, T.S., Walter, M.F., and C.A. Scott. 2002. A simple estimation of the prevalence of Hortonian flow in the New York City watersheds. J. Hydrol. Eng. 10: 169–170.

Weiler, M., and J.J. McDonnell. 2007. Conceptualizing lateral preferential flow and flow networks and simulating the effects on gauged and ungauged hillslopes, Water Resour. Res., 43, W03403, doi:10.1029/2006WR004867.

Woods, R., and L. Rowe. 1996. The changing spatial variability of subsurface flow across a hillside, J. Hydrol. N. Z., 35, 51– 86.

CHAPTER 3

A FIELD TEST OF THE VARIABLE SOURCE AREA INTERPRETATION OF THE CURVE NUMBER RAINFALL-RUNOFF EQUATION

Abstract

The Soil Conservation Service Curve Number (SCS-CN) method is a widely used empirical rainfall-runoff equation. Although the physical basis of the method has been debated, several researchers have suggested that it can be used to predict the watershed fraction that is saturated and generating runoff by saturation-excess from variable source areas (VSAs). In this paper we compared saturated runoff contributing areas predicted with the VSA interpretation of the SCS-CN method with field-measured VSAs in a 0.5 ha hillslope in central New York State. We installed a trench below a VSA and simultaneously recorded water flux from different soil layers at the trench face and water table dynamics upslope of the trench. This setup allowed us to monitor runoff initiation and saturation-excess overland flow in response to rainfall and different water table depths in the hillslope during 16 storm events. We found that the SCS-CN method accurately predicted the observed VSA and showed best agreement if the VSA was defined as the area where the water table was within 10 cm of the soil surface. These results not only demonstrate that the VSA interpretation of the SCS-CN method accurately predicts VSA extents in small watersheds but also that the transient water table does not necessarily need to intersect the land surface to cause a storm runoff response.

3.1 Introduction

The Soil Conservation Service Curve Number (SCS-CN) (U.S. Soil Conservation Service (SCS), 1972) method is an empirical rainfall-runoff relationship that is widely used to predict storm runoff in ungauged basins. While more sophisticated methods are available, its simplicity and dependence on readily available catchment properties has contributed to its continued popularity, particularly among practicing water resource engineers (Ponce and Hawkins, 1996: Garen and Moore, 2005). The rainfall-runoff principle of the SCS-CN method is such that no runoff occurs until a threshold in rainfall is met, above which the fraction of rainfall contributing to runoff increases with rainfall. The SCS-CN method in its original form (Victor Mockus, in Rallison, 1980) is independent of the underlying runoff generation mechanism, i.e. infiltration-excess, saturation-excess or something else.

Runoff generation based on the infiltration-excess, or the "Hortonian flow", concept occurs when rainfall intensity exceeds the rate at which water can infiltrate the soil (e.g., Horton, 1933, 1940). In contrast, saturation-excess occurs when rain (or snowmelt) encounters soils that are nearly or fully saturated, often due to a water table perched above a zone of low permeability, thus precluding infiltration (e.g., Dunne and Black, 1970; Hewlett and Nutter, 1970). The location of areas generating runoff by saturation-excess, typically called variable source areas (VSAs), depends on the topographic position in the landscape and the local soil transmissivity. As the adjective "variable" suggests, VSAs develop and expand spatially with rainfall and contract between storms (Dunne and Black, 1970; Hewlett and Nutter, 1970). One important aspect of the variable source area concept, also known as the partial area concept, is that the majority of the runoff is generated from small portions of the landscape (e.g., Dunne and Black, 1970) and, therefore, VSAs are important areas to target for

controlling non-point source pollutant transport (e.g., Walter et al., 2000; Gburek et al., 2002; Walter et al., 2007; Dahlke et al., 2010).

In agreement with this partial-area hydrology concept, Steenhuis et al. (1995) demonstrated that the SCS-CN relationship, in its most elementary form, can be derived from the assumption that only the saturated areas contribute to direct runoff. Although this VSA interpretation of the SCS-CN method has been incorporated into several continuous watershed models, which have been successfully applied to a variety of catchments (Schneiderman et al. 2007; Easton et al., 2008b, Dahlke et al., 2009), the fundamental concept still remains to be tested against field-measured VSAs to corroborate its physical accuracy.

3.2 Review of the SCS-CN method applied to VSA theory

The SCS (now Natural Resources Conservation Service, NRCS) runoff Curve-Number (CN) method (short SCS-CN) (USDA-SCS, 1972) is widely used in hydrologic engineering and is commonly used in water quality models to estimate the storm runoff response of a catchment (Eq. 3.1) (Garren and Moore, 2005):

$$Q = \frac{(P - I_a)^2}{P + S - I_a} \tag{3.1}$$

where Q (mm) is the total watershed runoff depth for a storm, P (mm) is the depth of rainfall, S (mm) is the potential maximum storage for water available in a watershed, and I_a (mm) is the initial abstraction or the amount of water required to initiate runoff. Traditionally, I_a is generally taken as $0.2S$ (USDA-SCS, 1972).

In its original form, the SCS-CN equation constitutes an empirical rainfall-runoff relationship that, according to its originator, Victor Mockus (Rallison, 1980), is independent of the underlying runoff generation mechanism (i.e. infiltration excess or saturation excess). Although many current water quality models use the SCS-CN equation in a way that implicitly assumes infiltration-excess is the dominant runoff mechanism (Walter and Shaw, 2005), Steenhuis et al. (1995) showed that Eq. 1 can be applied to predict saturation-excess runoff that results from rainfall onto saturated soils. The underlying principle of this VSA interpretation of the SCS-CN equation is that the area or fraction of the watershed that contributes runoff (A_f) can be estimated from the ratio of runoff depth (ΔQ) to precipitation depth (ΔP):

$$A_f = \Delta Q / \Delta P \tag{3.2}$$

Here, ΔQ (mm) is the incremental runoff depth or volume of excess rainfall generated during the storm event divided by the watershed area and ΔP (mm) is the incremental depth of runoff producing rainfall that occurred during the same time period. Introducing the effective precipitation, P_e (mm), which is equal to the total storm precipitation (P) after the initial abstraction (I_a) is subtracted, Eq. 3.1 can be rewritten as:

$$Q = \frac{P_e^2}{(P_e + S)} \tag{3.3}$$

The fractional area that is contributing saturation-excess runoff (A_f), according to Eq. 3.2, is equal to the derivative of Q with respect to P_e. Thus, by differentiating Eq. 3.3 with respect to P_e the saturated or runoff-generating fraction of the watershed generating runoff is:

$$A_f = 1 - \frac{S^2}{(P_e + S)^2} \tag{4}$$

In agreement with the mathematical limits of this equation, P_e = 0 when the contributing watershed area A_f equals zero and P_e goes to infinity as A_f approaches 1.

The amount of saturation-excess runoff generated during storm events is, to a great extent, controlled by the available soil water storage (S) in the watershed and depends largely on the moisture status of the watershed prior to storm events. The value of S can vary between some maximum, S_{max} (mm), when the watershed is dry (e.g. during the summer) and a minimum, S_{min} (mm), when the watershed is wet (e.g. late winter and spring) (Saxton et al., 1974; Saxton, 1984; Schneiderman et al., 2007). However, despite these seasonal and daily variations of S, engineers often assume that S is a storm invariant parameter that represents the potential maximum storage or the total amount of water that can be stored in the watershed (e.g., Steenhuis et al., 1995). Operationally, S is determined either using table-derived CN values for average soil and land use conditions (USDASCS, 1972; Chow et al., 1988) or it can be fitted to direct measurements of effective precipitation and runoff volume (e.g., Shaw and Walter, 2009).

3.3 Materials and Methods

A total of 16 storm events, monitored for a trenched, 0.5 ha hillslope from October 2009 through May 2010 (excluding the winter period) (Table 3.1) were used to test the CN-VSA approach of Steenhuis et al. (1995). The saturation-excess runoff generated in this hillslope site in response to these events was considered in detail using a network of direct measurements and analytical techniques.

3.3.1 Site description

This study was conducted on a 0.5 ha, N-NE facing hillslope in a crest position near Ithaca, New York, USA (76°14'48.44" W, 42°24'56.86" N). The hillslope is short (< 125 m), moderately steep (average 7°) and located in an elevation ranging from 482 to 499 m (Fig. 3.1). Annual precipitation averages 930 mm with an annual mean temperature of 7.8 °C (Climate station Cornell Game Farm). The vegetation in the study site is mixed grassland that is cut biannually (July, September) for hay production. Hardwood deciduous forest with American beech, oaks, and sugar maples bound the study site towards the western, steeper shoulder.

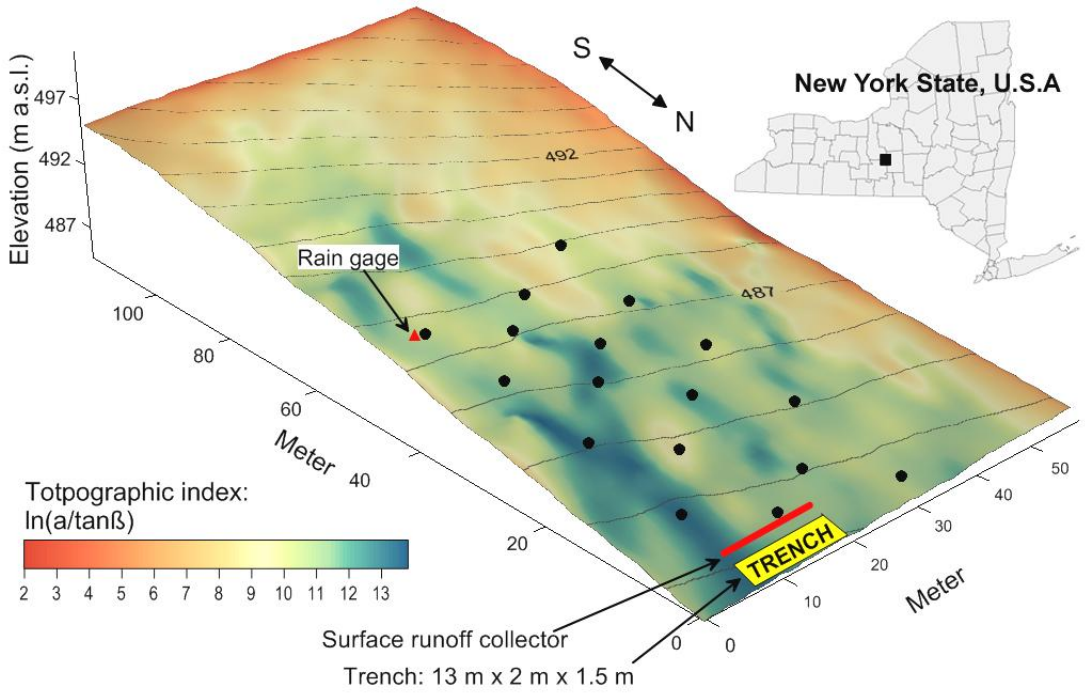

Figure 3.1: Location of study hillslope in central New York State, U.S.A. Black dots indicate locations of water level loggers.

The subsurface material consists of glacial till on middle Devonian shales and siltstones (Miller, 1993). The regional depth to the bedrock is locally variable and ranges between 1.5 m on the hilltops and several meters (> 25 m) in the main valley

around Harford (Miller, 1993). The dominant soil type at the site is a Mardin channery silt loam, which is classified as coarse-loamy, mixed, active, mesic typic Fragiudepts (parent material is glacial till) (Soil Survey Geographic Database, NRCS-USDA).

3.3.2 Hydrometric measurements and trench instrumentation

A 13 m long by 2 m wide trench was excavated in a persistent VSA located at the bottom of this ~100 m long hillslope (Fig. 3.1). The trench location was based on observed of topographic convergence and associated VSA formation. The trench face was constructed orthogonal to flowlines as derived from surface topography. The length of the trench was selected to span across the maximum extent of the VSA. The trench was dug to a depth of approximately 1.5 m to intersect the top of the fragipan horizon. Both the water flux draining through the trench as well as water level measurements within the soils in the drainage area of the trench face were monitored.

Three flow components were monitored using the trench: surface runoff, shallow interflow, and total discharge (Fig. 3.2). A surface runoff collector was installed 3 m upslope of the trench wall to collect flow from the upper 10 cm of the soil. This water is defined as "surface runoff". Two meters upslope of the trench face, a perforated drain tile with a 10 cm diameter was installed at the soil-fragipan interface in a ditch approximately 45 cm deep. When refilling the ditch, clay was used to seal the downslope face to intercept and collect shallow subsurface flow above the fragipan. This water is defined as "shallow interflow". Surface runoff and shallow interflow water were routed with pipes to the center of the trench for monitoring and collection. The amounts of both surface runoff and shallow interflow were measured with tipping buckets, each connected to a HOBO pendant event data logger (Onset Computer Corporation, Pocasset, MA, USA). The tipping buckets were leveled and fixed to a

solid wood structure to minimize changes in calibration with increasing tipping frequency. Surface runoff rate was measured with a tipping bucket that captured 4 L per tip while shallow interflow was measured with a bucket capacity of 430 mL per tip.

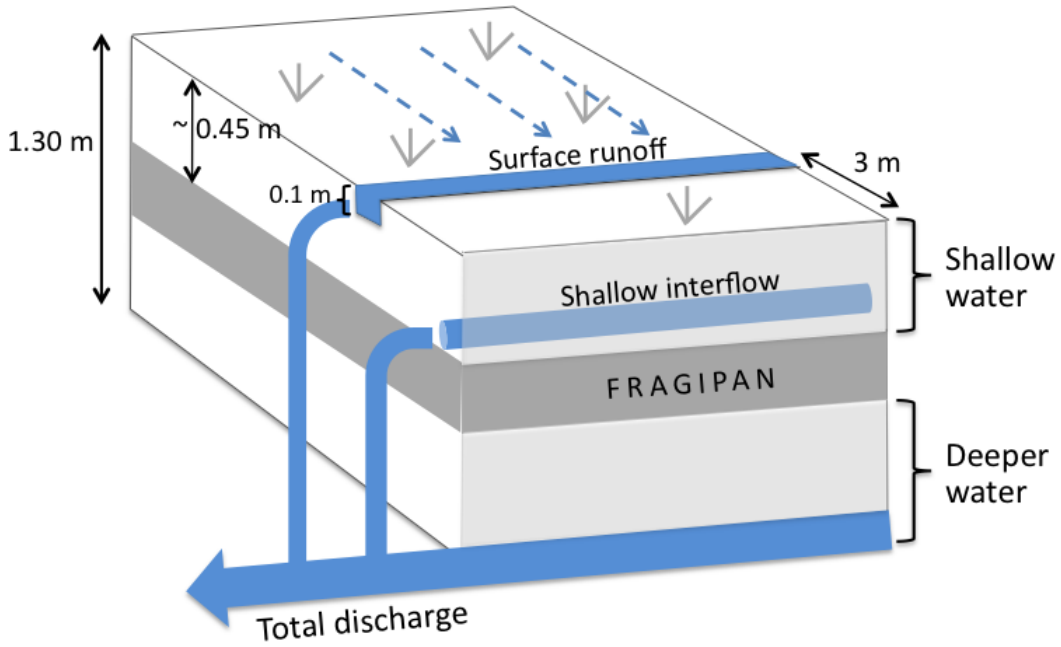

Figure 3.2: Schematic layout of the trench instrumentation and collectors of different flow components (surface runoff, shallow interflow) and total discharge.

A third perforated drain tile with a diameter of 10 cm was installed at the bottom of the trench (Fig. 2). This drain tile collected surface runoff, shallow interflow as well as deeper subsurface flow from underneath the fragipan. As this integrates across the entire soil profile, this water is defined as "total discharge" for the remainder of this paper. This total discharge was gauged at a 5-min interval using a compound weir equipped with a Telog Inc. (Victor, NY, USA) pressure transducer (1 psi). As the trench was left uncovered, total discharge was corrected for rainfall inputs into the trench by simply subtracting rainfall amounts times uncovered trench area (~26 m^2).

3.3.3 Hillslope instrumentation

A network of 17 water level loggers was installed in the lower half of the contributing area of the trench (Fig. 3.1). Water levels were measured at 5-min intervals using 500 mm and 1000 mm long capacitance probes (TruTrack Inc., New Zealand). The loggers were installed in four transects with a distance of 8 m across the slope and 14 m upslope between the loggers. This logger network covered 60 % of the total hillslope area. All capacitance probes were completely embedded in the soil inside 5 cm-PVC tubes, resulting in installation depths of 0.83 m for the WT-HR500 probes (wells P1 – P17, except well P3) and 1.30 m for one WT-HR1000 probe (well P3) respectively. The PVC tubing was screened over the lower 25 cm.

A tipping bucket rain gauge (Spectrum Technologies Inc., Plainfield, IL, USA) was installed on site that recorded rainfall amounts over 5-min intervals. Meteorological data (temperature, precipitation, wind, solar radiation) were concurrently available from a climate reference network station in Harford, NY, approximately 2.3 km north of the site.

3.3.4 Estimation of SCS-CN relevant parameters from field measured data

In this study the trench instrumentation allowed direct estimation of saturation excess overland flow through installation of collectors that recorded water flux from different soil horizons. We assume that the surface runoff, collected from the upper 10 cm of the soil, represents the amount of saturation-excess overland flow (Q_{obs}) generated during storm events. Observed flow volumes (L/hr) were converted to depth values (mm/hr) using an estimated contributing area of 2575 m^2, which was derived from the surface topography of the hillslope. To satisfy consideration of the initial abstraction I_a (the minimum amount of rainfall necessary to exceed field capacity) in the

determination of the effective precipitation (P_e) we obtained I_a as the sum of the precipitation before surface runoff commenced. The site-specific storage parameter, S, was back calculated from Eq. 3.3 for each storm event and then used in Eq. 3.4 to predict A_f based on observed Q and P_e.

The average fractional saturated area observed in the hillslope ($A_{f\text{-}obs}$) during storm events was determined using hourly averages of observed water table depths. During storm events, $A_{f\text{-}obs}$ can vary between zero (minimum extent) and some maximum extent, which is equal to the total hillslope contributing area. To reflect both, the influence of antecedent moisture conditions and total storm precipitation on VSA expansion we determined $A_{f\text{-}obs}$ as the average saturated area extend present in the hillslope for the duration of surface runoff generation. To obtain $A_{f\text{-}obs}$ we first interpolated observed water table depths using ordinary kriging (Ripley, 1981; Goovaerts, 1999) and then estimated $A_{f\text{-}obs}$ as the ratio of the area with water tables above a specified threshold to the total contributing area (2575 m^2). Lyon et al. (2006a, 2006b) found that the generation of saturation excess overland flow rapidly increased when the median water table was within the top 10 cm of the soil. However, in this paper we look at a range of possible thresholds (5, 10, 15 to 20 cm) and how the observed changes in A_f associated with each water table threshold compare to A_f predicted with Eq. 3.4.

3.4 Results

3.4.1 Rainfall-runoff response and saturation dynamics

The 16 storm events observed with the trenched hillslope showed rainfall depths and peak 1-hour rainfall intensities ranging from 2.5 mm to 46 mm and 0.7 to 9.8 mm/hr, respectively (Table 3.1). Ten of the 16 storm events had less than 10 mm of total

rainfall. Rainfall events lasted from 2 to 27 hours and generally had low intensities, common to rainfall in the northeastern US (Buda et al., 2009). At no time during the study was the infiltration capacity of the soil exceeded by the rainfall intensity. This was supported by estimates of the infiltration rate of the soil surface layer with a sprinkle infiltrometer (Ogden et al., 1997), which ranged from 148 to 334 mm/hr across the hillslope, and are far greater than any of the rainfall intensities.

Base flow, estimated as the minimum total discharge observed within the 24-hours prior to a storm event, ranged from 0.1 to 81 L/hr and reflected similarly the wide range of antecedent moisture conditions prior to storm events (Troch et al., 1993). Surface runoff or saturation-excess overland flow generated during the 16 storm events ranged from 0.005 (12 October 2009) to 6.7mm (28 October 2009).

Moisture conditions in the hillslope, as indicated by the hillslope average depth to the water table (average of 17 water level loggers) ranged from dry antecedent to saturated conditions during the study period (Fig. 3.3). The driest antecedent conditions, with an average water table depth of 780 mm, occurred prior to the storm event on 19 November 2009 after 14 days without rainfall. The lowest average water table depth monitored during the entire study period was reached during the largest storm event; on 28 October 2009 the site received 46 mm of rainfall within 12 hours, causing the average water table to rise from a depth of 473 mm prior to the storm to 74 mm two hours after peak flow with several areas of the hillslope completely saturating (e.g., water table at or near the soil surface).

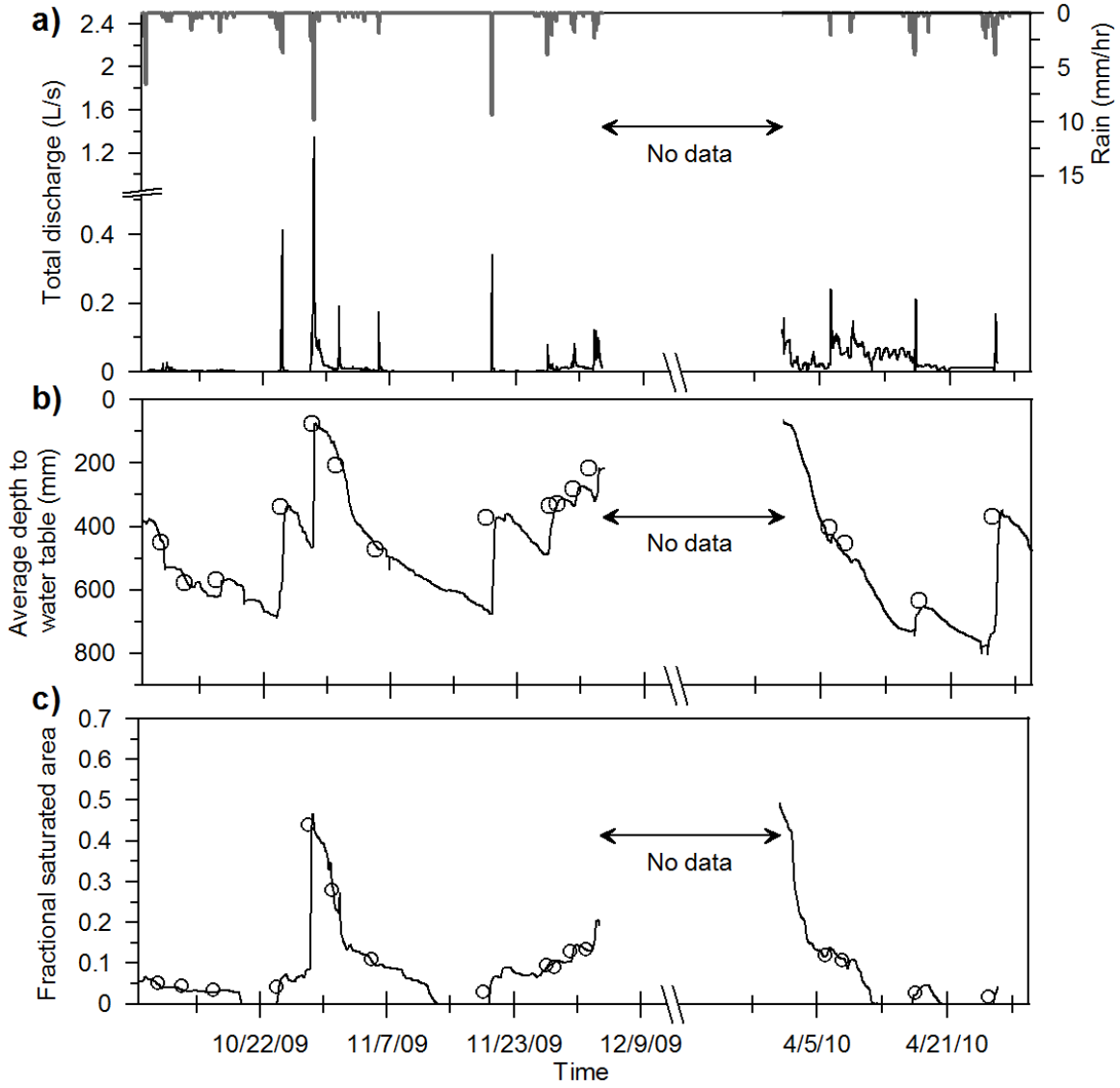

Figure 3.3: Rainfall and total discharge time series (a), dynamics of the average depth to the water table in the hillslope (b), and the fractional saturated area (c) recorded in the trench hillslope for the study period from 06 October 2009 until 31 May 2010. Measurements were discontinued from 9 December 2009 until 31 March 2010 due to snow cover and frozen soils.

Table 3.1: Rainfall and runoff information for the 16 storm events.

Event	Q_{obs}	Q_{base}	P_{tot}	I_a	$P_{i\text{-}1hr}$	API_7	API_{14}	API_{30}	Rainfall duration	Water table depth*
	(mm)	(mm/h)	(mm)	(mm)	(mm/h)	(mm)	(mm)	(mm)	(hrs)	(cm)
6-Apr-10	0.2	0.03	2.8	0.0	2.0	25	49	104	2	42
8-Apr-10	0.1	0.01	4.8	3.1	1.8	3	46	105	7	46
17-Apr-10	0.1	0.00	16.5	11.2	3.0	1	9	89	15	71
26-Apr-10	0.6	0.00	37.3	25.4	3.8	15	38	82	19	78
9-Oct-09	0.1	0.00	6.8	2.0	0.8	29	109	147	29	45
12-Oct-09	0.0	0.00	4.8	2.8	1.5	17	57	148	14	59
16-Oct-09	0.0	0.00	6.4	0.8	1.8	13	43	155	7	62
24-Oct-09	0.5	0.00	26.1	5.8	3.6	3	21	144	21	68
28-Oct-09	6.7	0.00	45.5	2.2	9.8	26	35	109	12	47
31-Oct-09	0.2	0.01	2.5	0.4	0.7	46	73	122	3	21
5-Nov-09	0.2	0.01	4.7	2.2	1.8	3	75	107	5	47
19-Nov-09	0.8	0.00	26.4	9.7	9.4	0	0	80	5	67
27-Nov-09	0.5	0.00	14.7	0.3	3.8	27	28	82	17	48
28-Nov-09	0.1	0.01	2.5	0.3	0.8	17	43	51	7	36
30-Nov-09	0.5	0.02	8.1	0.3	1.8	19	46	53	13	33
2-Dec-09	0.9	0.01	9.9	0.0	2.3	26	54	60	14	32

* Average depth to the water table in the hillslope prior to each storm event.

69

3.4.2 Influence of water table threshold on observed A_f

Table 3.2 summarizes values of the observed "saturated" fraction in the hillslope for each storm event for different average water table depth thresholds of 5 cm ($A_{f\text{-}5}$), 10 cm ($A_{f\text{-}10}$), 15 cm ($A_{f\text{-}15}$), and 20 cm ($A_{f\text{-}20}$). The average observed saturated fraction of the hillslope observed during any of the 16 storm events exhibited the smallest A_f -value range for the 5 cm threshold ($A_{f\text{-}5}$ = 0 – 6%) and largest value range for the 20 cm threshold ($A_{f\text{-}20}$ = 6 – 38%). The different thresholds influence $A_{f\text{-}obs}$ estimates mainly during large storm events or under dry antecedent conditions. If a threshold of 5 cm was used to estimate the saturated fraction, observed $A_{f\text{-}5}$ values were zero for most events except during events with greater rainfall amounts (P_e > 15 mm) when the water table rise was rapid or when the average water table depth was less than 400 mm below the soil surface prior to storm events (Tables 3.1 and 3.2). The maximum saturated fraction of the hillslope observed during the largest storm event on 28 October 2009 ranged from 11%, 38%, 49%, and 51% for the 5, 10, 15 and 20 cm thresholds, respectively.

3.4.3 Comparison of observed versus predicted A_f

Using the observed P_e and Q_{obs} to back calculate S from Eq. 3.3, predicted A_f (Eq. 3.4) ranged from 1% to 28% for the 16 storm events. To estimate the accuracy of predicted A_f and the effect of the average water table depth on the determination of the saturated hillslope fraction, we linearly regressed predicted versus observed A_f-values, derived for the four different thresholds (Fig. 3.4). A linear fit that approaches the 1:1 line closest indicates the best agreement between predicted and observed A_f; in this case $A_{f\text{-}10}$ produced the best agreement (Fig. 3.4) Additionally, the root-mean-square error (RMSE) and Nash-Sutcliffe criterion (E) (Nash and Sutcliffe, 1970) between predicted and observed A_f indicated the 10 cm water table threshold showed the closest fit;

RMSE = 0.11, 0.03, 0.03, and 0.04 and E = -22.1, 0.82, 0.78, and 0.57 for the 5, 10, 15 and 20 cm thresholds, respectively.

Table 3.2: Summary of predicted saturated areas (A_f) based on the VSA interpretation of the SCS-CN method and observed average saturated area extends, derived for water table depths of 5 cm ($A_{f\text{-}5}$), 10 cm ($A_{f\text{-}10}$), 15 cm ($A_{f\text{-}15}$) and 20 cm ($A_{f\text{-}20}$) respectively. The RMSE and Nash-Sutcliffe coefficient list statistical measures for the comparison of predicted and observed A_f.

					Observed average VSA			
Events	**P_e**	**Q_{obs}**	**S**	**$A_{f\text{-}pred}$**	**$A_{f\text{-}5}$**	**$A_{f\text{-}10}$**	**$A_{f\text{-}15}$**	**$A_{f\text{-}20}$**
	(mm)	(mm)	(mm)					
6-Apr-10	2.8	0.20	37	0.14	0	0.12	0.16	0.19
8-Apr-10	1.8	0.10	31	0.11	0	0.08	0.12	0.15
17-Apr-10	5.3	0.14	203	0.05	0	0	0.04	0.06
26-Apr-10	11.9	0.62	219	0.10	0	0.01	0.04	0.10
9-Oct-09	4.8	0.06	410	0.02	0	0.03	0.05	0.08
12-Oct-09	2.0	0.01	786	0.01	0	0.02	0.04	0.06
16-Oct-09	5.6	0.03	1243	0.01	0	0.02	0.04	0.06
24-Oct-09	20.3	0.45	895	0.04	0	0.01	0.03	0.07
28-Oct-09	43.4	6.68	238	0.28	0.06	0.27	0.35	0.38
31-Oct-09	2.1	0.22	18	0.20	0	0.16	0.28	0.32
5-Nov-09	2.5	0.19	32	0.14	0	0.08	0.11	0.14
19-Nov-09	16.7	0.78	343	0.09	0	0.02	0.07	0.09
27-Nov-09	14.5	0.53	379	0.07	0.03	0.08	0.10	0.12
28-Nov-09	2.3	0.06	84	0.05	0.04	0.09	0.12	0.15
30-Nov-09	7.9	0.45	130	0.11	0.05	0.11	0.15	0.18
2-Dec-09	9.9	0.90	99	0.17	0.06	0.16	0.21	0.24
RMSE*					0.11	0.03	0.03	0.04
E**					-22.1	0.82	0.78	0.57

* Root-mean-squared-error

** Nash-Sutcliffe coefficient (Nash and Sutcliffe, 1970).

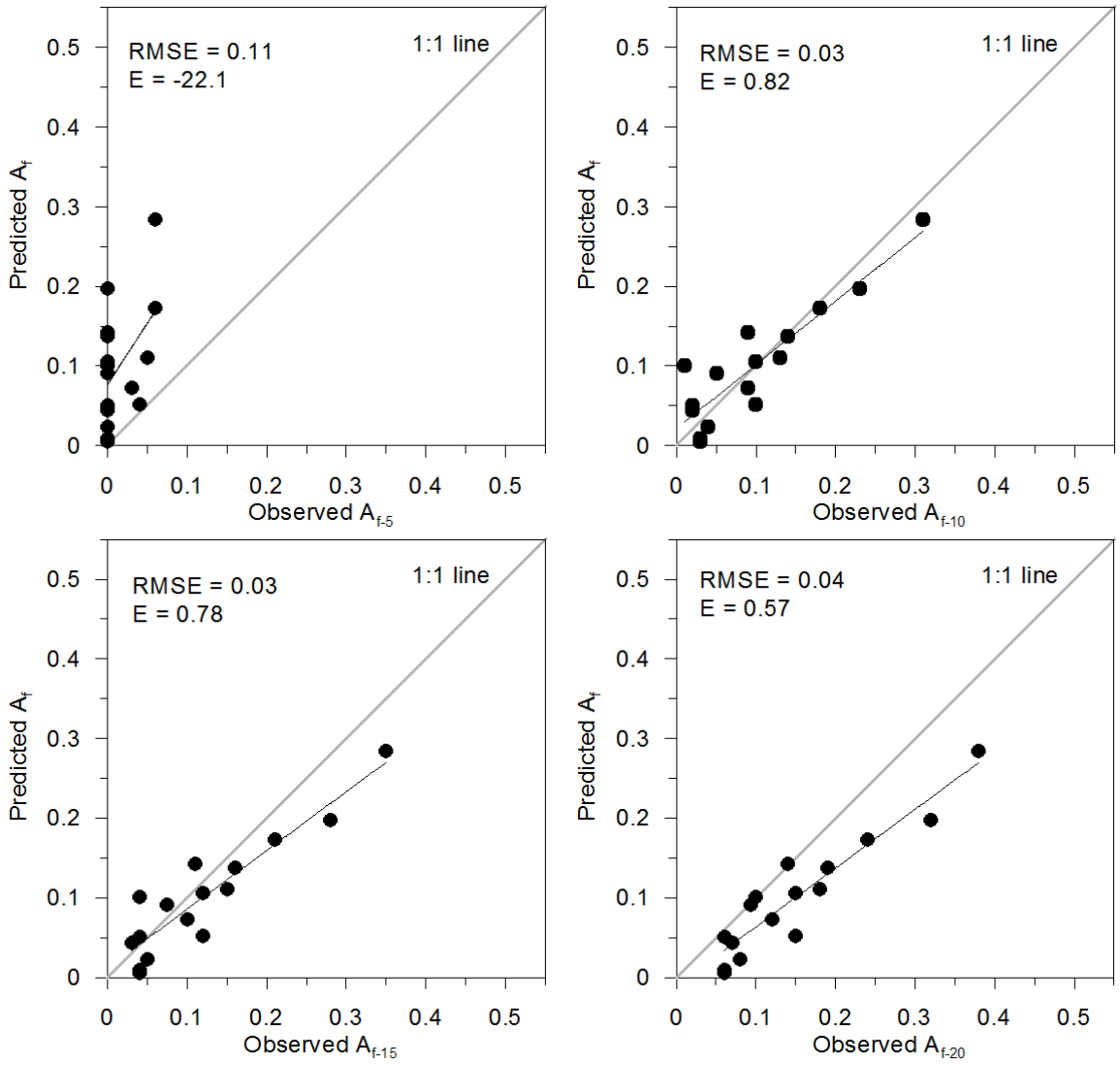

Figure 3.4: Linear regressions between predicted saturated areas using the VSA interpretation of the SCS-CN method and observed average saturated area extends, which were derived for different water table depths below the soil surface. Best agreement is achieved if the regression line approaches closely the 1:1 line. RMSE is the root-mean-squared error and E shows the Nash-Sutcliffe coefficient (Nash and Sutcliffe, 1970).

3.4.4 Physical rainfall-runoff relationships

3.4.4.1 Initial abstraction

As outlined in Tables 3.1 and 3.2, the observed 16 storm events showed a high variability in antecedent moisture conditions that influenced generated runoff volumes

and saturated area extents. In our analysis, the influence of antecedent moisture on runoff generation is addressed by both S and I_a (Table 3.2). Traditionally, I_a is considered a linear function of S in the original SCS-CN equation (USDA-SCS, 1972; Rallison, 1980). However, we found no coherent relationship between the two; for a linear regression $r^2 < 10^{-5}$ and log- and power-functions produced $r^2 < 0.1$ (analyses not shown, data in Table 3.2). This was curious because both S and I_a exhibit power-function-like relationships with respect to antecedent base flow (Q_{base}) or $A_{f\text{-}obs}$ (Fig. 3.5; S relationships not shown). The S-Q_{base} and S-I_a relationships were almost a threshold relationship similar to what Shaw et al. (2008) observed for very small watersheds. The initial abstraction observed during the 16 storm events showed an exponential increase with the average water table depth (Fig. 3.5a). This suggests, as expected, that dry antecedent conditions require more precipitation to satisfy the soil moisture deficit before runoff is initiated than for wet antecedent conditions. If the water table was at a depth of 700 mm or more, approximately 15 - 25 mm of rainfall were needed to initiate surface runoff. Under wet antecedent conditions, an average water table depth of less than 350 mm below the soil surface, less than 5 mm of rainfall were needed to initiate surface runoff (Table 3.1, Fig. 3.5a). The initial abstraction showed a similar behavior with the base flow observed 24-hours prior to storm events (Fig. 3.5b). The initial abstraction exponentially increased under dry antecedent conditions when the hillslope received less than 36 mm of rainfall within 14 days prior to the storm event as indicated by a base flow rate of 0.004 mm/hr (10 L/hr) or less.

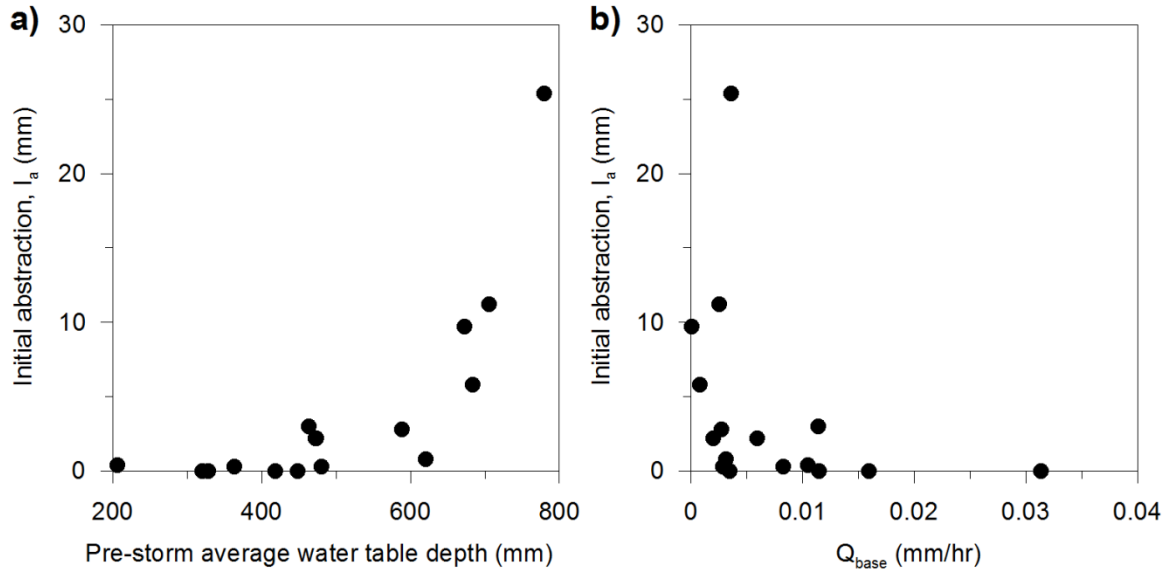

Figure 3.5: Relationship between (a) the initial abstraction or amount of water required to initiate runoff and the average depth to the water table in the hillslope prior to each storm event, and (b) the initial abstraction and base flow observed within the 24-hour period prior to each storm event.

In this study we were able to account for both the variability of I_a and S with respect to antecedent conditions because we were able to directly measure all parameters except S, which weback-calculated from Eq. 3.1. Operationally, it would be convenient to eliminate one of these variables. Contrary to the common assumption that I_a=0.2S (or sometimes 0.05S), we did not find a relationship between S and I_a. Thus, we explored the possibility of using an average S-value such that only I_a varied with antecedent conditions; this is somewhat akin to the approach of Steenhuis et al. (1995) and Lyon et al. (2004) who used the Thornthwaite-Mather soil water budget to estimate I_a. We fitted an average S of 15.5 cm (CN = 62) from Q-P and A_f - P_e pairs using the method outlined by Steenhuis et al. (1995). Based on the fitted average S and observed Q and P we then back-calculated I_a using Eq. 3.1. The field-observed I_a and predicted I_a relative to Q_{base} (Fig. 3.6) is similar to the relationship in Figure 3.5b, which included the effect of variability of antecedent moisture conditions on S. For some events with

wet antecedent conditions there were negative values of the back-calculated I_a, reflecting that the soils in the trenched hillslope were already saturated prior to the storm event resulting in a soil water surplus and higher runoff volumes than predicted with the SCS-CN equation due to hillslope drainage. In this interpretation of the SCS-CN equation, S is a static watershed-specific parameter, However, in order to use the SCS-CN method in continuous watershed models or to predict runoff from specific events, more work is needed to incorporate soil-moisture accounting schemes (e.g., Michel et al., 2005), or proxies for soil moisture (e.g., Shaw and Walter, 2009) into the SCS-CN method.

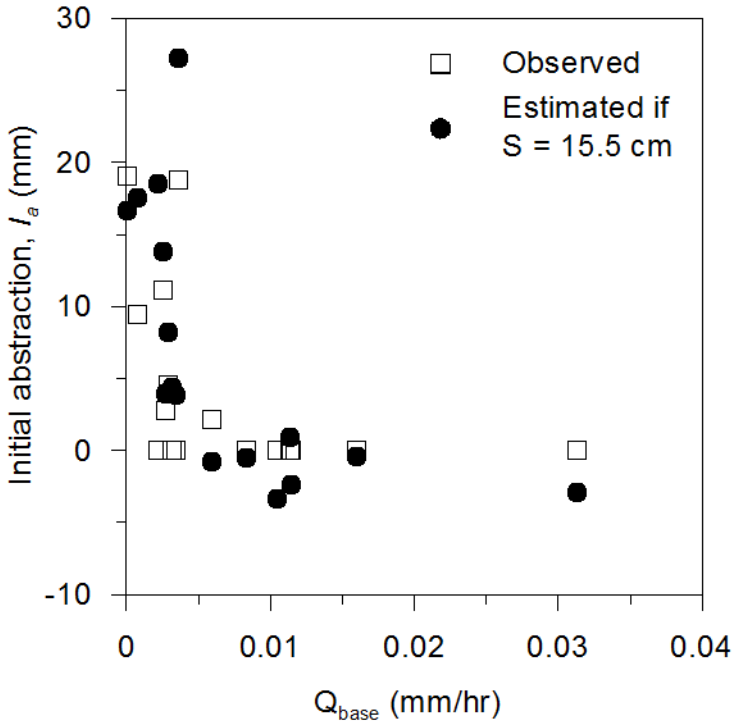

Figure 3.6: Comparison of observed initial abstraction and calculated initial abstraction if the watershed storage equals S=15.5 cm. The estimated initial abstraction shows negative values for events with wet antecedent conditions when discharge was greater than rainfall inputs. For these events the observed I_a was set to zero.

3.4.4.2 Predicted runoff volumes

As stated in Eq. 3.2, the VSA hydrology concept is based on the assumption that the amount of runoff generated during a storm event is a function of the rainfall amount and the saturated fraction of the watershed that is contributing runoff during a storm event. Thus, beside the statistical comparison of observed and predicted A_f, we tested whether the product of effective rainfall multiplied by the average saturated hillslope area ($A_{f\text{-}obs}$ x P_e) derived for each of the water table thresholds would match the observed runoff depths (Q_{obs}) (Fig. 3.7). The slope of the predicted verses observed Q is closest to unity for the 10 cm water table threshold (Fig. 3.7). The root-mean-squared-error (RMSE) between observed discharge (Q_{obs}) and the product of effective precipitation and the average fractional saturated area ($A_{f\text{-}obs}$ x P_e) were 1.10, 1.27, 2.18, and 2.58 mm respectively for the 5, 10, 15 and 20 cm thresholds (Table 3.3). Nash-Sutcliffe efficiencies were 0.51, 0.34, -0.94, and -1.71 respectively for the 5, 10, 15 and 20 cm water table thresholds (Table 3.3). Statistical measures might be mostly driven by the large storm event on October 2009. However, when plotting linear regression between Q_{obs} and the product of effective rainfall times the saturated hillslope area leaving the largest storm event out (Fig. 3.7, inserts), RMSE = 0.31, 0.27, 0.49, and 0.78 and E = 0.54, 0.68, -0.02, and -1.57 for the 5, 10, 15 and 20 cm thresholds, respectively (Table 3.3, Fig. 3.7). These results corroborate our conclusion that the runoff-generating, saturated fractional hillslope area is the area for which the water table was at 10 cm (or less) below the soil surface. In addition the results validate that runoff generation is dominated by saturation-excess and well predicted by the VSA interpretation of the SCS-CN method; note, although many of the statistical comparisons were actually stronger for the 5 cm threshold, the predicted values were systematically lower than the observed (Fig. 3.7a).

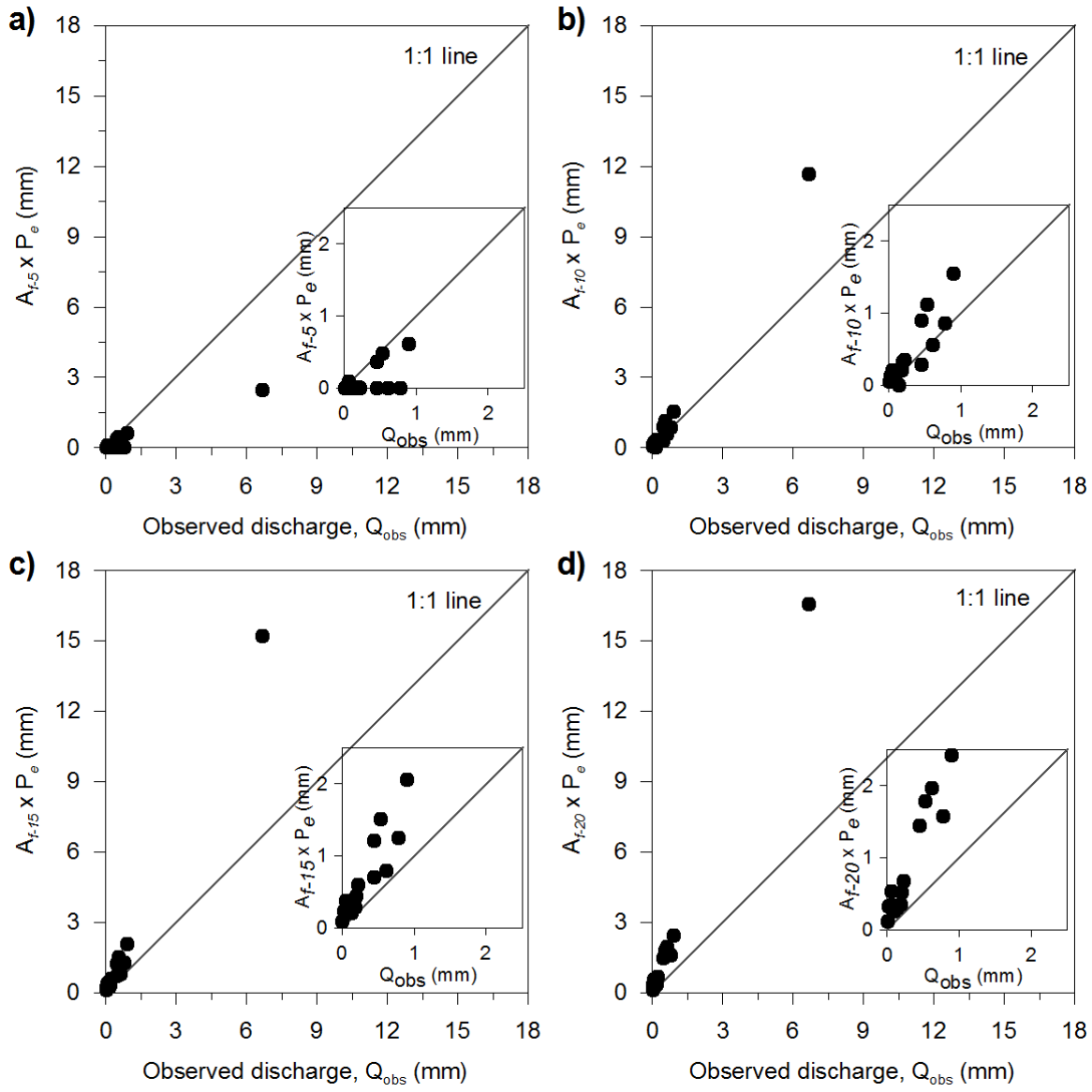

Figure 3.7: Relationship between total observed saturation-excess runoff and the product of effective precipitation times the average fractional saturated hillslope area as observed if the water table was at 5 cm (a), 10 cm (b), 15 cm (c), or 20 cm (d) below the soil surface. Inserts show data pairs for 15 storm events excluding the largest storm on 28 October 2009.

Table 3.3: Statistical comparison of observed runoff volumes (Q_{obs}) versus predicted runoff volumes based on the product of effective precipitation and the average fractional saturated area (A_f *x* P_e) for each water table depth threshold. Statistical measures comprise of the Nash-Sutcliffe efficiency (E) (Nash and Sutcliffe, 1970) and the root-mean-squared-error (RMSE).

Water table threshold	All events		All events except the largest storm event	
	E	RMSE	E	RMSE
5 cm	0.51	1.1	0.59	0.31
10 cm	0.34	1.27	0.68	0.27
15 cm	-0.94	2.18	-0.02	0.49
20 cm	-1.71	2.58	-1.57	0.78

3.5 Discussion

Our field monitoring setup allowed us to investigate the effect of the depth to the water table on runoff initiation. Similar to the findings of Lyon et al. (2006b), in this study we found that A_f predicted based on observed Q and effective precipitation agreed best with observed A_f if the water table was at or above a depth of 10 cm in the soil; i.e., rapid storm flow is initiated when the water table rises to within 10 cm of the surface. This indicates an important, although common, misinterpretation of saturation-excess stormflow, namely, soil saturation and water tables do not necessarily need to intersect the land surface to cause significant storm runoff. A rise of the water table to the zone of higher transmissivity, generally near the soil surface, (Brooks et al., 2004, Lyon et al. 2006b) can produce rapid runoff despite the lack of clear signs of surface saturation. Thus, if the water table is at a depth of 10 cm "direct runoff", which by definition can be of the form of direct precipitation on stream channels, overland flow, or shallow subsurface flow (USDA-SCS, 1972), is generated as defined in the curve number procedure.

Estimation of the runoff contributing area in watershed and field plot studies is important for water quality studies (Allan, 1995; Walter et al., 2000; DeLaune et al., 2004; Hamilton et al., 2004; Sharpley et al., 2004m, Easton et al. 2008a). The good statistical fit obtained for the linear regression of predicted versus observed average saturated area extends, if the water table was at 10 cm (or less) below the soil surface, corroborates the theorized accuracy of the underlying VSA interpretation of the SCS-CN method. Despite the "antiquated" image of the SCS-CN method held by many hydrologists, our results indicate that in the correct settings and with the correct assumptions the prediction of VSAs using the CN method is surprisingly robust in watersheds (Lyon et al., 2004; Schneiderman et al., 2007; Easton et al., 2008a, b) and even small plots (this study) dominated by saturation-excess overland flow. Complete field estimates of VSA extents in small or large watersheds are difficult to obtain and require either time consuming and cost intensive field mapping or remote sensing imagery and reliable interpretation. However, a few studies have indirectly shown that watershed models using the VSA hydrology concept perform better in the northeastern U.S. than models that assume infiltration-excess as the underlying runoff generation process (e.g. Lyon et al., 2004; Schneiderman et al., 2007; Easton et al., 2008a,b; Walter et al., 2008).

The amount of saturation-excess runoff generated during storm events is, to a great extent, controlled by the available soil water storage, which changes daily and seasonally with antecedent moisture conditions. However, the traditional SCS-CN method (USDA-SCS, 1972) adjusts *S* based on antecedent rainfall, which has been shown to be a poor index for antecedent conditions with respect to *S* (Shaw and Walter, 2009). To incorporate the variable *S* for each storm event into the analysis requires a better method for determining antecedent moisture conditions. Several

methods have been proposed to improve estimates of *S* based on various measures or indicators of antecedent conditions ranging from deriving *S* from soil moisture data (Saxton et al., 1982), the effective available soil water storage proposed by Schneiderman et al. (2007) to the storage versus base flow relationship proposed by Troch et al. (1993) and applied to the SCS-CN method by Shaw and Walter et al. (2009). The latter may be more readily applicable because there are relatively few places where soil moisture is continuously monitored and remotely sensed soil moisture is not well developed while there are many stream gages throughout much of the world.

One unique aspect of this study was that the initial abstraction was directly measured as the sum of the precipitation before surface runoff commenced. In both the standard SCS-CN procedure and the VSA interpretation of the SCS-CN method the initial abstraction is assumed to be a function of *S*, generally taken as 0.2*S* (USDA-SCS, 1972). However, soil water contents can vary between the wilting point at minimum and field capacity at maximum making the initial abstraction dependent on the actual soil water content. Studies from Jiang (2001) and Shaw and Walter (2009) have shown that much smaller I_a of 0.05*S* and 0.03*S*, respectively, resulted in better estimates of runoff than the traditional 0.2*S*. Walter and Shaw (2009) also suggested that when considering only storm events with rainfall amounts greater than 10 mm, neglecting the initial abstraction in watersheds on the order of 100 km^2 seems to results in suitable estimates of discharge. However, in smaller watersheds, particularly with a limited amount of riparian or wetland areas, the initial abstraction serves an important role in runoff production.

In this study I_a was estimated independent from S, which resulted in a storm variant S (back-calculated using Eq. 3.3) that reflects changes in antecedent moisture conditions. However, if using a site specific, constant S, which can be fitted by plotting observed effective precipitation versus runoff depths for several storm events (Steenhuis et al., 1995), variation of I_a with total rainfall and runoff can be estimated for each storm event (Fig. 3.6). Both the estimated and observed I_a show similar values depending on antecedent moisture conditions. Although S is representing the potential average storage or the total amount of water that can be stored in the watershed, differences in the soil moisture prior to storm events (i.e. negative I_a values for storms with wet antecedent conditions) have a large impact on the amount of runoff generated for a given rainfall amount (Fig. 3.6). As shown in this study the initial abstraction is highly variable in response to differences in antecedent moisture but shows good relations to indirect indicators such as the average water table depth and base flow rate prior to storm events (Figs. 3.3a,b). Thus, unlike the standard SCS-CN method, which assumes a fixed initial abstraction of 0.2S, more variable, continuous solutions of determining S or I_a that reflect antecedent wetness conditions need to be developed.

3.6 Conclusion

We compared variable source runoff areas predicted with the VSA interpretation of the SCS-CN method (Steenhuis et al., 1995) and field-observed spatial extends of variable source areas in a 0.5 ha trenched hillslope in central New York State. The trench instrumentation in conjunction with continuous measurements of upslope water table dynamics in the hillslope allowed quantification of lateral flow from different soil layers. Initiation and total volume of saturation-excess overland flow in response to rainfall could be directly monitored for different water table depths in the upslope

contributing area of the trench for 16 storm events between October 2009 and May 2010. Using field measured precipitation and discharge amounts, the comparison showed that the VSA interpretation of the SCS-CN method accurately predicted the runoff contributing area observed during the 16 storm events. We further demonstrate that predicted and observed saturated areas showed the best agreement if the water table was within 10 cm of the soil surface during storm events. These results not only provide evidence that the VSA interpretation of the SCS-CN method accurately predicts VSA extends in small watersheds or plots but also that the method has a physical basis and is not simply a curve fitting routine of observed rainfall and runoff depths. In addition, the results clarify that if the water table is at a depth of 10 cm below the soil surface, direct runoff in the form of shallow subsurface flow is initiated. Thus, not all stormflow is generated as overland flow due to intersection of the water table with the land surface, or, the term "overland" is perhaps misleading.

REFERENCES

Allan, J.D. 1995. Stream ecology: Structure and function of running waters. Chapman and Hall, London, United Kingdom.

Brooks, E.S., Boll, J., and P.A. McDaniel. 2004. A hillslope-scale experiment to measure lateral saturated hydraulic conductivity. Water Resources Research 40. doi:10.1029/2003WR002858.

Buda, A.R., Kleinman, P.J.A., Srinivasan, M.S., Bryant, R.B., and G.W. Feyereisen. 2009. Factors influencing surface runoff generation from two agricultural hillslopes in central Pennsylvania. Hydrological Processes 23: 1295-1312.

Dahlke, H.E., Easton, Z.M., Fuka, D.R., Lyon, S.W., and T.S. Steenhuis. 2009. Modeling Variable Source Area Dynamics in a CEAP Watershed. Ecohydrology 2: 337-349.

DeLaune, P.B., Moore, P.A., Carman, D.K., Sharpley, A.N., Haggard, B.E., and T.C. Daniel. 2004. Evaluation of the phosphorus source component in the phosphorus index for pastures. Journal of Environmental Quality 33:2192–2200.

Dunne, T., and R.D. Black. 1970. Partial area contributions to storm runoff in a small New England watershed. Water Resources Research 6, 1296–1311.

Easton, Z.M., Walter, M.T., and T.S. Steenhuis. 2008a. Combined monitoring and modeling indicate the most effective agricultural best management practices. Journal of Environmental Quality 37, 1798–1809.

Easton, Z.M., Fuka, D.R., Walter, M.T., Cowan, D.M., Schneiderman, E.M., and T.S. Steenhuis. 2008b. Re-conceptualizing the soil and water assessment tool (SWAT) model to predict runoff from variable source areas. Journal of Hydrology 348: 279– 291.

Garen, D.C., and D.S. Moore. 2005. Curve number hydrology in water quality modeling: Uses, abuses, and future directions. J. Am. Water Resour. Assoc. 41: 377–388.

Gburek, W.J., Drungil, C.C., Srinivasan, M.S., Needelman, B.A., and D.E. Woodward. 2002. Variable-source area controls on phosphorus transport: Bridging the gap between research and design. Journal of Soil and Water Conservation 57(6): 534–543.

Goovaerts, P. 1999. Geostatistics in soil science: state-of-the-art and perspectives. Geoderma 89: 1-45.

Hamilton, P.A., Miller, T.L., and D.N. Myers. 2004. Water quality in the nation's streams and aquifers: Overview of selected fi ndings. USGS, Washington, DC. 1265. p. 1–19.

Hewlett, J.D., and A.R. Hibbert. 1967. Factors affecting the response of small watersheds to precipitation in humid regions. In: Forest Hydrology (Sopper WE, Lull HW, eds.). Pergamon Press, Oxford.

Hewlett, J.D., and W.L. Nutter. 1970. The varying source area of streamflow from upland basins, Proceedings of the Symposium on Interdisciplinary Aspects of Watershed Management. Bozeman, MT. ASCE, New York, pp. 65–83.

Horton, R.E. 1933. The role of infiltration in the hydrologic cycle. Eos (Transactions of the American Geophysical Union) 14: 44–460.

Horton, R.E. 1940. An approach toward a physical interpretation of infiltration capacity. Soil Science Society of America Proceedings 4: 399-417.

Jiang, R. 2001. Investigation of runoff curve number initial abstraction ratio, M.S. thesis, Univ. of Ariz., Tucson.

Lyon, S.W., Gérard-Marchant, P., Walter, M.T., and T.S. Steenhuis. 2004. Using a topographic index to distribute variable source area runoff predicted with the SCS-Curve Number equation. Hydrological Processes 18(15): 2757–2771.

Lyon, S.W., Lembo, A.J., Walter, M.T., and T.S. Steenhuis. 2006a. Defining probability of saturation with indicator kriging on hard and soft data. Advances in Water Resources 29: 181–193.

Lyon, S.W., Seibert, J., Lembo, A.J., Walter, M.T., and T.S. Steenhuis. 2006b. Geostatistical investigation into the temporal evolution of spatial structure in a shallow water table. Hydrology and Earth System Sciences 10: 113–125.

Michel, C., Andréassian, V., and C. Perrin. 2005. Soil Conservation Service curve number method: How to mend a wrong soil moisture accounting procedure? Water Resour. Res., 41, W02011, doi:10.1029/ 2004WR003191.

Miller, T.S. 1993. Glacial geology and the origin and distribution of aquifers at the Valley Heads moraine in the Virgil Creek and Dryden Lake-Harford valleys, Tompkins and Cortland counties, New York. U.S. Geological Service Water-resources investigations report, 90-4168.

Nash, J.E., and J.V. Sutcliffe. 1970. River flow forecasting through conceptual models, Part 1 - a discussion of principles. Journal of Hydrology 10: 282–290.

Ogden, C.B., van Es, H.M., and R.R. Schindelbeck. 1997. Miniature rain simulator for measurement of infiltration and runoff. Soil Sci. Soc. Am. J. 61:1041-1043.

Ponce, V.M., and R.H. Hawkins. 1996. Runoff curve number: Has it reached maturity?, J. Hydrol. Eng., 1: 11 –19, doi:10.1061/(ASCE)1084-0699(1996)1:1(11).

Rallison, R.E. 1980. Origin and evolution of the SCS runoff equation. Symposium on Watershed Management, American Society of Civil Engineers: New York, NY; 912–924.

Ripley, B.D. 1981. Spatial Statistics Wiley, New York.

Saxton, K.E., Johnson, H.P., and R.H. Shaw. 1974. Modeling evaptranspiration and soil moisture. Transactions of the American Society of AgriculturalEngineers 17(4): 673–677.

Saxton, K.E. 1982. SPAW model predicts crop stress. Agric. Res. 30: 16–26.

Schneiderman, E.M., Steenhuis, T.S., Thongs, D.J., Easton, Z.M., Zion, M.S., Mendoza, G.F., Walter, M.T., and A.L. Neal. 2007. Incorporating variable source area hydrology into the curve number based Generalized Watershed Loading Function model. Hydrological Processes 21: 3420–3430, DOI: 10.1002/hyp6556.

Sharpley, A.N., Kleinman, P., and J. Weld. 2004. Assessment of best management practices to minimize the runoff of manure-borne phosphorus in the United States. N. Z. J. Agric. Res. 47: 461–477.

Shaw, S.B., and M.T. Walter. 2009. Improving runoff risk estimates: Formulating runoff as a bivariate process using the SCS curve number method, Water Resour. Res., 45, W03404, doi:10.1029/2008WR006900.

Shaw, S.B., Walter, M.T., and R.D. Marjerison. 2008. Grouping like catchments: A novel means to compare 40+ watersheds in the Northeastern U.S. American Geophysical Union Fall Meeting, December 14–19, 2008, San Francisco, CA, USA. -- Eos Trans. AGU, 89(53), Fall Meet. Suppl. Abstract H33D-1038.

Soil Survey Staff, Natural Resources Conservation Service, United States Department of Agriculture. Soil Survey Geographic (SSURGO) Database for [Tompkins County, Cayuga County, New York State]. Available online at http://soildatamart.nrcs.usda.gov accessed [06/20/2008].

Steenhuis, T.S., Winchell, M., Rossing, J., Zollweg, J.A., and M.F. Walter. 1995. SCS Runoff Equation Revisited for Variable-Source Runoff Areas. J. Irrig. Drain. E-ASCE 121: 234-238.

Troch, P.A., De Troch, F.P., and W. Brutsaert. 1993. Effective water table depth to describe initial conditions prior to storm rainfall in humid regions, Water Resour. Res., 29: 427– 434, doi:10.1029/92WR02087.

USDA-SCS (Soil Conservation Service). 1972. National Engineering Handbook, Part 630 Hydrology, Section 4, Chapter 10.

Walter, M.T., and S.B. Shaw. 2005. Discussion of Curve number hydrology in water quality modeling: uses, abuses, and future directions by Garen and Moore. J. Am. Water Resour. Assoc., 41(6): 1491–1492.

Walter, M.T., Walter, M.F., Brooks, E.S., Steenhuis, T.S., Boll, J., and K.R. Weiler. 2000. Hydrologically sensitive areas: Variable Source Area hydrology implications for water quality risk assessment. J. Soil Water Conserv. 55(3): 277-284.

Walter, M.T., M. Dosskey, M. Khanna, J. Miller, M. Tomer, and J. Wiens. 2007. The science of targeting within landscapes and watersheds to improve conservation

effectiveness. In (M. Schnepf and C. Cox, eds.) Managing Agricultural Landscapes for Environmental Quality, Strengthening the Science Base, Soil and Water Conservation Society, Ankeny, IA pp 63-91.

Walter, M.T., Archibald, J.A., Buchanan, B., Dahlke, H., Easton, Z.M., Marjerison, R.D., Sharma, A.N., and S.B. Shaw. 2009. A new paradigm for sizing riparian buffers to reduce risks of polluted storm water: A practical synthesis. ASCE Journal of Irrigation and Drainage Engineering 135(2): 200-209.

CHAPTER 4

MODELING VARIABLE SOURCE AREA DYNAMICS IN A CEAP WATERSHED

Abstract

In the Northeast US, saturation excess is the most dominant runoff process and locations of runoff source areas, typically called variable source areas (VSAs), are determined by the available soil water storage and the landscape topographic position. To predict runoff generated from VSAs some water quality models use the Soil Conservation Service Curve Number equation (SCS-CN), which assumes a constant initial abstraction of rainfall is retained by the watershed prior to the beginning of runoff. We apply a VSA interpretation of the SCS-CN runoff equation that allows the initial abstraction to vary with antecedent moisture conditions. We couple this modified SCS-CN approach with a semi-distributed water balance model to predict runoff, and distribute predictions using a soil topographic index for the Town Brook watershed in the Catskill Mountains of New York State. The accuracy of predicted VSA extents using both the original and the modified SCS-CN equation were evaluated for fourteen rainfall-runoff events through a comparison with average water table depths measured at 33 locations in Town Brook from March – September 2004. The modified SCS-CN equation captured VSA dynamics more accurately than the original equation. However, during events with high antecedent rainfall VSA dynamics were still under-predicted suggesting that VSA runoff is not captured solely by knowledge of the soil water deficit. Considering the importance of correctly predicting runoff generation and pollutant source areas in the landscape, the results of this study demonstrate the feasibility of integrating VSA hydrology into water quality models to reduce non-point source pollution.

4.1 Introduction

Water quality risks arise in areas where pollutant sources coincide with areas that are prone to generating runoff during storm events. These saturated areas are more likely to serve as rapid hydrological transport pathways for potential pollutants, thus they are often referred to as hydrologically sensitive areas (HSAs) (Walter et al., 2000; Gburek and Sharpley, 1998; Walter et al., 2001; Gburek et al., 2002). To reduce the contribution of non-point source pollution (NPS) to water bodies, managing and protecting HSAs is critical and consideration should be given to the location of areas generating saturation-excess runoff (Rao et al., 2008). These areas, typically called variable source areas (VSAs), expand and contract in size with changing rainfall depth. In regions dominated by saturation excess overland flow there is a need for water quality models that incorporate VSA hydrology in order to identify HSAs and optimize NPS pollution reduction (Heathwaite and Jones, 1996; Gburek and Sharpley, 1998; Gburek et al., 2000, 2002; Walter et al., 2000, 2001). Therefore, accurately predicting the locations of HSAs with hydrologic models is important to provide detailed information to mitigate contamination of surface waters.

More than 75 years ago Horton (1933, 1940) and Hursh (1944), and later Dunne (1970), identified HSAs in the landscape based on whether runoff was generated by infiltration excess overland flow (Horton 1933, 1940) or saturation excess overland flow (Hursh, 1944; Dunne, 1970). Infiltration excess overland (e.g., Hortonian flow) occurs when the rainfall intensity exceeds the infiltration capacity of the soil. The soil infiltration capacity is influenced by soil characteristics and vegetation, but also land use practices that cause a change in the infiltration capacity through compaction, surface sealing or other processes. Saturation excess runoff occurs in humid, well-vegetated regions where the soil capacity to store water is exceeded. Rainfall or

snowmelt water that cannot enter the saturated soil runs off as overland flow or flows shallowly as interflow (Hursh, 1944; Dunne, 1970). These VSAs are found in areas of the landscape characterized by shallow soils underlain by a restricting layer or spots where the topographic slope decreases causing surface and lateral flow to converge. VSAs develop within hours or days and expand and contract spatially depending on the rainfall depth (Dunne and Black, 1970; Hewlett and Nutter, 1970). Since landscape factors that control infiltration excess runoff differ from the factors that control saturation excess runoff from VSAs, watershed models that assume Hortonian flow as the primary runoff-generating process will predict different locations of runoff than models that assume saturation excess is the dominant runoff generating process (Schneiderman et al., 2007).

In the northeast US, saturation excess runoff generation from VSAs is the dominant runoff process (Walter et al., 2003). However, many water quality models such as AGNPS (Young et al., 1989), CREAMS (USDA, 1980), SWAT (Arnold et al., 1993) and GWLF (Haith and Shoemaker, 1987) implicitly assume that infiltration excess is the runoff generating mechanism. These models all use the USDA Soil Conservation Service Curve-Number (SCS-CN) equation (USDA, 1972) to predict runoff based on land use and soil type. Although the SCS-CN runoff equation was originally developed to estimate design storm flows for flood forecasting where the location of runoff production was not important, it is increasingly being used for NPS pollution management where identifying the correct location of runoff generation is critical, and thus capturing the processes controlling runoff generation is important.

In its most elementary form, the SCS-CN method is not based on any particular runoff generation mechanism (Rallison, 1980), and in fact Victor Mockus, to whom most of

the preceding work to the SCS-CN runoff equation can be attributed, said that the CN produces "rainfall-runoff curves of a type found on natural watersheds" (Rallison, 1980). Steenhuis et al. (1995) proposed a re-interpretation of the SCS-CN equation that allows prediction of the magnitude of the area that contributes direct runoff to the stream. However, this re-conceptualization of the SCS-CN equation could lead to imprecise predictions of runoff contributing areas if applied on a daily basis. The spatial dynamics of VSAs are dependent on the amount of water required to initiate runoff at the selected temporal scale and on the magnitude of the soil water deficit before a rainfall event. However, the original SCS-CN runoff equation accounts for the depth of precipitation before runoff begins as a constant fraction of the watershed's overall available soil storage, called the initial abstraction (I_a). Schneiderman et al. (2007) presented a VSA interpretation of the SCS-CN runoff equation that accounts for the effects of antecedent moisture conditions on VSA dynamics by scaling the time-varying storage parameter (S) in the SCS-CN to unsaturated zone soil moisture storage as simulated in the GWLF daily water balance. However, a simpler method for planning purposes would be to account for the effect of antecedent moisture conditions on VSA dynamics by determining the initial abstraction in the SCS-CN runoff with a water balance model.

The objective of this paper is to predict the dynamics of VSAs on a daily basis using a VSA interpretation of the original SCS-CN runoff equation modified with a dynamic initial abstraction term and a semi-distributed water balance model. The initial abstraction was revised to account for antecedent moisture conditions and the amount of rainfall retained by the watershed prior to the beginning of runoff, as estimated with a daily water balance model. The VSA dynamics predicted with constant and dynamic initial abstraction are compared to ground water levels observed at 33 locations on a

hillslope in Town Brook watershed in the Catskill Mountains, NY. This method presents a new, improved technique that is essential for water quality management and risk assessment.

4.2 Site Description

The study was conducted on a 2.5 ha hillslope in the southeast area of the 37 km² Town Brook watershed (42°21´N and 74°35´W) in the Catskill Mountains of New York State (Fig. 4.1). The Town Brook watershed is a headwater catchment in the Cannonsville Reservoir basin, which is part of the drinking water supply system for New York City. Elevation in Town Brook watershed ranges from 493 to 989 m and slopes range from 0 to 43°. The mean annual temperature is 7.7 °C and the mean annual precipitation is 905 mm/year (NRCS station Hobart, NY). Land use in Townbrook consists predominately of deciduous and coniferous forest (60%), pasture and crop lands for dairy farming (20%) and shrubs/bushes (18%). The study hillslope is moderately sloping with shallow soils generally characterized as gravelly silt loams over glacial till and fractured bedrock (shale). Using refraction seismic methods the thickness of the glacial till deposit was estimated at a maximum depth of 4 m in the near stream areas of the study site but became shallow moving up the hillslope to an approximate depth of 1.5 m (Dahlke et al., in preparation). According to the Soil Survey Geographic Database (SSURGO) soil maps, two soil types dominate the study hillslope: the northern (down slope) half consists of shallow gravely silt loam with a fragipan at approximately 55-60 cm depth, and the southern (up slope) half consists of moderately well drained silt loam with a fragipan at approximately 65-70 cm depth. These shallow soils are typified by a highly conductive ($1.4x10^{-5}$ m s^{-1}) surface material (less than 40 cm deep) overlaying a less conductive ($1.4x10^{-6}$ m s^{-1}) base material deeper than 40 cm with large fractures.

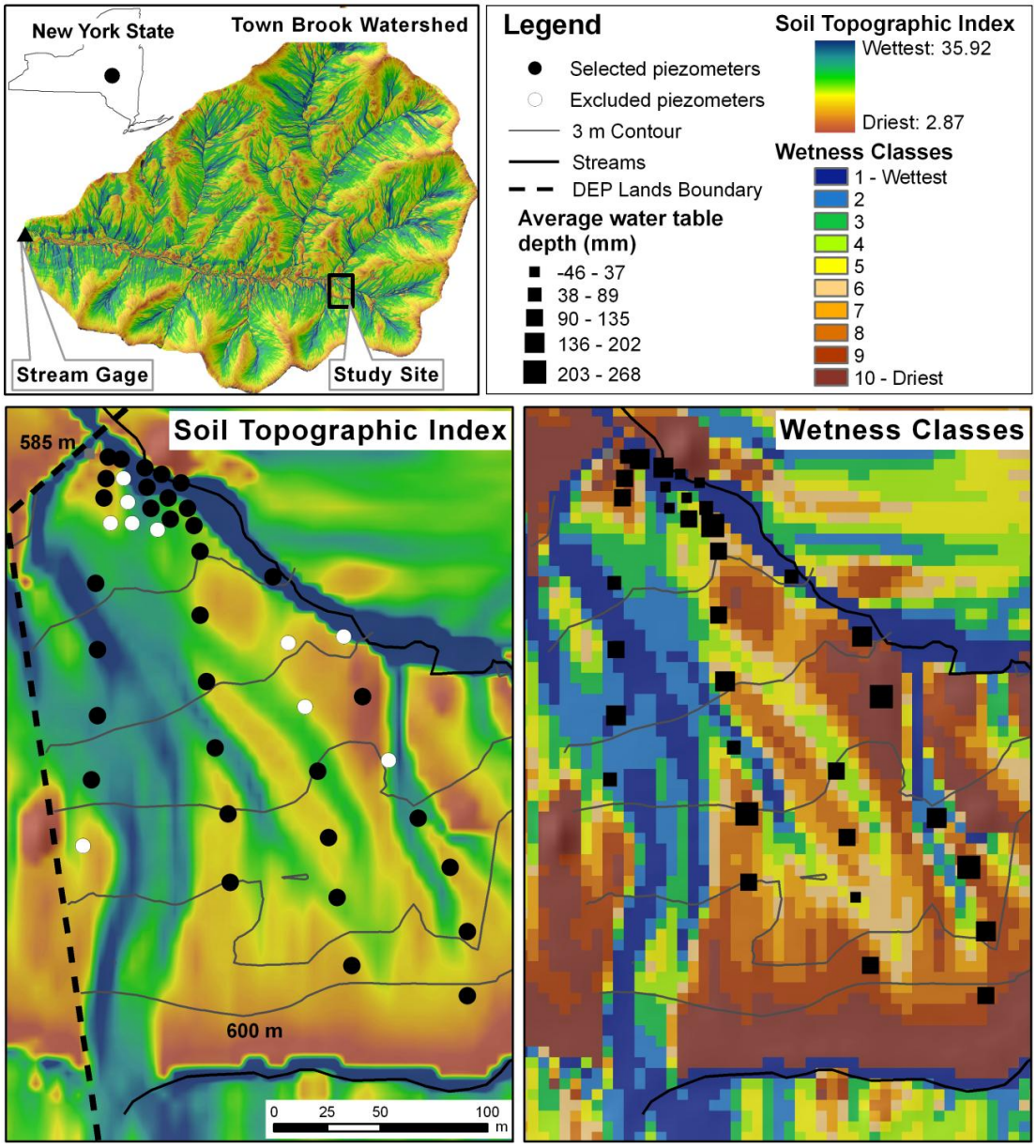

Figure 4.1: Location of Town Brook watershed in the Catskill Mountains, New York State (upper left). The left panel shows locations of water level loggers (black dots) considered in and excluded from this analysis (white dots) and the soil topographic index (STI) for the hillslope. The right panel shows the event-averaged depth to the water table for each water level logger underlain by a map of the wetness classes (as reclassified from the STI).

4.3 Methods

4.3.1 VSA prediction with the revised SCS-CN equation

In watersheds that are dominated by saturation overland flow Steenhuis et al. (1995) showed that the fraction of the watershed that produces runoff (A_f) can be estimated from the ratio of runoff depth (ΔQ) to precipitation depth (ΔP). The SCS curve number equation is often used to predict storm runoff from a watershed. The form typically used is (USDA-SCS, 1972):

$$Q = \frac{(P - I_a)^2}{(P - I_a) + S} = \frac{P_e^2}{P_e + S} \tag{4.1}$$

where I_a (mm) is the initial abstraction, S (mm) is the depth of the watershed-wide storage in the soil profile, P_e (mm) is the depth of effective precipitation after runoff begins. The initial abstraction is the amount of water required to initiate runoff or in terms of VSA hydrology, I_a is the soil water deficit to be satisfied before complete saturation of the soil profile is reached, after which additional rainfall becomes surface runoff. In the standard SCS-CN procedure I_a is generally taken as *0.2S*, which implies that the fraction of rainfall retained by the watershed prior to the beginning of runoff is storm invariant. However, soil water contents can vary between the wilting point at minimum and field capacity at maximum making the initial abstraction dependent on the actual soil water content. Therefore, a more accurate way of determining the initial abstraction for saturation-excess dominated watersheds would be to calculate I_a using a water balance model to estimate the soil water deficit or the variable initial abstraction before runoff is initiated.

Initial model tests showed that using a constant fraction of watershed storage for the initial abstraction (i.e., 0.2S) resulted in an over-prediction of A_f after a sustained

period without rain and in an under-prediction of A_f after long periods of rainfall. Therefore, we assumed that the initial abstraction is a function of the overall watershed wetness. We incorporated a dynamic initial abstraction term for the effective precipitation (P_e) in Eq. 1 by adjusting the amount of effective precipitation for a given day, *t,* depending on the antecedent rainfall surplus or deficit in the watershed. Considering antecedent moisture conditions P_e including I_a for a period prior to rainfall is calculated as the amount of precipitation on the day of the event minus the sum of the actual evapotranspiration (E_a) of all days (t) since the last rainfall event:

$$P_e = P_t - \sum_{t=1}^{n} E_{a,t} \tag{4.2}$$

If there is rain or snowmelt on the previous day the water deficit is calculated differently, because the watershed is not in equilibrium. In this case we subtract the previous day's saturation excess runoff and the previous and current day's evapotranspiration from the precipitation of the previous and current day.

$$P_e = P_t + P_{t-1} - Q_{t-1} - E_{a,t-1} - E_{a,t} \tag{4.3}$$

As shown by Steenhuis et al. (1995) the saturated fraction of the watershed contributing runoff areas can be estimated by integrating the SCS-CN runoff equation (Rallison, 1980) (Eq. 4.1) with respect to the effective precipitation, P_e:

$$A_f = 1 - \frac{S^2}{\left(P_e + S\right)^2} \tag{4.4}$$

where S (mm) in accordance to Eq. 1 is the depth of the watershed-wide storage in the soil profile, and P_e is the amount of rainfall after the runoff starts, or the total storm precipitation subtracted by the moisture deficit dependent initial abstraction (I_a) from Eq. 4.2 and Eq. 4.3. At a minimum, when $P_e = 0$ the fractional, runoff contributing area is zero and when P_e approaches infinity the contributing area equals 1.

4.3.2 Spatial Locations of VSAs

To find the spatial location of the fractional runoff contributing area A_f calculated with Eq. 4.5, the soil topographic index (*STI*) was employed (Beven and Kirkby, 1979). Several studies have shown that the soil topographic index is a good predictor of VSA locations in humid regions where water distributions are strongly driven by topography (O'Loughlin, 1986; Western et al., 2002; Lyon et al., 2004; Lyon et al., 2006a,b; Schneiderman et al., 2007; Easton et al., 2007; Easton et al., 2008). For instance, Agnew et al. (2006) demonstrated for three watersheds dominated by saturation excess runoff that the *STI* showed a strong correlation to locations of saturated areas. The *STI*, is calculated based on a raster Digital Elevation Model (DEM):

$$STI = \ln\left(\frac{\alpha}{\tan(\beta) D \hat{K}_s}\right) \tag{4.5}$$

where α is the upslope contributing area (m²), β is the local surface topographic slope (radians), D is the local soil depth (m), and $\hat{K}_s$ is the saturated hydraulic conductivity (m d^{-1}). Large *STI* values indicate locations that are more prone to saturation than locations with a small *STI*. Based on the assumption that areas saturate in the order

from highest to lowest *STI* value the index is used to qualitatively rank locations in the watershed in terms of their propensity of producing runoff.

4.3.3 Definition of Wetness Classes

We divided the watershed into ten unit areas, called wetness classes that are defined based on the relative propensity of each unit to become saturated or generate saturation excess runoff. Each wetness class is of equal size and derived through a reclassification of the soil topographic index (*STI*) into ten equal area classes. Thus, A_f -values of 0.1 (10%) or smaller are associated with the highest *STI* values, representing the wettest 10% of the watershed in wetness class one, A_f –values of 0.1 – 0.2 (10 – 20%) are associated with the next wettest 10% of the watershed and the second highest STI values in wetness class two, etc. These wetness classes are introduced because different areas of the watershed begin contributing runoff at different times depending on the amount of rainfall the watershed receives and their relative storage. However, the number of wetness classes is arbitrary and can be varied depending on the purpose of the study. The differentiation of the ten equal-area units generalizes spatial VSA predictions in order to simplify the applicability of the presented method for planners and farmers as NPS protection measures in the field.

4.3.4 VSA Water Balance Model

The daily available water storage in Town Brook watershed is estimated with a simple water budget model based on the Thornthwaite-Mather procedure and scripted in Python (Thornthwaite and Mather, 1955; Steenhuis and van der Molen, 1986; Collick et al., 2006). This model estimates the moisture storage, *S* (mm), of the topmost layer and the saturation excess runoff at the watershed outlet using precipitation, *P* (mm d^{-1}), potential evapotranspiration, E_p (mm d^{-1}), percolation to the subsoil, *Perc* (mm d^{-1}),

and storage, $S_{t-\Delta t}$ (mm). In the water balance model the depth of the watershed-wide soil water storage, *S,* (Eq. 4.1) becomes a calibration parameter that can be derived directly from baseflow-separated streamflow data and is not based on averaging the curve numbers of the various land uses in the watershed. During wet periods, when rainfall exceeds evapotranspiration (i.e. $P > E_p$) or the moisture content exceeds field capacity, the moisture storage S_t is determined from the previous day moisture, $S_{t-\Delta t}$ (mm), plus the effective precipitation ($P - E_p$) during the time step. During dry periods when evapotranspiration exceeds rainfall (i.e. $P < E_p$), the moisture content of the soil decreases linearly by actual evapotranspiration, E_a (mm), from the potential evapotranspiration rate at field capacity to zero at the wilting point. Potential evapotranspiration (E_p) is calculated using a sinusoidal function that is calibrated by fitting against observed E_p data. For a more detailed description of the model see Collick et al. (2006).

We integrated several modifications to the original water balance model described above to better capture the spatial/temporal dynamics of the VSA hydrology in the Town Brook watershed. In accordance with the ten wetness classes the moisture storage in each wetness class is estimated with the water balance model. Each wetness class is characterized by a maximum effective storage ($\sigma_{e,j}$), above which runoff is generated. The maximum effective storage ($\sigma_{e,j}$) for each wetness class was assigned using a method derived by Schneiderman et al. (2007):

$$\sigma_{e,j} = S\left(\sqrt{\frac{1}{1-A_{s,j}}} - 1\right) \tag{3.6}$$

where $\sigma_{e,j}$ is the maximum effective storage of a defined fraction j of the watershed, S is the depth of the watershed-wide storage, and $A_{s,j}$ (%) is the percent of the watershed area that has a local effective soil water storage less than or equal to $\sigma_{e,j}$. In accordance with Schneiderman et al. (2007), areas with a high propensity of generating runoff are characterized by a small maximum effective storage, ($\sigma_{e,j}$), while areas of the watershed that are dryer have a greater maximum effective storage. At any time the available water content in each wetness class varies between zero (wilting point) and $\sigma_{e,j}$.

Since watersheds in northeast US exhibit large runoff fractions resulting from spring snowmelt a snow energy budget model by Walter et al. (2005) was incorporated into the water balance model. Measured precipitation is first processed in the snow energy budget, which uses only minimum and maximum temperature data, before being distributed evenly over the watershed. Any water added in exceedance of the $\sigma_{e,j}$ of each wetness class is partitioned between saturation excess runoff, R (mm d^{-1}), and a bedrock reservoir that acts as the source of baseflow in the stream. Streamflow, Q, is computed for each time step by adding a fraction of the bedrock reservoir to the saturation excess runoff, R, by calibrating a baseflow recession coefficient (Easton et al., 2007). Two different baseflow recession coefficients are used to model variations in baseflow during the summer and winter months (Easton et al., 2007). Although we distinguish ten wetness classes in the watershed, there is no hydrologic connection among them (i.e., no interflow) so any runoff generated is routed to the outlet.

4.4 Input Data

4.4.1 Weather

Precipitation and temperature data for Town Brook were downloaded from the NRCC (Northeast Regional Climate Center) weather station located in Stamford, NY approximately 5 km northwest of the site, which recorded for the period 01 Jan 1997 to 31 Dec 2004. Minimum and maximum potential evapotranspiration varied between 0 mm and 5 mm (Steenhuis and van der Molen, 1986). Streamflow data were available since 01 Oct 1997 measured by the US Geological Survey (USGS) at the outlet of the Town Brook watershed in Hobart, NY.

4.4.2 Soil Topographic Index

The soil topographic index was computed for Town Brook watershed using Eq. 4.5 and a Lidar Digital Elevation Model with 5 m resolution (Fig. 4.1). Values for the contributing area, α, were determined using the D∞ flow algorithm of Tarboton et al. (1997); the local slope was calculated using a method of Horn (1981). The soil depth and the saturated hydraulic conductivity data for the study area were taken from the digital Soil Survey Geographic Database (SSURGO). We chose to divide the continuous *STI* map into ten-equal area classes (Table 4.1) with the highest *STI* values, representing the wettest 10% of the watershed in wetness class one to wetness class 10 and the lowest *STI* values, representing the driest 10% of the watershed area, as wetness class 10.

Table 4.1: Characterization of the ten wetness classes used in the VSA water balance model. For each wetness class the maximum effective storage σ_e, the threshold for the classification of the soil topographic index, the number of data loggers available, and event-averaged depths to the water table are listed.

Wetness classes	σ_e [mm]	*STI*	No of available data logger per wetness class	Average depth to water table [mm]
1	3.6	15.1-35.92	6	35.7
2	11.7	13.8-15.1	3	88.4
3	21.4	12.9-13.8	2	78.1
4	33.3	12.1-12.9	2	82.0
5	48.2	11.4-12.1	2	76.6
6	68.0	10.9-11.4	4	163.8
7	95.8	10.1-10.9	4	125.6
8	139.3	9.4-10.1	3	132.5
9	223.4	8.3-9.4	5	168.0
10	734.3	2.9-8.3	3	207.5

4.4.3 Water Table Depths

Water table measurements at 43 locations on a 2.5 ha hillslope in Town Brook watershed were available for the period from 05 March 2004 to 27 November 2004 (Fig. 4.1) (Lyon et al., 2006a). The water levels in the upper 50 cm of the soil were recorded at 5-min intervals using WT-HR 500 capacitance probes (TruTrack, Inc, New Zealand) and averaged to daily values. The capacitance probes have an accuracy of ± 1% of full scale (TruTrack Inc, New Zealand). Nineteen of the 43 loggers were located in the near stream area in a grid of 10 x 10 m and 24 loggers were spread along four transects up the hillslope (Fig. 4.1). To validate the model predictions of the timing and magnitude of fractional runoff contributing areas, 14 of the larger runoff events during March to September were chosen (Table 4.2, Fig. 4.2). The durations of four of the 14 events were longer than one day. The four storm events in March were caused by snowmelt. All other events received more than 20 mm per day of rainfall.

We used data from 33 of the 43 data loggers. Ten data loggers could not be included in the analysis because they did not record data during the selected events.

Table 4.2: Summary statistics of observed and predicted average streamflow, runoff and baseflow for the watershed outlet of Town Brook watershed. Hydrograph separation was performed according to Hewlett and Hibbert (1967).

Period[a]	Observed			Predicted			E[b]	r^{2c}
	Runoff [mmd^{-1}]	Baseflow [mmd^{-1}]	Streamflow [mmd^{-1}]	Runoff [mmd^{-1}]	Baseflow [mmd^{-1}]	Streamflow [mmd^{-1}]		
Winter 2003	13.6	2.3	3.7	20.5	1.4	2.7	0.65	0.72
Summer 2003	7.5	1.3	2.5	11.6	0.7	2.2	0.64	0.68
Winter 2004	6.4	1.5	2.3	18.1	1.1	2	0.66	0.75
Summer 2004	8.7	1.1	2.2	12.7	0.7	1.9	0.61	0.62
Total	9.1	1.6	2.7	14.8	1	2.2	0.65	0.7

[a] Summer is May – October. Winter is November – April.

[b] Nash-Sutcliffe efficiency comparison with measured streamflow.

[c] Coefficient of determination comparison with measured streamflow.

Each data logger is associated with one of the 10 wetness classes based on the *STI* value of the data logger location. This association is used to compare the spatial dynamics predicted with the water balance model with measured water table dynamics in the hillslope. In other words, if wetness classes one to three are predicted to be saturated with the water balance model for a given event the water level loggers located in the wetness classes one to three should indicate saturated conditions (i.e., water tables close to the soil surface). For each wetness class a minimum of two and a maximum of seven data loggers were available to evaluate the fraction of the Town Brook watershed contributing runoff (Table 4.1).

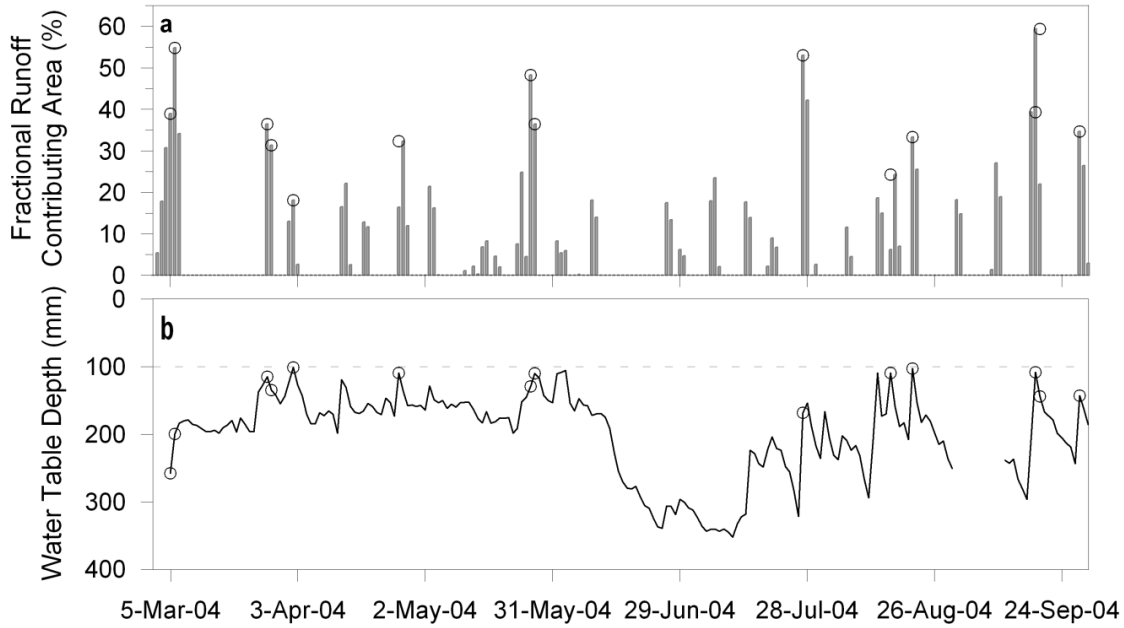

Figure 4.2: (a) Fractional runoff contributing area (A_f) and (b) average depth to water table of all sampling locations for the event analysis period March – September 2004. Circles indicate the 14 selected events. The horizontal, dashed line in (b) indicates the threshold water table depth above which runoff generation is initiated.

In this study the average depth to the water table of all loggers in a wetness class was used to validate the predicted runoff contributing area of Town Brook watershed as reflected by changes in the shallow water table. Based on the results of Lyon et al. (2006a) the soils in the study hillslope are characterized by a highly conductive top layer. Using the same time series of water level data Lyon et al. (2006a) showed that if the water table was within 10 cm of the soil surface the nearby stream exhibited a response. Subsequently Lyon et al. (2006b) speculate that both interflow and surface runoff increase at the 10 cm threshold depth (e.g. the interflow and runoff signal were indistinguishable). Therefore, if the average depth to the water table of all data loggers in a wetness class was less than 10 cm below the soil surface the wetness class was assumed saturated and contributing runoff to the stream.

4.5 Results

4.5.1 Model Calibration

Due to limited availability of rainfall data the VSA water balance model was calibrated using time series data available for 2004 and validated using time series data available for 2003. During 2003 and 2004 there was a time lag between rainfall and observed runoff, although it was not constant and thus could not be remedied by incorporating a time lag directly in the model. Due to the lack of a time adjustment factor in the model we consequently shifted the rainfall data by one day to match runoff peaks. The shift in observed rainfall is most likely caused by the station's recording method. Daily rainfall values cover a 24-hour period ending at 8 am on the date of record starting at 8 am on the previous day.

The VSA water balance model requires calibration of only a few parameters. First the overall effective storage of the watershed is calibrated to baseflow separated runoff (S = 13.8 cm) Then the maximum effective storage, σ_e, for each of the ten wetness classes is determined using Eq. 4.6 (Table 4.1). The baseflow recession coefficients for the summer and winter season were calibrated from baseflow separated streamflow (Hewlett and Hibbert, 1967; Arnold et al., 1995) and equaled a = 0.49 (d^{-1}) for summer (May – October) and a = 0.20 (d^{-1}) for winter (November – April), while the percolation fraction was calibrated to Q_p = 0.87 (mm d^{-1}). The VSA water balance model was run to predict streamflow at the outlet of the Town Brook watershed for 2004.

4.5.2 VSA Model Validation and Performance

The model performance was validated with a comparison of predicted to observed daily streamflow data for 2003. The water balance simulation agreed well with

observed streamflow measured at the outlet of Town Brook (Fig. 4.3). The Nash-Sutcliffe efficiency (Nash and Sutcliffe, 1970) (E) was $E = 0.65$ and the $r^2 = 0.70$ for the entire modeling period (2003-2004) and for the 2003 the $E = 0.66$ and $r^2 = 0.72$. Table 4.3 gives summary statistics for observed and modeled average streamflow, runoff, and baseflow amounts for the years 2003-2004. Streamflow was generally well predicted during the entire modeling period and the magnitudes of major storm events were particularly well predicted during 2004 (Table 4.3) but slightly over-predicted during 2003.

Table 4.3: Summary of hydrological parameters, the antecedent moisture conditions and the effective precipitation calculated with the original and revised SCS-CN equation observed and predicted for 14 events in 2004.

			Effective Precipitation				Fractional Areas			
							Original SCS-CN equation		Revised SCS-CN equation	
Event	**Q_{obs} [mm]**	**Q_{pred} [mm]**	**Days since last rainfall**	**Antecedent rainfall[a] [mm]**	**Rainfall[b] [mm]**	**P_e [mm]**	**A_f [%]**	**Wetness class**	**A_f [%]**	**Wetness class**
03/05/04	10.2	8.85	1	19.6	26.1	38.5	0.29	3	0.39	4
03/06/04	15.4	17.97	1	26.1	52.0	67.3	0.47	5	0.55	6
03/27/04	5.1	5.11	19	0.0	37.0	35.1	0.37	4	0.36	4
03/28/04	6.1	2.20	1	37.0	0.0	28.5	0.00	0	0.31	4
04/02/04	6.7	3.24	1	13.0	8.0	14.5	0.08	1	0.18	2
04/26/04	6.7	28.15	2	0.0	61.0	53.8	0.18	2	0.32	4
05/26/04	5.9	5.35	1	17.0	20.0	29.7	0.50	6	0.48	5
05/27/04	7.5	15.42	1	61.0	10.0	35.1	0.09	1	0.36	4
07/27/04	19.8	16.52	3	0.0	68.0	63.4	0.53	6	0.53	6
08/16/04	9	5.41	1	11.0	18.0	20.6	0.18	2	0.24	3
08/21/04	13.3	12.35	4	0.0	37.0	31.0	0.35	4	0.33	4
09/18/04	55.4	29.11	8	0.0	43.0	39.1	0.40	4	0.39	4
09/19/04	20.2	13.24	1	43.0	53.0	78.5	0.46	5	0.59	6
09/28/04	9.8	8.22	10	0.0	36.0	32.8	0.35	4	0.35	4

[a] Antecedent rainfall includes precipitation and snowmelt.

[b] Rainfall includes precipitation and snowmelt.

The timing and magnitudes of snowmelt runoff events, typically a challenge in hydrological modeling, were predicted correctly. Given the simplicity of the model (i.e., no interflow component) and the lack of measured rainfall data in the basin, the

baseflow predictions, while under-predicted, do indeed capture the response of the watershed. Under-prediction of streamflow was likely the result of deep percolation, which ultimately ends up as regional flow leaving the basin, due to the presence of complex geological formations in the Catskill Mountains. Precise predictions of stream discharge are further complicated because locally variability in precipitation is common in the Catskill Mountains (Mehta et al., 2004). The meteorological data used for this study were obtained from a station located 5 km northwest of the watershed but topographically separated by a mountain ridge. The station was chosen because it showed the best correlation coefficient with observed runoff (r=0.53). Other climate stations located in the central part of the Catskill Mountains, approximately 12-15 km south of Town Brook watershed, showed lower correlation coefficients.

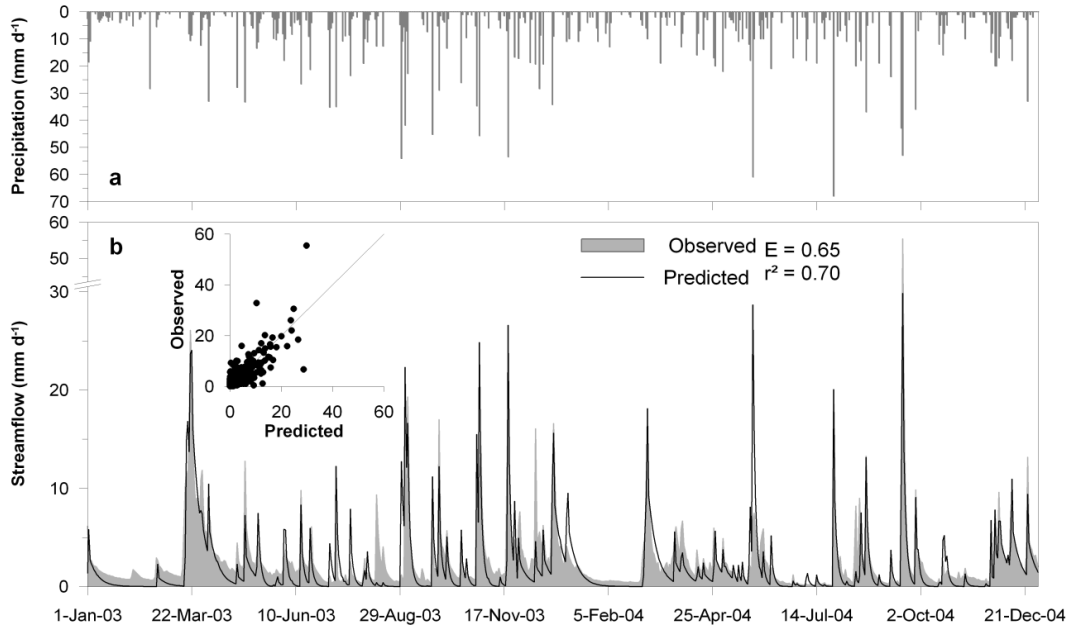

Figure 4.3: (a) Precipitation, and (b) observed and predicted streamflow for the water balance model from January 2003 to December 2004.

4.5.3 Evaluation of VSA extents

The validation of the daily extents of runoff contributing areas predicted with the water balance model and the revised version of the SCS-CN runoff equation is based

on a hypothesized correlation between measured average water table depths and the *STIs* of each data logger location. Each logger showed a good correlation of *STI* values to average event water table depths (r^2=0.51) (Fig. 4.4). However, the coefficient of correlation improved considerably when water table depths of all data loggers located in the same wetness class (e.g. seven data loggers in wetness class one) were averaged to one value per wetness class (r^2=0.81) (Fig. 4.4). The correlation coefficients indicate that most of the variation in the depth to water table can be explained by topography. However, some of the sampling locations, especially in the mid-slope areas, showed both rapid water table fluctuations in response to storm events and low average depths to water table (Fig. 4.1) that were not captured by the *STI* and resulted in the spread of observations in Fig. 4.4a. The water tables heights at these sampling locations reached or exceeded the ground surface quickly during storm events indicating transient perched water table, and rapid runoff of infiltrated rainfall and subsurface flow from the upslope areas.

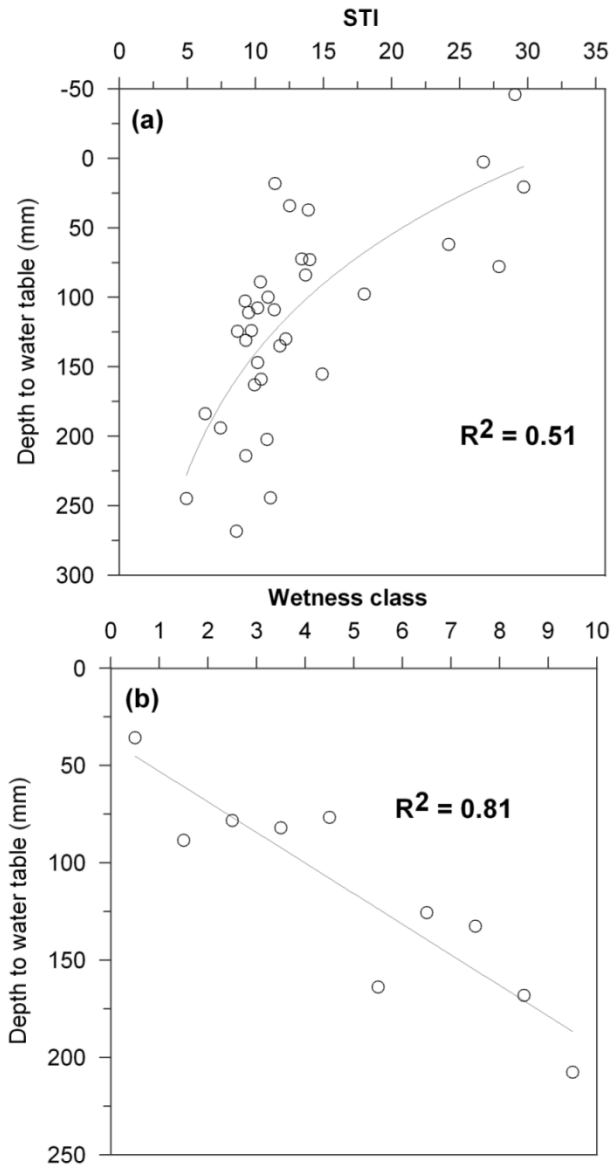

Figure 4.4: Correlation of the soil topographic index (*STI*) and average event water table depth of each sampling location (a), and wetness class vs. average water table depth based on all data loggers located in any wetness class.

Accurate prediction of the magnitude of a storm event and the extent of VSAs is important as the focus of nutrient management shifts to the timing of applications of potential pollutants such as fertilizers, manures, and pesticides. To evaluate the dynamics of the runoff contributing areas in Townbrook, 14 storm events were

selected from the sampling period March – September 2004. These events were selected because they produced distinct runoff peaks for which the VSA model predicted 18 – 59% of the watershed to be saturated.

The storm events from March through mid-May were dominated by low-intensity storms, or snowmelt induced events causing prolonged saturation of 18 – 55 % of the watershed. Measured peaks producing most of the runoff coincided with the large rainfall amounts that were estimated with the snowmelt energy budget during March (Fig. 4.2b). During this period the average depth to the water table on the hillslope maintained a constant depth of approximately 15 cm below the soil surface and peaked in response to rainfall events often peaking at 10 cm below the soil surface (Fig. 4.3b). During June through mid-July small rainfall events and higher P_e caused a drop in water tables across the hillslope, and low streamflow. From the end of July through September the region experienced high intensity storms with 20 – 60 % of the watershed contributing runoff. Water tables in the hillslope fluctuated quickly in response to single storm events and dropped abruptly in the dry periods (Fig. 4.3b). The two largest runoff events after days without high antecedent rainfall were recorded on 27 July 2004 and on 18 September 2004 (Table 4.3). Both events showed single day rainfall amounts of more than 40 mm resulting in runoff contributing areas of 53 % and 39 %. Events with single day antecedent rainfall amounts greater than 20 mm followed by rainfall events of 50 mm or more occurred on 6 March and 19 September 2004 (Table 4.3). For these events, runoff contributing areas of 55 % and 59 % respectively were predicted with the revised SCS-CN runoff equation while the original runoff equation predicted areas of 47 % and 46 % respectively. The difference of approximately 10 % achieved with the revised SCS-CN equation indicates the reduction in effective available soil storage prior to the rainfall events.

Seasonal trends can be observed repeatedly in the event responses of average water tables in each wetness class (Figs. 4.5 and 4.6). The first two selected storm events in early March 2004 miss the clear trend in observed average water table depths for all wetness classes. The data show a high variability but remain below the 10 cm threshold for most wetness classes, above which runoff is assumed to be initiated (Fig. 4.5). The locations of runoff contributing areas were well predicted with the revised SCS-CN equation (black vertical line) in wetness classes one and four in the close proximity of the stream. Runoff peaks at the beginning of March are the product of snowmelt runoff from near stream areas and groundwater springs in the hillside leading to a discontinuous response at some of the sampling locations in the field where soils remained frozen. However, saturated wetness classes predicted with the revised version of the SCS-CN equation capture the dynamics of the runoff source areas and the magnitude of the snowmelt event better than the original SCS-CN equation (Fig. 4.5).

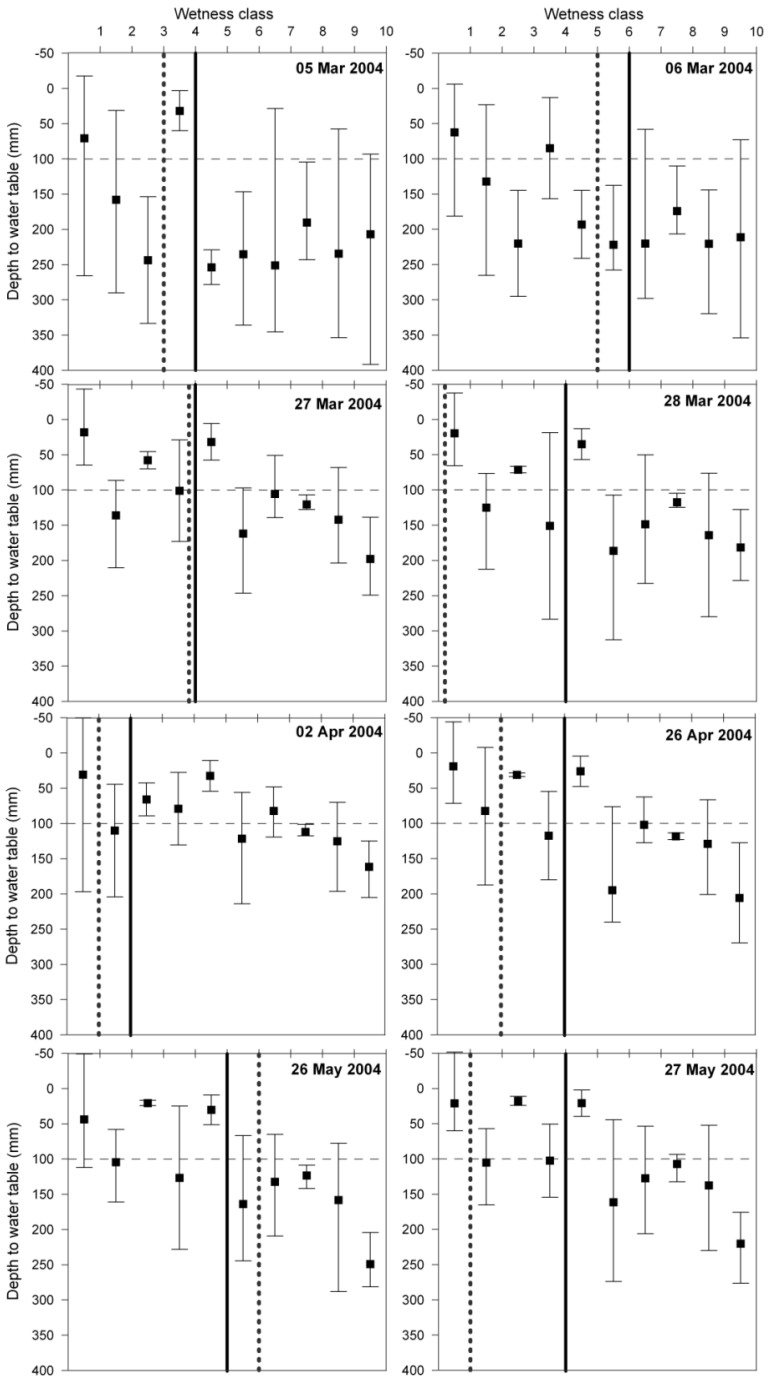

Figure 4.5: Average, minimum and maximum water table depths shown for each wetness class for events from 05 March until 27 May 2004. The vertical lines show the maximum range of wetness classes contributing runoff during this storm event as predicted with the original SCS-CN equation (dotted line) and the revised SCS-CN runoff equation (black line). The thin, horizontal dashed lines show the threshold water table depth above which the sampling locations indicate that runoff generation is initiated.

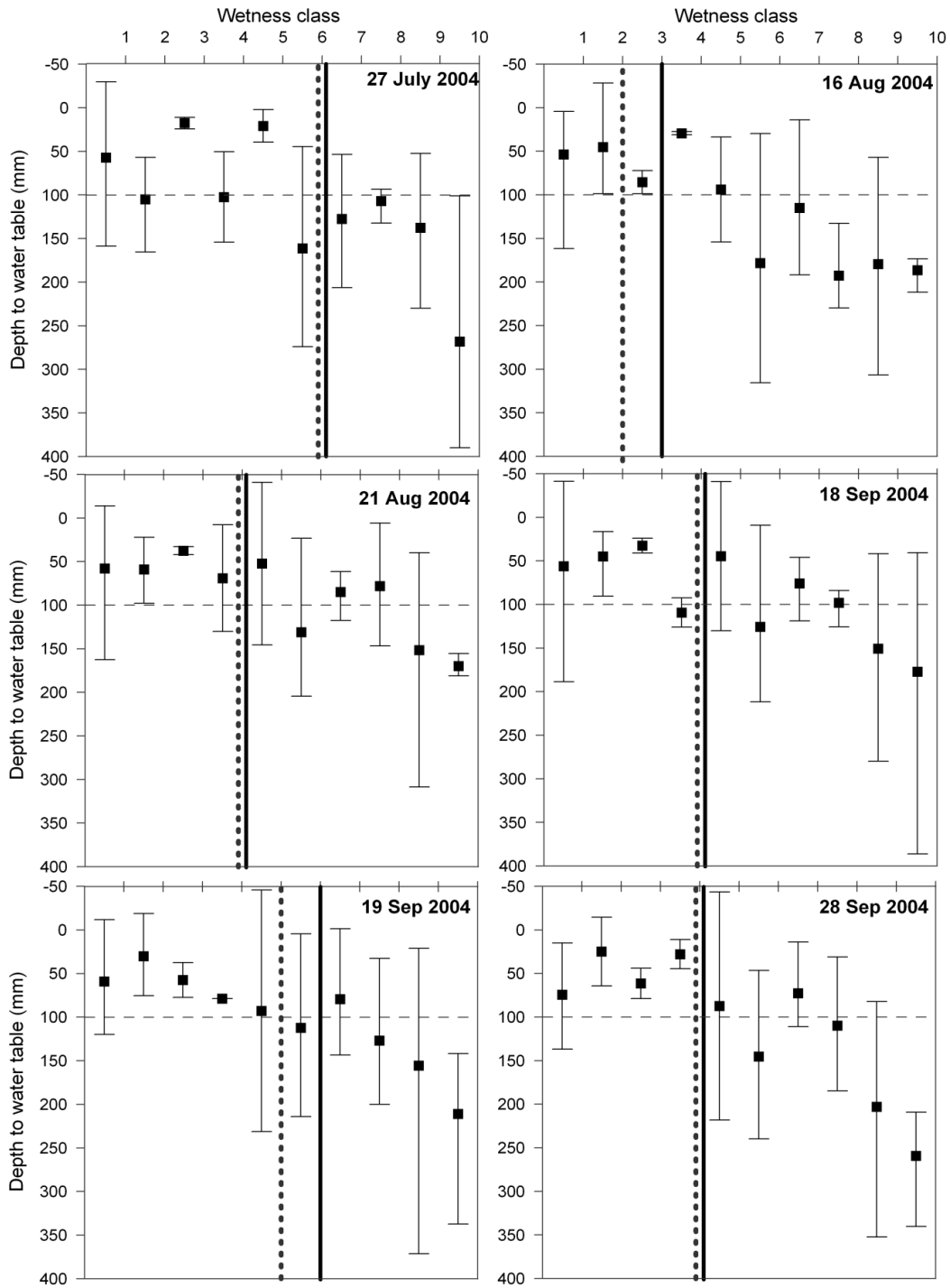

Figure 4.6: Average, minimum and maximum water table depths shown for each wetness class for events from 27 July until 28 September 2004. The vertical lines show the maximum range of wetness classes contributing runoff during this storm event as predicted with the original SCS-CN equation (dotted line) and the revised SCS-CN runoff equation (black line). The thin, horizontal dashed lines show the threshold water table depth above which the sampling locations indicate that runoff generation is initiated.

The range of average water table depths across wetness classes decreased throughout April and May indicating that the response of the water table to rainfall input becomes more homogeneous, likely the result of increasing E_p. Wetness classes predicted to contribute runoff (e.g., one – five) during rainfall events in April and May 2004 show average depths in close proximity to the 10 cm threshold, while water tables in wetness classes that are not expected to saturate (e.g., six – ten) remain below the threshold. This trend continues throughout the second half of the study period (Fig. 4.6). For the events on 16 and 21 August 2004 and 18 and 28 September 2004 the fractions of runoff contributing areas were correctly predicted with the revised SCS-CN equation, as indicated by the average water table depths of 10 cm and less for wetness classes one – five, while the average water tables of the drier wetness classes (six – ten) remain well below the 10 cm threshold (Fig. 4.6). For the two largest runoff events (27 July and 18 September 2004) average water tables show a trend of greater depth in the lower wetness classes and a lower depth in the higher wetness classes but also a greater range in measured water tables. For the largest event measured in 2004 (18 September) average water table depth are closer to the ground surface in all wetness classes indicating a large contributing runoff area in Town Brook for this event.

4.6 Discussion

By modifying the initial abstraction term of the SCS-CN runoff equation (Eq. 4.1) to account for antecedent moisture conditions in the estimation of runoff contributing areas we are able to more accurately predict the spatial extent of VSA dynamics on a daily basis. However, the average measured water table depth did not always coincide with the VSAs predicted with the wetness class distribution. Some of this variability is expected because the soil topographic index, in this model used as a proxy to identify

the location of VSA, is unlikely to capture all of the complex spatial variability describing runoff generation in real world applications. Some variability in the water table depths, measured in the transition zone between typical wet areas (low wetness classes) and dry areas (high wetness classes), may be influenced by unknown soil hydraulic properties or bedrock topographic features that change on a scale less than the *STI* (Fig. 4.1).

Similar to the findings of Lyon et al. (2006b), we found that the water table response to rainfall events was primarily driven by the antecedent moisture conditions in the watershed. During wet conditions, when the water table is likely to be close to the soil surface, the VSA water balance model correctly predicted more wetness classes to have greater saturation (e.g., 10 cm threshold). However, water table dynamics were generally better predicted during the summer months than during the snowmelt events when frozen soils impede the connectivity of hillslopes and riparian areas. Although the runoff peaks of snowmelt events during March 2004 were correctly predicted with the water balance model and the revised SCS-CN equation the measured data in the study site indicate that water table dynamics react slowly to snowmelt and that runoff generation results most likely from snowmelt runoff from frozen soils. These snowmelt driven VSA dynamics indicate that more work is needed to understand the processes governing the formation of VSAs and water table fluctuation during snowmelt. During low antecedent rainfall conditions (i.e., dry initial conditions), such as the 27 July 2004 and 16 August 2004 event, predicted and observed runoff contributing areas coincide well, but the measured water table depths in each wetness class show a large range. Rainfall events occurring after prolonged dry periods initially saturate preferential flow paths and expand laterally from topographically converging areas in the hillslope. Thus, water level loggers located nearby (but not in)

these preferential flow paths show water table responses only during storm events with high antecedent moisture conditions.

By considering antecedent moisture conditions in the SCS-CN runoff equation, we re-conceptualized one of the simplest methods used by hydrologists and engineers to predict the extent of the area that contributes direct runoff to streams. Previously, water quality models of varying complexity have been used to effectively delineate saturated areas in the landscape. These include SMDR (Frankenberger et al., 1999; Mehta et al., 2004; Gérard-Marchant et al., 2006), which is a spatially distributed model more appropriate to small catchments due to extensive simulation run times; SWAT (Easton et al., 2008), which requires extensive expertise and data collection efforts; and VSLF (Schneiderman et al., 2007; Easton et al. 2008), which takes a relatively simple water balance model approach. However, these models often require extensive expertise and data collection efforts to be used on a routine basis for planning and monitoring purposes. Although physically realistic VSA hydrology models for NPS pollution control are available there is a gap between scientifically proven models and tools readily available for planners and stakeholders that incorporate our current knowledge. The VSA water balance model presented in this study provides current research on VSA hydrology in a semi-distributed model that requires calibration of four key parameters. In areas where saturation excess overland flow is the dominant runoff generating process the recognition of VSA hydrology is crucial in the water quality management process. People familiar with using the USDA-SCS method (USDA-SCS 1972) in the decision process of water quality protection measures might be more inclined to use this simple model that captures the geographical distribution of runoff producing areas and their temporal dynamics correctly.

Previous studies from Lyon et al. (2004), Agnew et al. (2006), and Gérard-Marchant et al. (2006) have shown how monthly statistics of the probability of saturation could help to identify critical source areas through an overlay of VSA maps on field boundaries. They demonstrated that knowledge of long-term saturation extents could improve the proposed placement of potential pollutants by avoiding some fields that are identified as hydrologically sensitive during critical months (e.g. March-April, October-November). Considering the daily VSA status could potentially reduce restrictions on landowners (i.e., reduce the amount of land restricted for application of manures) through identification of fields that could potentially receive more nutrient applications without increasing the risk nutrient runoff.

This is especially important for watershed management under a changing climate. As climate records of the past 20 years indicate seasonal rainfall patterns are changing in the northeast and typical dry months like July and August can receive larger amounts of rainfall in single storm events (Mortsch and Quinn, 1996; Kunkel et al., 1999) than previously recorded. Thus, while seasonal or monthly saturation probabilities might remain unchanged, the daily risk of fertilizer or manure applications will potentially change, and better consideration needs to be given to the tools used to capture these processes. Daily predictions of VSA dynamics, as shown with the VSA water balance model, and even forecasts of hydrologically sensitive areas based on the knowledge of antecedent moisture conditions in the watershed could potentially reduce these daily pollution risks.

4.7 Conclusion

This study presents an alternative form of the SCS-CN runoff equation and a semi-distributed water balance model to predict the daily dynamics of VSAs for the Town

Brook watershed in the Catskill Mountains of New York State. The initial abstraction term of the original SCS-CN runoff equation was modified to account for antecedent moisture conditions, obtained with a daily water balance model based on the Thornthwaite-Mather procedure. Geographical locations of VSAs were predicted using a soil topographic index reclassified into ten equal-area classes. In the 14 events considered, the modeled VSA extents were correctly predicted as verified by average water table depths observed at 33 locations on a hillslope in Town Brook watershed. However, during events with high antecedent rainfall conditions, measured water table depths still showed more wetness classes to be contributing runoff than predicted with the water balance model. As agricultural watershed management begins to focus more on the timing of activities, correct identification of HSAs and VSAs in space and time becomes increasingly important. The model demonstrates an easy-to-implement method to predict the daily dynamics of VSAs by combining VSA hydrology and existing engineering methods such as the SCS-CN runoff equation. The expertise, calibration, and low data requirements of this model facilitate its implementation into water quality management tools and support its applications in ungaged watersheds. The model could also help delineate fields with low saturation potential that could potentially receive more nutrient applications without increasing the pollution risk. Thus, it could potentially reduce pollution risks if antecedent moisture conditions are considered in the daily schedule of management activities in the watershed. This kind of methodology provides the foundation for the next generation of water quality risk-assessment tools valuable to watershed managers and stakeholders.

REFERENCES

Agnew, L.J., Lyon, S., Gérard-Marchant, P., Collins, V.B., Lembo, A.J., Steenhuis, T.S., and M.T. Walter. 2006. Identifying hydrologically sensitive areas: Bridging science and application. Journal of Environmental Management 78: 64-76.

Arnold JG, Allen PM, Bernhardt G. 1983. A comprehensive surface-groundwater flow model. Journal of Hydrology 142: 47–69.

Beven, K.J., and M.J. Kirkby. 1979. A physically-based, variable contributing area model of basin hydrology. Hydrologic Science Bulletin 24: 43–69.

Collick, A.S., Easton, Z.M., Montalto, F.A., Gao, B., Kim, Y., Day, L., and T.S. Steenhuis. 2006. Hydrological Evaluation of Septic Disposal Field Design in Sloping Terrains. Journal of Environmental Engineering, 132(10): 1289–1297.

Dunne, T. 1970. Runoff production in humid areas. U.S. Department of Agriculture Publication ARS-41–160.

Dunne, T, and R.D. Black. 1970. Partial area contributions to storm runoff in a small New England watershed. Water Resources Research 6: 1296–1311.

Easton, Z.M., Gerard-Marchant, P., Walter, M.T., Petrovic, A.M., and T.S. Steenhuis. 2007. Hydrologic assessment of a urban variable source watershed in the Northeast US. Water Resources Research 43, W03413, DOI:10.1029/2006WR005076, 2007.

Easton, Z.M., Fuka, D.R., Walter, M.T., Cowan, D.M., Schneiderman, E.M., and T.S. Steenhuis. 2008. Re-conceptualizing the Soil and Water Assessment Tool (SWAT) model to predict runoff from variable source areas. Journal of Hydrology 348: 279–291.

Frankenberger, J.R., Brooks, E.S., Walter, M.T., Walter, M.F., and T.S. Steenhuis. 1999. A GIS-based variable source area model. Hydrological Processes 13(6): 805–822.

Gérard-Marchant, P., Hively, W.D., and T.S. Steenhuis. 2006. Distributed hydrological modelling of total dissolved phosphorus transport in an agricultural landscape, part I: distributed runoff generation. Hydrology and Earth System Sciences 10: 245–261.

Gburek WD, and A.N. Sharpley. 1998. Hydrologic controls on phosphorus loss from upland agricultural watersheds. Journal of Environmental Quality 27: 267–277.

Gburek, W.J., Sharpley, A.N., Heathwaite, L., and G.J. Folmar. 2000. Phosphorus management at the watershed scale: a modification of the phosphorus index. Journal of Environmental Quality 29: 130–144.

Gburek, W.J., Drungil, C.C., Srinivasan, M.S., Needelman, B.A., and D.E. Woodward 2002.Variable-source area controls on phosphorus transport: Bridging the gap between research and design. Journal of Soil and Water Conservation 57(6): 534–543.

Gunter, A., Seibert, J., and S. Uhlenbrook. 2004. Modeling spatial patterns of saturated areas: an evaluation of different terrain indices. Water Resources Research 40: W0114.

Haith, D.A., and L.L. Shoemaker. 1987. Generalized watershed loading functions for stremflow nutrients. Water Resources Research 23(3): 471–478.

Heathwaite, A.L., and P.J. Johnes. 1996. The contribution of nitrogen species and phosphorus fractions to stream water quality in agricultural catchments. Hydrological Processes 10: 971–983.

Hewlett, J.D., and A.R. Hibbert. 1967. Factors affecting the response of small watersheds to precipitation in humid regions. In: Forest Hydrology (Sopper WE, Lull HW, eds.). Pergamon Press, Oxford.

Hewlett, J.D., and W.L. Nutter. 1970. The varying source area of streamflow from upland basins, Proceedings of the Symposium on Interdisciplinary Aspects of Watershed Management. Bozeman, MT. ASCE, New York, pp. 65–83.

Hjelmfelt, A.T. 1980. Curve number procedure as infiltration method. Journal of Hydrology 106: 1107 –1111.

Horn, B.K.P. 1981. Hill shading and the reflectance map. Proceedings of the IEEE 69(1): 14- 47.

Horton, R.E. 1933. The role of infiltration in the hydrologic cycle. Transactions American Geophysical Union 14: 446–460.

Horton, R.E. 1940. An approach toward a physical interpretation of infiltration capacity. Soil Science Society of America Proceedings 4: 399–417.

Hursh, C.R. 1944. Report of the subcommittee on subsurface flow. Transactions of the American Geophysical Union 25: 743–746.

Kunkel, K.E., Andsager, K., and D. Easterling. 1999. Long-term trends in extreme precipitation events over the conterminous United States and Canada. Journal of Climate 12: 2515–2527.

Lyon, S.W., Gérard-Marchant, P., Walter, M.T., an T.S. Steenhuis. 2004. Using a topographic index to distribute variable source area runoff predicted with the SCS-Curve Number equation. Hydrological Processes 18(15): 2757–2771.

Lyon, S.W., Lembo, A.J., Walter, M.T., and T.S. Steenhuis. 2006a. Defining probability of saturation with indicator kriging on hard and soft data. Advances in Water Resources 29: 181–193.

Lyon, S.W., Seibert, J., Lembo, A.J., Walter, M.T., and T.S. Steenhuis. 2006b. Geostatistical investigation into the temporal evolution of spatial structure in a shallow water table. Hydrology and Earth System Sciences 10: 113–125.

Nash, J.E., and J.V. Sutcliffe. 1970. River flow forecasting through conceptual models, Part 1 — a discussion of principles. Journal of Hydrology 10: 282–290.

Mehta, V.K., Walter, M.T., Brooks, E.S., Steenhuis, T.S., Walter, M.F., Johnson, M., Boll, J., and D. Thongs. 2004. Application of SMR to modeling watersheds in the Catskill mountains. Environmental Modeling and Assessment 9: 77–89.

Mortsch, L.D., and F.H. Quinn. 1996. Climate change scenarios for Great Lakes basin ecosystem studies. Limnology and Oceanography 41(5): 903–911.

O'Loughlin, E.M. 1986. Prediction of surface saturation zones in natural catchments by topographic analysis. Water Resources Research 22: 794–804.

Rallison, R.K. 1980. Origin and evolution of the SCS runoff equation. In Proceedings of Symposium on Watershed Management, 21–23 July, Boise, ID. American Society of Civil Engineers: New York, NY, 912–924.

Rao, N.S., Easton, Z.M., Schneiderman, E.M., Zion, M.S., Lee, D.R., and T.S. Steenhuis. 2009. Modeling Watershed-Scale Effectiveness of Agricultural Best Management Practices to Reduce Phosphorus Loading. Journal of Environmental Management 90: 1385-1395.

Schneiderman, E.M., Steenhuis, T.S., Thongs, D.J., Easton, Z.M., Zion, M.S., Mendoza, G.F., Walter, M.T., and A.L. Neal. 2007. Incorporating variable source area hydrology into the curve number based Generalized Watershed Loading Function model. Hydrological Processes 21: 3420–3430, : 10.1002/hyp6556.

Steenhuis, T.S., and W.H. van der Molen. 1986. The Thornthwaite-Mather Procedure as a Simple Engineering Method to Predict Recharge. Journal of Hydrology 84: 221–229.

Steenhuis, T.S., Winchell, M., Rossing, J., Zollweg, J.A., and M.F. Walter. 1995. SCS Runoff Equation Revisited for Variable-Source Runoff Areas. ASCE Journal of Irrigation and Drainage 121: 234–238.

Tarboton, D.G. 1997 A new method for the determination of flow directions and contributing areas in grid digital elevation models. Water Resources Research 33(2): 309–319.

Thornthwaite, C.W., and J.R. Mather. 1955. The water balance. Pub. No. 8, Laboratory of Climatology, Centerton, NJ.

USDA. 1980. CREAMS —a Field Scale Model for Chemicals, Runoff, and Erosion from Agricultural Management Systems. Science and Education Administration, Congressional Research Report 26, U.S. Department of Agriculture: Washington, DC.

USDA-SCS (Soil Conservation Service). 1972. National Engineering Handbook, Part 630 Hydrology, Section 4, Chapter 10.

Walter, M.T., Walter, M.F., Brooks, E.S., Steenhuis, T.S., Boll, J., and K.R. Weiler. 2000. Hydrologically sensitive areas: Variable Source Area hydrology implications for water quality risk assessment. Journal of Soil and Water Conservation 55(3): 277–284.

Walter, M.T., Brooks, E.S., Walter, M.F., Steenhuis, T.S., Scott, C.A., and J. Boll. 2001. Evaluation of soluble phosphorus transport from manure-applied fields under various spreading strategies. Journal of Soil and Water Conservation 56(4): 329–336.

Walter, M.T., Mehta, V.K., Marrone, A.M., Boll, J., Steenhuis, T.S., and M.F. Walter. 2003. Simple estimation of prevalence of Hortonian flow in New York City watersheds. ASCE Journal of Hydrology and Engineering. 8(4): 214–218.

Western, A.W., Grayson, R.B., and G. Blöschl. 2002. Scaling of soil moisture: a hydrologic perspective. Annual Reviews in Earth Planetary Science 205: 20–37.

Young, R.A., Onstad, C.A., Boesch, D.D., and W.P. Anderson. 1989. AGNPS—a nonpoint-source pollution model for evaluating agricultural watersheds. Journal of Soil and Water Conservation 44(2): 168–173.

CHAPTER 5

A WEB-BASED DECISION SUPPORT SYSTEM TO FORECAST HYDROLOGICALLY SENSITIVE AREAS

Abstract

In order to reduce the risk of nonpoint source pollution from agricultural fields, it is important to know where runoff-producing areas are in the landscape. In the northeastern U.S., hilly topography and shallow, permeable soils play central roles in controlling where saturated soils conditions and associated runoff generation occur in the landscape. These areas of the landscape are termed hydrologically sensitive areas (HSA). Where agricultural lands coincide with HSAs there is a potential risk of contaminant transport to streams during rainfall events. Watershed management in this region is often too static to account for the highly variable, spatio-temporal dynamics of HSAs. In this paper we present a web-based decision support system (DSS), HSA-DSS, displaying maps of HSAs in the landscape that are predicted with a hydrologic model and ensemble atmospheric forecasts of weather conditions. The HSA-DSS utilizes the ArcIMS GIS platform, implemented using a web server, Java virtual machine, and servlet engine technology to support data access and a dynamic display of geospatial information. The ArcIMS application server has been coupled with a hydrologic assessment tool that predicts current conditions as well as 48-hr forecasted HSA locations and updates HSA maps displayed in the DSS using a management interface programmed in Python. As a proof of concept, a prototype of this HSA-DSS was developed to simulate runoff generation and HSAs in the Salmon Creek watershed, NY. We intend to apply the HSA-DSS to other watersheds in central NY to enable producers and environmental planners to better plan the day-to-day locations

and timing of nutrient and pesticide applications to reduce potential non-point source contamination of water bodies.

5.1 Introduction

Nonpoint source pollution (NPS) from agricultural activity contributes substantially to surface water quality degradation in the United States (Puckett, 1995; Ekholm et al., 2000; Sharpley et al., 2001; Andraski and Bundy, 2003). During the last 30 years various environmental standards (e.g. NRCS 590 standard, Phosphorus Index) and watershed management practices have been implemented in an attempt to reduce NPS of surface water bodies but have been found in practice to be highly variable in their effectiveness (Brannan et al., 2000; Lee et al., 2000; Gitau et al., 2006). This is partly because their "demonstrated" effectiveness is based on simplified watershed-scale models that do not consider the spatial variability of natural landscapes (e.g., Sorrano et al., 1996; Walter et al., 2001; Santhi et al., 2003, Walter and Shaw, 2005). Thus, tools are needed that capture this spatial variability and can help producers and watershed managers better assess and plan management to reduce NPS pollution based on proven scientific principles.

The effectiveness of watershed management practices to reduce NPS pollution is influenced by numerous, interrelated factors, such as landscape position, soil chemical, physical and microbial characteristics, land use, hydrology, meteorology, and pollutant transport and transformation properties. Given this multitude of controlling factors, it is perhaps unsurprising that early attempts to control NPS pollution were not consistently effective because they were largely based on historical soil conservation practices (Walter et al., 1979; Clark et al., 1985; Walter et al., 2000; Novotny, 2003; Walter et al., 2003). During the 1990s, so-called Source Control Best

Management Practices (BMPs) were introduced to reduce nutrient and pesticide contamination (McKell and Peiretti, 2004); these BMPs were based on the scientific evidence that certain parts of the landscape contribute proportionally greater pollutant loads with storm water than other parts (Pionke et al., 1996; Haygarth et al., 1998; Easton et al., 2008a).

Source Control BMPs can be especially effective in regions where storm runoff is principally governed by saturation excess (Hewlett and Hibbert, 1967; Dunne and Black, 1970). In regions like the northeastern U.S., saturation excess occurs primarily where there is a sufficiently large, often steep, upslope area that contributes drainage too rapidly for the local soil hydraulics to accommodate; additionally, shallow restrictive subsoil layers (hardpans or bedrock) are nearly ubiquitous and prevent downward drainage, which also promotes saturation excess. These saturated areas expand and contract from storm to storm, as well as seasonally and, thus, are referred to as variable source areas (VSAs) (Dunne and Leopold, 1978; Walter et al., 2000; Srinivasan et al. 2002; Walter et al. 2003; Needleman et al. 2004, Easton et al., 2007, 2008b). Where VSAs coincide with potential pollutant sources (e.g., animal manures), there is a heightened risk of NPS pollution (Walter et al., 2000; Gburek et al., 2000, 2002; Qui et al., 2007). Unfortunately, the dynamic nature of VSAs makes it difficult to consistently predict where (or when) they will occur. The concept of hydrologically sensitive areas (HSAs) was proposed to refer to parts of the landscape most prone to being VSAs (Walter et al., 2000, 2001). Hydrologically sensitive areas were defined as areas that were saturated or generate saturation excess more often than some threshold (e.g., more than 30% of the days in a month) and were identified using distributed hydrological model runs using many decades of weather data (e.g., Walter et al., 2000, 2001). Agnew et al. (2006) showed that HSAs could be regionalized using

relationships between the frequency that a point in the landscape saturates (as determined by a model) and its topographic index (see Beven and Kirkby, 1979; Ambroise et al. 1996; Walter et al. 2002), which can be determined with readily available geospatial data for most of U.S. and much of the World. Once HSAs are mapped, managers can prioritize potentially polluting activities to parts of the landscape that are not hydrologically sensitive (e.g. Walter et al., 2000, 2001; Gburek et al., 2002; Marjerison et al., 2010, in press).

The New York State (NYS) Phosphorus Runoff Index (P-Index) is an example of a water quality management tool that made an early attempt to incorporate the HSA concept. The P-Index is used in the development of farm level nutrient management plans (NMPs) to assess the vulnerability (risk) to phosphorus (P) export from agricultural fields to streams (Czymmek et al., 2003). The P loss risk is evaluated based on two factors, i) the amount of P available on a field (P source factor), and ii) the presence of potential ways of hydrological transport to the stream (P transport factor). Currently, the NYS P-Index considers HSAs based on distance from a stream, i.e., areas close to streams are more likely to saturate and generate runoff than areas farther from streams (Gburek et al., 2000, 2002; Agnew et al., 2006). Additionally, NMPs generally include consideration of seasonal hydrologic landscape dynamics and associated runoff risks (Czymmek et al., 2003). Several researchers have proposed approaches for identifying HSA-locations more precisely and accounting for month-to-month risks (Walter et al., 2000; Agnew et al., 2006; Marjerison et al., 2010, *in press*) or even on a storm-size basis (e.g., Gburek et al., 2000, 2002; Shaw and Walter, 2009). However, these approaches have not been widely adopted, probably because they require GIS and, sometimes, hydrological modeling expertise, which is not ubiquitously available to nutrient managers and conservation planners.

This paper presents our prototype, web-based, decision support system (DSS) to assist producers and planners in quickly identifying fields or portions of fields at high risk of generating storm runoff (i.e., HSAs) so that those areas can be avoided from potentially polluting activities. Furthermore, this HSA-DSS uses real-time weather forecasts so that HSAs are not based on long-term average conditions, as previously proposed (Walter et al., 2000, 2001; Agnew et al., 2006), but current and forecasted conditions. We first describe the structure and implementation of the HSA-DSS within ArcIMS (ESRI, 2005a, b) that fully integrates a hydrologic assessment tool to predict daily saturated and runoff generating areas. The HSA-DSS is designed to function as a guidance tool for farmers and planners in the daily decision of nutrient (e.g. manure, fertilizer) and pesticide applications. To enhance the supportive capabilities of the HSA-DSS we use the hydrologic assessment tool to predict current conditions, using the Northeastern Regional Climate Center (NRCC) weather data, as well as 24-48 hr forecasted VSA dynamics based on NOAA GFS MOS (National Oceanic and Atmospheric Administration Global Forecast System Model Output Statistic) ensemble temperature and precipitation data. We present a test of our prototype HSA-DSS in the Salmon Creek watershed in central New York State.

5.2 HSA-DSS architecture

The HSA-DSS application is based on the ArcIMS 9.2 software (ESRI Inc.), which provides a highly scalable framework for GIS Web publishing. We integrated a geospatial database, a hydrologic assessment tool (Steenhuis et al., 1995; Lyon et al., 2004; Collick et al., 2006; Dahlke et al., 2009) and a hydrologic forecast module into the ArcIMS framework of the HSA-DSS (Antolik and Baker, 2009) (Fig. 5.1) to provide a user-friendly interface for the access of scientific predictions of runoff generation and hydrologic solute transport without the need for local model calibration

by the user. The integrated HSA-DSS is developed for standard Internet browser and allows a dynamic display of maps and geospatial data that is updated daily based on the VSA predictions estimated with the hydrologic assessment tool. Below we describe in detail the design and functionality of the three main components of the HSA-DSS, *i)* the hydrologic assessment tool, *ii)* the hydrologic forecast module, and *iii)* the presentation tier of the HSA-DSS.

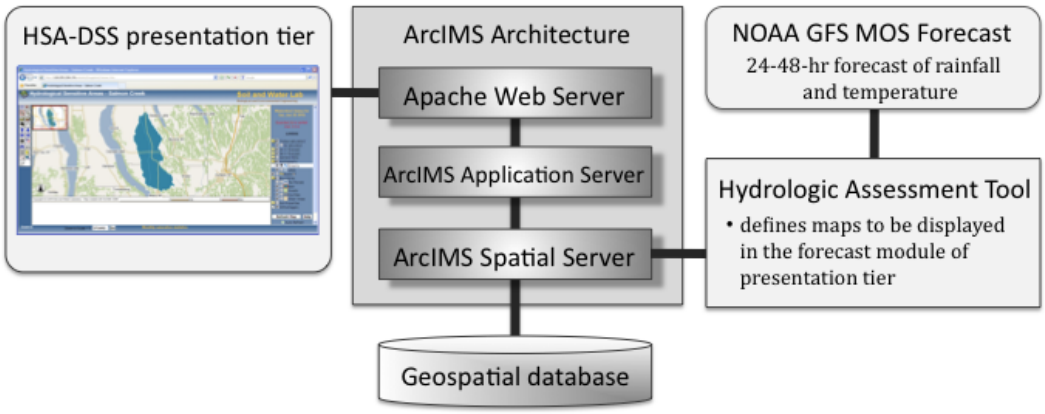

Figure 5.1: Integrated system components of the HSA-DSS.

5.2.1 Hydrologic Assessment tool

The developed HSA-DSS is connected to a pre-calibrated (watershed specific) hydrologic assessment tool (HAT) that is invisible to the DSS user. The hydrologic assessment tool represents the integration of several standard hydrologic models used to predict VSA dynamics and runoff generation in watersheds dominated by saturation excess overland flow (Collick et al., 2006; Dahlke et al., 2009). The model operates on a daily time step and predicts daily total streamflow, saturation excess runoff (or quickflow in terms of Hewlett and Hibbert, 1967) and the percentage of the watershed that is "saturated" and generating runoff during storm events (note, we use the term saturated areas and runoff generating areas interchangeably recognizing that the soil may not need to be fully saturated to generate storm runoff) using the Soil

Conservation Service-Curve Number (SCS-CN) equation (Eq. 4.1) (Steenhuis et al. 1995). The tool uses readily available inputs (precipitation, minimum and maximum temperature) as well as topography (digital elevation model) and soil characteristics (soil depth and saturated hydraulic conductivity) to distribute and locate saturated areas in the landscape with the soil topographic index (Beven and Kirkby, 1979; Ambroise et al., 1996; Walter et al., 2002; Agnew et al., 2006; Lyon et al., 2006a, b; Easton et al., 2008b; Dahlke et al., 2009). The mathematical formulation of HAT is described in chapter 4 and is essentially a compilation of methods used in Collick et al. (2006), Easton et al. (2007), Schneiderman et al. (2007), and Dahlke et al. (2009). Data inputs (i.e. GFS MOS (Global Forecast System Model Output Statistic) forecasted climate data) and model outputs of HAT are interfaced with the ArcIMS framework via a Python script.

The HSA-DSS uses past temperature and precipitation time series data to simulate current soil moisture patterns across a watershed. The system also uses the current weather predictions and those for the next 24-48 hr to simulate soil moisture and associated storm runoff for "today," "tomorrow," and "the next day". The HAT model output results in the estimation of the fraction of the watershed (A_f) (Eq. 4.4) that will potentially saturate and generate runoff. To simplify the presentation of this information to the user of the HSA-DSS the predicted watershed fractions are summarized in ten-percent incremental classes (e.g. 10%, 20%, 30% etc.), shown as red areas on top of air photographs (Fig. 5.4). For more general risk information, the user can also view each potential ten-percent (see section 5.2.3) runoff risk class (e.g. 90%) in the watershed, which is provided by separate "General HSA" layers in the presentation tier of the HSA-DSS (Fig. 5.4).

5.2.2 Hydrologic forecast module

The 24-48 hr hydrologic forecast of HSA dynamics is using contents of the Model Output Statistics (MOS) (Glahn and Lowry, 1972) extended-range alphanumeric messages generated with the Global Forecast System (GFS). GFS forecasts are released through the National Weather Service via online providers such as NOAA. The messages contain forecasts of different meteorological parameters such as maximum daytime and minimum nighttime temperature, wind speed, probability and quantity of precipitation, snow, and mean total sky cover that are valid over at least a 12-h period (Fig. 5.2).

```
KITH   GFSX MOS GUIDANCE   7/01/2010  0000 UTC
FHR  24| 36  48| 60  72| 84  96|108 120|132 144|156 168|180 192
THU  01| FRI 02| SAT 03| SUN 04| MON 05| TUE 06| WED 07| THU 08 CLIMO
X/N  68| 45  73| 52  84| 56  87| 61  89| 63  89| 65  85| 60  81 57 79
TMP  61| 53  66| 61  74| 65  77| 69  79| 70  79| 71  75| 67  73
DPT  49| 47  53| 52  57| 57  59| 61  65| 63  65| 64  63| 61  62
CLD  CL| CL  CL| CL  CL| CL  CL| CL  PC| PC  PC| OV  PC| PC  PC
WND  14|  7   8|  3   8|  4   9|  3   8|  4   7|  4   8|  6   8
P12   6|  2   0|  3   0|  8   7|  9  13| 20  25| 27  33| 35  38999999
P24    |      2|      4|      8|     14|     29|     46|     53   999
Q12   0|  0   0|  0   0|  0   0|  0   0|  0   0|  0   0|
Q24    |      0|      0|      0|      0|      0|      0|
T12   2|  0   9|  3   9|  3   0|  2  12| 13  29| 16  25| 18  21
T24    |  2    |  9    |  9    |  4    | 26    | 34    | 34
```

Figure 5.2: Sample message of the Global Forecast System (GFS) Model Output Statistic (MOS) for the Ithaca, NY climate station. Elements used in the forecast module of the HSA-DSS are FHR = forecast hour, X/N = daytime max, nighttime min temperature, P24 = 24-hr probability of precipitation, and Q24 = 24-hr quantitative precipitation forecast.

The GFS MOS guidance data result from the Medium Range Forecast (MRF) run of the NCEP's (National Centers for Environmental Prediction) Global Spectral Model (Kanamitsu, 1989), which has been referred to as the Global Forecast System (GFS) model since 2002 (Maloney et al., 2010). The medium range MOS guidance provides projections of 24 to 192 hours for most weather elements (Fig. 5.2). The extended-

range GFS-based alphanumeric message is published twice a day at 0000 and 1200 UTC (Universal Time Coordinate) for approximately 1,693 sites in the contiguous United States and Alaska (Maloney et al., 2010).

Only three parameters, the 24-hr quantitative precipitation forecast (Q24), the 24-hr probability of precipitation (P24), and the predicted maximum daytime and minimum nighttime temperature (X/N) are used in the hydrologic forecast module of the HSA-DSS. The MOS guidance for liquid-equivalent precipitation accumulated during a 24-hr period is given in categorical form in the alphanumerical message (Table 5.1). To convert the quantitative precipitation forecast into actual precipitation amounts the maximum value of the precipitation range predicted with the category number used as precipitation input into HAT.

Table 5.1: Categories of the quantitative precipitation forecast provided with in the Global Forecast System alphanumerical message.

0 = no precipitation expected
1 = 0.01 – 0.09 inches
2 = 0.10 – 0.24 inches
3 = 0.25 – 0.49 inches
4 = 0.50 – 0.99 inches
5 = 1.00 – 1.99 inches
6 = ≥ 2 inches

Likewise the maximum predicted daytime and minimum nighttime temperature for the 24-hr and 48-hr period is extracted from the message and added to the existing time series of meteorological input data for the hydrologic assessment tool. In addition, the probability of precipitation (P24) is extracted from the alphanumerical message and parsed into a HTML file with the Python script that gives a short text summary of expected rainfall amounts and hydrologic conditions in the watershed (Fig. 5.5). The P24 forecast publishes the probability that 0.01 inches or more of liquid-equivalent

precipitation occur during a 24-hr period. If the probability reaches values greater than 50% the predicted maximum precipitation amount is added to the precipitation time series used in the hydrologic assessment tool to predict future HSA extends.

5.2.3 Presentation tier of the HSA-DSS

When consulting the HSA-DSS web site to locate HSAs or to retrieve weather updates for the next 24-48 hours, the user is presented with the page depicted in Fig. 5.3 (http://www.hsadss.bee.cornell.edu/Website/SalmonCreek/viewer.htm). The page provides standard interface features such as a main map display, an overview map, a tool bar, a layer list and legend frame, as well as a query and feature information retrieval I/O window (Fig. 5.4). For geospatial information control, the frame on the right side of the window shows in the top three layers the daily updated HSA forecast maps for "today", "tomorrow" and "the next day". These areas are ultimately visible to the user as red areas in the display window when the HSA-DSS web site is consulted and the user has zoomed into an area of interest with a scale of less than 1:100,000 (Fig. 5.4). If the hydrologic assessment tool predicts runoff-generating areas of zero percent in the total watershed area HSAs are not displayed on the map and the message "no saturation!" appears next to each forecast layer.

Below the three layers the HSA-DSS lists static layers that provide more general information such as the potential HSA risk maps, administrative boundaries or physical characteristics of the target watershed. At the top of the frame a hyperlink (highlighted in yellow) opens the "status report" window that informs the user about the current and forecasted hydrologic and weather conditions in the area (Fig. 5.5). Below the yellow highlighted link a news-feed informs the user about the most-up-to-date forecast of expected rainfall amounts within the next 24 hours (Fig. 5.4).

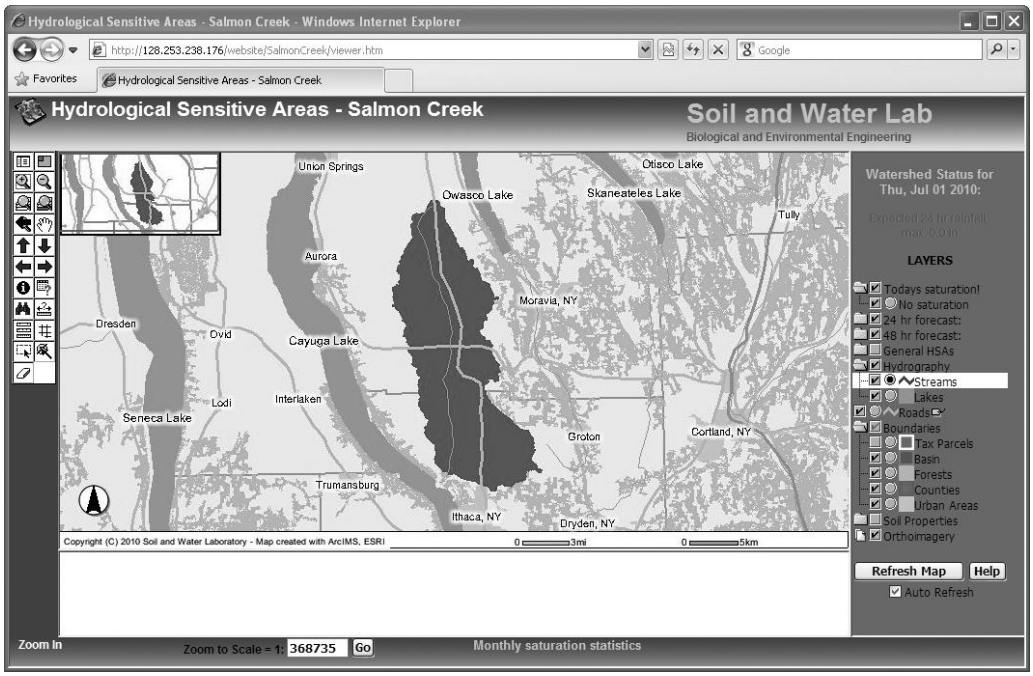

Figure 5.3: Presentation tier and start page of the HSA-DSS.

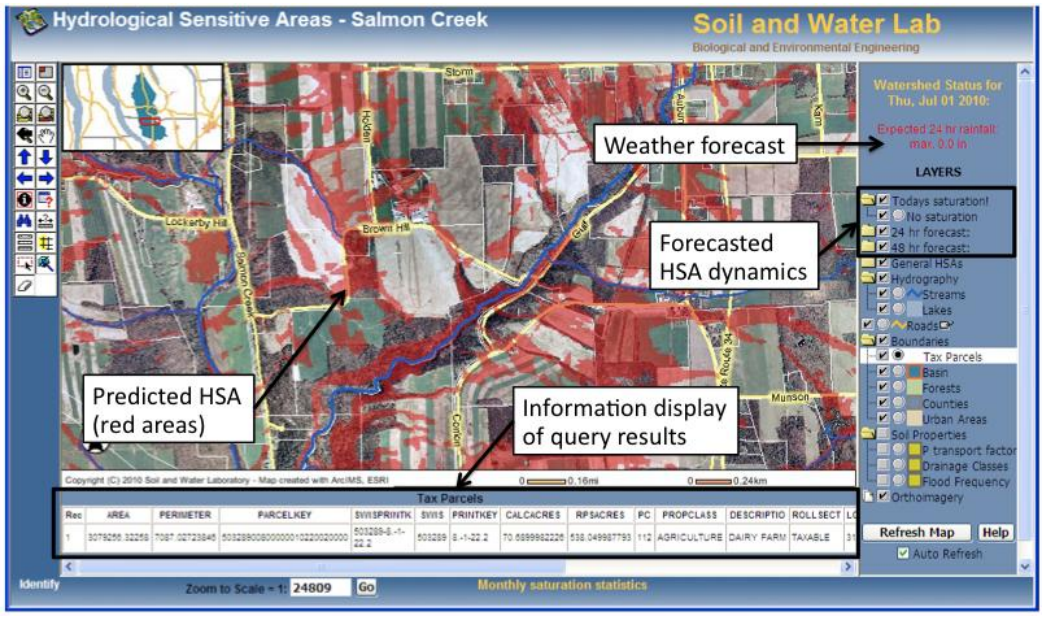

Figure 5.4: Presentation tier of the HSA-DSS. Red areas show HSA predicted with the hydrologic assessment tool. A daily update of forecasted weather conditions and HSA dynamics in Salmon Creek watershed is given in the top of the right frame.

The remaining layers display geospatial data sets comprising general HSA information, hydrography (e.g. rivers and lakes), infrastructure (e.g. roads), administrative boundaries and areas (e.g. county or tax parcel boundaries), soil property maps (e.g. flood frequency, soil drainage), and ortho-images containing the air photographs for the area of interest. Each geospatial data set listed in the layer list can be controlled to either toggle visibility, select, query, or identify features within the display window using the toolbar on the left side of the HSA-DSS. The geospatial datasets provided in the HSA-DSS are intended to help the user identify their general area of interest and to retrieve property and field boundary information (e.g. via tax parcel code) and physiographic information (e.g. soil characteristics, rivers and creeks) required in the NYS P-Index to estimate the nutrient loss risk from specific fields.

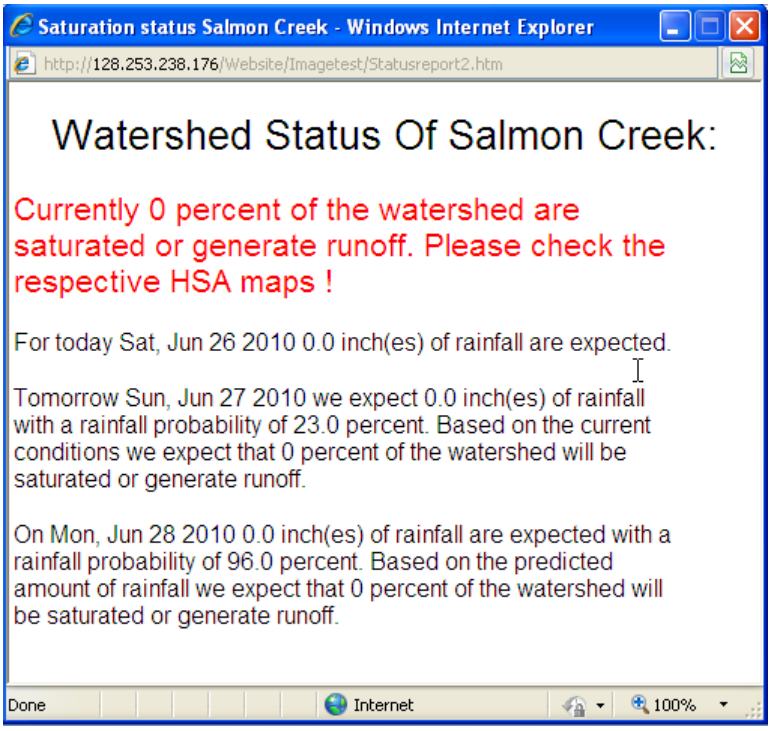

Figure 5.5: Daily updated status report showing forecasted rainfall amounts, rainfall probability and expected percent area of the watershed that could saturate or generate runoff.

5.3 Application of HSA-DSS: Proof of Concept

As a proof of concept, a prototype HSA-DSS was developed for the 230 km^2 Salmon Creek watershed (Fig. 5.6), located north of Ithaca, NY. The watershed is located in the glaciated Allegheny Plateau physiographic region. The annual average temperature is 8°C, average annual precipitation is 93 cm, with 173 cm of snowfall annually. Land use consists of 70% agricultural land, 28% mixed forest, and the remaining 2% is residential, commercial, and urban. Soils are generally silt loams and gravelly silt loams, 200 cm deep (Soil Survey Staff NRCS-USDA). Elevations range from 320 to 378 m. The watershed exhibits typical HSA type hydrology due to the shallow highly permeable soils overlaying a dense fragipan at a shallow depth (Marjerison et al., 2010, in press).

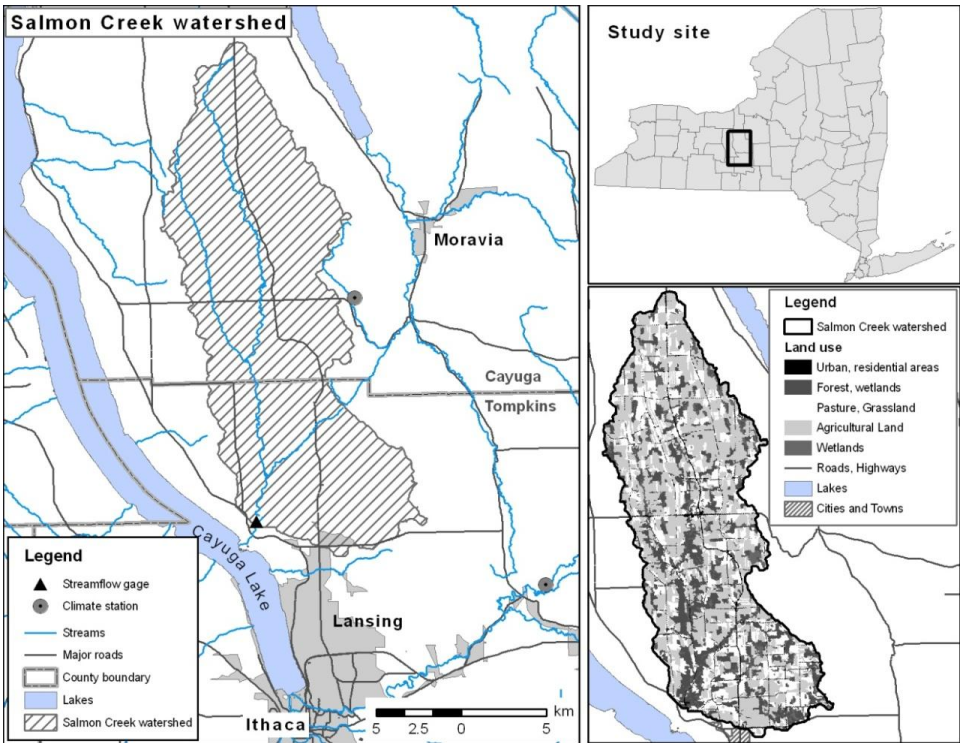

Figure 5.6: Location and characteristics of Salmon Creek watershed.

5.3.1 Geospatial database for Salmon Creek

A geospatial database was developed for the HSA-DSS containing image raster and vector data for Salmon Creek watershed and surrounding areas. Table 5.2 provides a summary of the geospatial dataset characteristics and sources. All data displayed in the HSA-DSS are projected in UTM coordinates, Zone 18 with the North American Datum 1983. The geospatial database developed for Salmon Creek watershed is comprised of 63 layers including air-photo imagery, ArcGIS data (shapefiles), and derived features such as the HSA maps. Datasets in the database are only available for interrogation to users and no modification of existing data is made.

Table 5.2: Multisource geospatial database developed for the HSA-DSS.

Data	Resolution/ Scale	Source	Description
Air photographs	2 m	NY State GIS Clearinghouse	Natural color image. Cayuga County 2007, Tompkins County 2006.
DEM	10 m	NYS DEC, USGS (distributed via http://cugir.mannlib.cornell.edu)	Elevation, slope, flow direction, flow accumulation, HSAs
Forest	30 m	Multi-Resolution Land Characteristics (MRLC) Consortium	Land Use, Land Cover data set, 2001
Lakes	1:2,000,000	National Atlas, New York State	Lakes and surface water bodies
Roads	1:100,000	U.S. Census Bureau (distributed via http://cugir.mannlib.cornell.edu)	
Soils	1:15,840 (Cayuga County) 1:20,000 (Tompkins County)	SSURGO (USDA-NRCS Soil Data Mart)	Soil depth, saturated hydraulic conductivity, drainage class, flood frequency
Streams	1:100,000	U.S. Census Bureau (distributed via http://cugir.mannlib.cornell.edu)	Hydrography
Tax Parcels	1:10,000	Tompkins County and Cayuga County Clerk's Office (distributed via http://cugir.mannlib.cornell.edu)	Municipal Tax Parcels (year 2000)
Urban areas	1:100,000	U.S. Census Bureau (distributed via http://cugir.mannlib.cornell.edu)	Urbanized areas and municipalities

A 10 m USGS digital elevation model (DEM) obtained from the USDA-NRCS data gateway was used to delineate the Salmon Creek watershed boundary, which defines the main modeling unit for HAT. HSA maps were likewise derived from the DEM using the soil topographic index method (Eq. 4.5) described by Agnew et al. (2006) and Dahlke et al. (2009). The continuous raster map of the soil topographic index was reclassified in ArcGIS (ESRI Inc.) into ten equal-area classes, each covering ten percent of the Salmon Creek watershed. The wettest 10% of the watershed, predicted by the hydrologic assessment tool as the most frequently saturating and runoff-generating parts of the landscape, were associated with the highest values in the soil topographic index map. If a storm runoff event causes 20% of the watershed to saturate or generate runoff, based on the prediction with the hydrologic assessment tool, red HSA maps covering the wettest 0-20% of the watershed are automatically displayed to the user.

5.3.2 Model calibration and validation

HAT for the Salmon Creek watershed uses weather data from two NRCC weather stations located in Locke (42.67 N, 76.47 W) and Freeville (42.52 N, 76.33 W), NY. Predicted streamflow was calibrated and validated using observed stream gage data from the USGS gage in Ludlowville, NY (42.55 N, 76.53 W. HAT was calibrated for Salmon Creek watershed using observed streamflow and climate data for the period July 2006 to December 2008. Streamflow data observed since January 2009 were used to validate the model performance. The coefficient of determination (r^2) for the linear regression between daily observed and predicted streamflow for the calibration period is $r^2 = 0.85$ and Nash-Sutcliffe efficiency (E) (Nash and Sutcliffe, 1970) is $E = 0.72$ and for the validation period $r^2 = 0.83$ and $E = 0.67$ respectively.

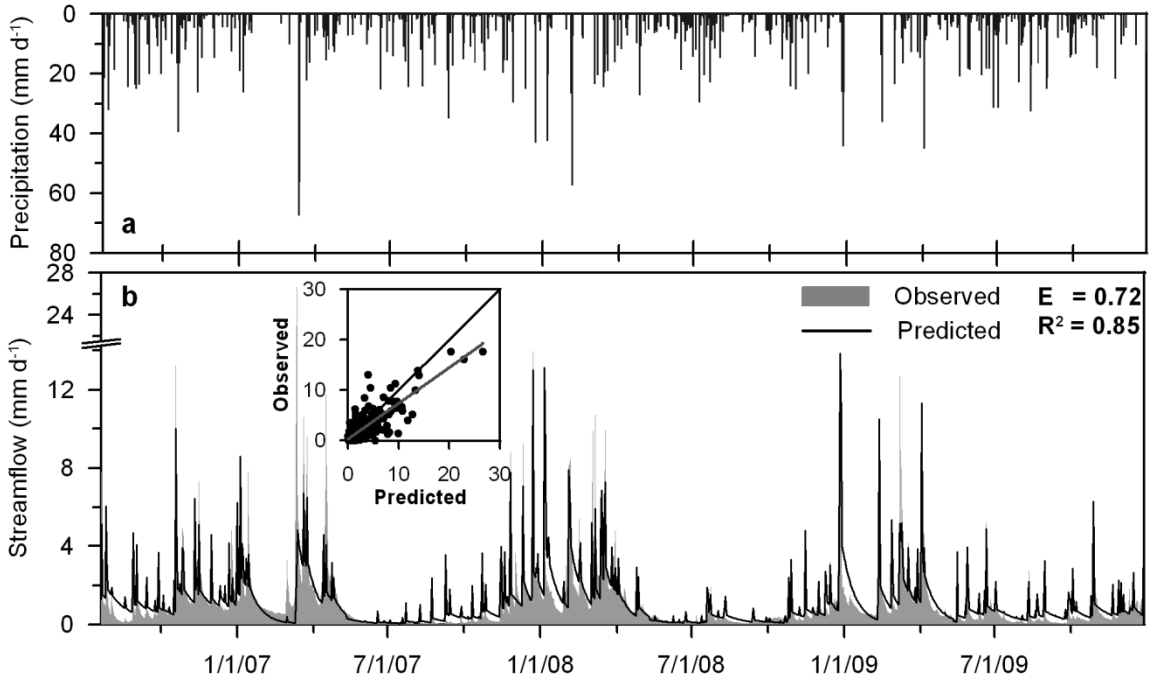

Figure 5.7: Precipitation (a), and measured and modeled discharge (b) for the water balance model of Salmon Creek watershed from July 2006 to January 2010.

Table 5.3 summarizes statistical evaluation measures for the comparison between observed and predicted streamflow for each hydrological season since summer 2006. Streamflow was generally well predicted during the entire modeling period (Fig. 5.7) and particularly well predicted during the wet winter months. During this period the majority of total and dissolved P is exported from watersheds in the humid northeastern U.S. (Edwards and Owens, 1991; Pionke et al., 1999; Smith et al., 1991; Vanni et al., 2001

Table 5.3: Summary of seasonal and yearly observed and predicted streamflow of Salmon Creek watershed.

Period[a]	Predicted			Observed			E[b]	r^2[c]
	Minimum mm d^{-1}	Mean mm d^{-1}	Maximum mm d^{-1}	Minimum mm d^{-1}	Mean mm d^{-1}	Maximum mm d^{-1}		
Summer 2006	0.52	1.48	10.03	0.11	1.23	13.25	0.64	0.81
Winter 2006-2007	0.08	1.81	17.62	0.53	2.33	26.71	0.69	0.86
Summer 2007	0.06	0.38	3.66	0.02	0.23	1.63	0.57	0.62
Winter 2007-2008	0.39	2.24	17.63	0.14	2.28	20.3	0.65	0.81
Summer 2008	0.08	0.32	3.3	0.04	0.33	3.33	0.61	0.81
Winter 2008-2009	0.25	1.7	13.87	0.21	1.56	13.78	0.69	0.84
Summer 2009	0.14	0.72	6.29	0.05	0.52	5.23	0.46	0.78
Calibration period[d]	0.06	1.24	17.63	0.02	1.28	26.71	0.72	0.85
Validation period[e]	0.14	1.08	11.33	0.00	0.94	12.72	0.67	0.83
Entire Period	0.01	1.43	18.8	0.02	1.54	26.7	0.72	0.85

[a] Summer is May-October. Winter is November-April.

[b] Nash-Sutcliffe comparison with measured streamflow.

[c] Coefficient of determination comparison with measured streamflow.

[d] Calibration period is 21 July, 2006 – 31 December, 2008.

e Validation period is 01 January – 31 December 2009.

5.3.3 Hydrologic forecast for Salmon Creek watershed

For the 24-48 hr forecast of HSA dynamics of Salmon Creek temperature and precipitation data from the GFS MOS guidance dataset are used. The closest available GFS MOS site to Salmon Creek watershed is the Ithaca airport station (KITH) (42.48 N, 76.47 W), approximately 10 km southeast of the Salmon Creek stream gage. The station's coefficient of determination (r^2) values for the linear regression of daily temperature data with the two NRCC stations in Locke and Freeville are both $r^2 = 0.99$ (n = 1613, p = 0.00). The coefficient of determination values of regressed daily precipitation data are $r^2 = 0.82$ (n = 1613, p = 0.0005) and $r^2 = 0.86$ (n=1613, p = 0.015), respectively. Temperature and precipitation time series data for the future 24-48 hrs are daily updated at 4:00 AM local time with GFS MOS forecasted data from the KITH station, while current and past time series data used in the HAT are

updated with temperature data from the NRCC station in Freeville, NY and precipitation data from the NRCC station in Locke, NY.

5.3.4 Predicted saturation dynamics

We used the calibrated HAT to determine long-term monthly saturation dynamics in the Salmon Creek watershed that can be accessed by the user through a hyperlink in the bottom frame of the HSA-DSS (Fig. 5.3). Average moisture and runoff conditions in Salmon Creek show, in general, a high level of seasonal variability. For each month the probability of saturation can be estimated by taking the ratio of the number of days for which a location within the watershed is saturated to the total number of rainfall-days (Walter et al., 2000; Lyon et al., 2004). The number of saturation days is predicted with the HAT; the number of precipitation days is taken from climate stations in Locke and Freeville, NY. The probability of saturation shown in Table 5.4 and Fig. 5.8 present monthly and annual averages estimated over the period July 2006 to December 2009. The months December-March are on average the wettest months of the year where more than 50% of the rainfall and snowmelt events cause the whole watershed to saturate. During October, November, and April 25% of the rainfall events cause the entire watershed area to contribute runoff. Only during the drier summer months (May-August) does the saturation probability decreases below 25%, with May being the driest month and July being the wettest summer month on average (Table 5.4). The annual probability of saturation shows that the wettest 10% of the watershed saturate and generate runoff for more than 50% of the annual rainfall events. The remaining areas of the watershed have the potential to transport nutrients and pollutants to streams, on average, in over 25% of the rainfall events.

Table 5.4: Probability of saturation for each 10% fractional area in Salmon Creek watershed as predicted by the hydrologic assessment tool.

	Fraction of the total watershed area										
	Wettest									Driest	
	10%	20%	30%	40%	50%	60%	70%	80%	90%	100%	Average number of rainfall days
Jan	0.94	0.94	0.94	0.94	0.94	0.94	0.94	0.94	0.94	0.94	7.9
Feb	0.71	0.71	0.71	0.71	0.71	0.71	0.71	0.71	0.71	0.71	3.5
March	0.82	0.82	0.82	0.82	0.82	0.82	0.76	0.76	0.76	0.76	8.5
Apr	0.62	0.55	0.41	0.41	0.38	0.38	0.38	0.38	0.38	0.38	14.5
May	0.05										10.0
June	0.29	0.16	0.03								15.5
July	0.36	0.31	0.26	0.24	0.24	0.19	0.19	0.17	0.12	0.10	18.1
Aug	0.26	0.21	0.14	0.09	0.07	0.02	0.02	0.02	0.02	0.02	14.3
Sept	0.42	0.28	0.22	0.22	0.22	0.22	0.11	0.11	0.11	0.11	12.0
Oct	0.61	0.57	0.46	0.41	0.37	0.37	0.35	0.28	0.22	0.22	15.3
Nov	0.55	0.50	0.50	0.50	0.50	0.50	0.50	0.50	0.48	0.23	13.3
Dec	0.77	0.73	0.73	0.68	0.68	0.68	0.68	0.68	0.68	0.68	7.3
Year	0.51	0.44	0.38	0.36	0.35	0.34	0.32	0.31	0.29	0.26	140.3

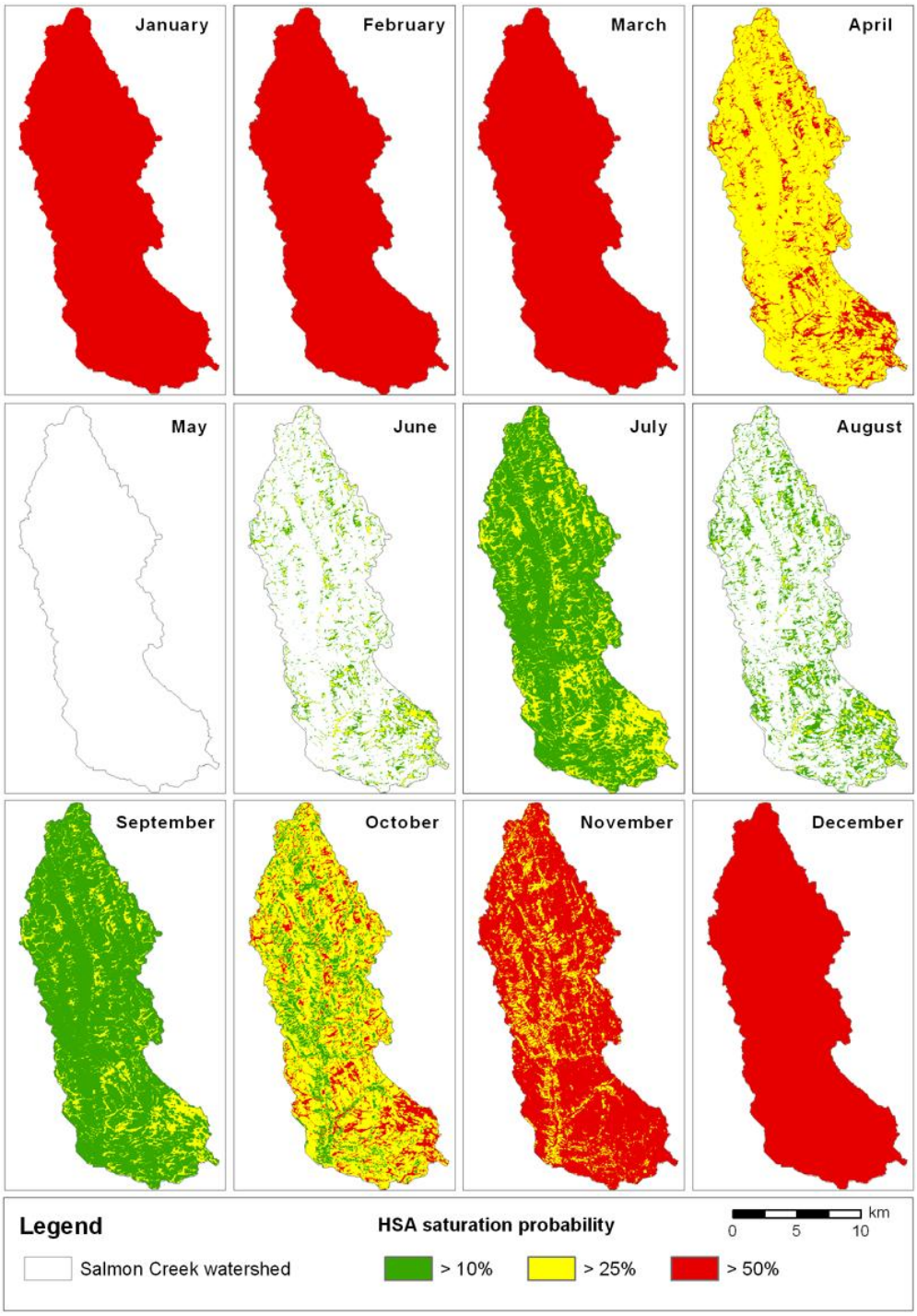

Figure 5.8: Monthly probability of saturation for Salmon Creek watershed. For each month the fraction is shown that saturates or generates runoff in more than 50% (red areas), 25% (yellow areas), 10% (green areas), and 0% (white areas) of the rainfall events.

5.3.5 Management implications and conclusions

The HSA-DSS presented in this paper integrates a hydrologic assessment tool and a 24-48 hr forecast mode of saturation dynamics into the industry-standard Internet mapping software ArcIMS. The HSA-DSS is aimed at identifying and displaying specific parts of the landscape that show a high risk of transport of agricultural chemicals and nutrients to streams with storm runoff. The use of the ArcIMS framework provides an intuitive and user-friendly environment to learn about variable source area hydrology and its implications for non-point source pollutant transport. It also enables users to utilize the system without an in-depth knowledge of the individual components and the expertise required to calibrate the hydrologic assessment tool. The prediction of wetness conditions and saturated areas is automatically daily updated based on weather data of nearby NRCC climate stations and GFS MOS forecasted temperature and precipitation data, making it widely applicable. The framework is designed such that watershed planners and stakeholders can easily access the HSA-DSS via a web site that provides basic geographical data for orientation. The usage of the HSA-DSS requires no expertise in VSA hydrology or BMP planning.

The implementation of the HSA-DSS, as presented in this paper, identifies not only the locations of areas prone to saturation or surface runoff, but also determines the risk of NPS pollution by estimating the relative risk of saturation or runoff. The extent of HSAs is modeled based on antecedent moisture conditions and daily rainfall data within a hydrologic assessment tool that allow the usage of the HSA-DSS for the prediction of HSA dynamics and the scheduling of management activities in the watershed in real-time. The HSA-DSS can be used to locate fields with low saturation potential that could, potentially receive more liberal manure applications without

increasing the risk of NPS pollution. We find that implementing a DSS that provides real-time and 24-48 hr HSA predictions will be valuable to watershed managers and stakeholders to, for instance, schedule manure or pesticide applications more precisely; in essence this sort of tool provides another dimension to precision agricultural management. In essence, we propose that the targeting of potentially polluting activities away from HSAs constitutes a none-structural, dynamic Control Source BMP. The HSA-DSS ultimately redefines the HSA-concept such that "areas most likely to generate runoff" no longer refers to the probability based on past weather but, rather, based on current and near-forecast conditions. This is an important paradigm shift in HSAs.

In addition to being a potential component of precision agriculture, the HSA-DSS has the potential to improve transport-factor estimates in the NYS P-Index, which is used for longer-term nutrient management planning. Specifically, it can provide general geospatial data sets used to calculate the P-Index transport factor (e.g. soil drainage, flood frequency) and, more importantly, provide better and more precise information about the coincidence of fields and HSAs. Recall that the current NYS P-Index identify high-risk runoff areas based largely on proximity to a water course, which is not consistently an adequate proxy of runoff risk (Agnew et al., 2006; Marjerison et al., 2010, in press). Additionally, the current NYS P-Index transport factor is more or less static, restricting the application of manure within 30 m of a stream. Recognizing that the location where runoff occurs varies both spatially and temporally and depends on the amount of rainfall and antecedent moisture conditions in the watershed (Dahlke et al., 2009), the HSA-DSS can provide sub-field information about the month-to-month variability in hydrologic sensitivity for longer-term manure-application scheduling. Thus, using the HSA-DSS planners and farmers can achieve more

flexibility in planning applications of nutrients or pesticides based on the characteristics of the land at larger spatial and temporal scales than they currently use. However, the web-based approach provides unlimited opportunities to update the HSA-DSS continuously with new scientific findings, which will help to improve management decisions and water quality in VSA-dominated watersheds.

REFERENCES

Agnew, L., Kendall, C., Hooper, R.P., Freer, J.E., Peters, N.E., Beven, K., and P. Schlosser. 2003. The geochemical evolution of riparian groundwater in a forested Piedmont catchment. Groundwater 41(7): 913–925.

Dahlke, H.E., Easton, Z.M., Fuka, D.R., Lyon, S.W., and T.S. Steenhuis. 2009. Modeling Variable Source Area Dynamics in a CEAP Watershed. Ecohydrology 2: 337-349.

Day, R.L., Calmon, M.A., Stiteler, J.M., Jabro, J.D., and R.L. Cunningham. 1998. Water balance and flow patterns in a fragipan using in situ soil soil block. Soil Science 163(7): 517-528.

de Alwis, D.A., Easton, Z.M., Dahlke, H.E., Philpot, W.D., and T.S. Steenhuis. 2007. Unsupervised classification of saturated areas using a time series of remotely sensed images. Hydrol. Earth Syst. Sci. 11: 1609–1620.

Dunne, T., and R.D. Black. 1970. Partial area contributions to storm runoff in a small New England watershed. Water Resources Research 6: 1296–1311.

Dunne, T., Moore, T.R., and C.H. Taylor. 1975. Recognition and prediction of runoff-producing zones in humid regions. Hydrol Sci Bull, 20(3): 305–327.

Easton, Z.M., Gerard-Marchant, P., Walter, M.T., Petrovic, A.M., and T.S. Steenhuis. 2007. Hydrologic assessment of an urban variable source watershed in the Northeast US. Water Resources Research 43, W03413, doi:10.1029/2006WR005076, 2007.

Easton, Z.M., Fuka, D.R., Walter, M.T., Cowan, D.M., Schneiderman, E.M., and T.S. Steenhuis. 2008. Re-conceptualizing the Soil and Water Assessment Tool (SWAT) model to predict runoff from variable source areas. Journal of Hydrology 348: 279–291.

Ekholm, P., Kallio, K., Salo, S., Pietilainen, O.P., Rekolainen, S., Laine, Y., and M. Joukola. 2000. Relationship between catchment characteristics and nutrient concentrations in an agricultural river system. Water Res., 34: 3709-3716.

Freer, J., McDonnell, J., Beven, K.J., Brammer, D., Burns, D., Hooper, R.P., and C. Kendal. 1997. Topographic controls on subsurface storm flow at the hillslope scale for two hydrolog- ically distinct small catchments. Hydrological Processes 11(9): 1347–1352.

Freer, J., McDonnell, J., Beven, K.J., Peters, N.E., Burns, D.A., Hooper, R.P., Aulenbach, B., and C. Kendall. 2002. The role of bedrock topography on subsurface storm flow. Water Resour. Res. 38:1269 doi:10.1029/2001WR000872.

Garen, D.C., and D.S. Moore. 2005. Curve number hydrology in water quality modeling: Uses, abuses, and future directions. J. Am. Water Resour. Assoc. 41: 377–388.

Gburek, W.D., and A.N. Sharpley. 1998. Hydrologic controls on phosphorus loss from upland agricultural watersheds. Journal of Environmental Quality 27: 267–277.

Gburek, W.J., Sharpley, A.N., Heathwaite, L., and G.J. Folmar. 2000. Phosphorus management at the watershed scale: a modification of the phosphorus index. Journal of Environmental Quality 29: 130–144.

Gburek, W.J., Drungil, C.C., Srinivasan, M.S., Needelman, B.A., and D.E. Woodward. 2002.Variable-source area controls on phosphorus transport: Bridging the gap between research and design. Journal of Soil and Water Conservation 57(6): 534–543.

Gitau, M.W., Veith, T.L., Gburek, W.J., and A.R. Jarrett. 2006. Watershed-level BMP selection and placement in the Town Brook watershed, NY. J. Am. Water Resour. As. 42 (6): 1565-1581.

Haith, D.A., and L.L. Shoemaker. 1987. Generalized watershed loading functions for stremflow nutrients. Water Resources Research 23(3): 471–478.

Harpold, A.A., Lyon, S.W., Troch, P.A., and T.S. Steenhuis. 2010. The Hydrological Effects of Lateral Preferential Flow Paths in a Glaciated Watershed in the Northeastern USA. Vadose Zone Journal, 9: 397–414.

Hewlett, J.D., and A.R. Hibbert. 1963. Moisture and energy conditions within a sloping soil mass during drainage. Journal of Geophysical Research 68(4): 1081–1087.

Hewlett, J.D., and W.L. Nutter. 1970. The varying source area of streamflow from upland basins, Proceedings of the Symposium on Interdisciplinary Aspects of Watershed Management. Bozeman, MT. ASCE, New York, pp. 65–83.

Hinton, M.J., Schiff, S.L., and M.C. English. 1993. Physical properties governing groundwater flow in a glacial till catchment. Journal of Hydrology, 142: 229-249.

Hooper, R.P., Aulenbach, B.T., Burns, D.A., McDonnell, J., Freer, J., Kendall, C., and K. Beven. 1998. Riparian control of stream-water chemistry: implications for hydrochemical basin models. IAHS Publications-Series of Proceedings and Reports-Intern Assoc Hydrological Sciences, 248: 451–458.

Horton, R.E. 1933. The role of infiltration in the hydrologic cycle. Transactions American Geophysical Union 14: 446–460.

Horton, R.E. 1940. An approach toward a physical interpretation of infiltration capacity. Soil Science Society of America Proceedings 4: 399–417.

Huisman, J.A., Sperl, C., Bouten, W., and J.M. Verstraten. 2001. Soil water content measurements at different scales: Accuracy of time domain reflectometry and ground-penetrating radar. J. Hydrol. 245: 48–58.

Huisman, J.A., Hubbard, S.S., Redman, J.D., and A.P. Annan. 2003. Measuring soil water content with ground penetrating radar: a review. Vadose Zone Journal 2: 476-491.

Kirkby, M.J. 1978: Hillslope hydrology. Chichester, Wiley.

Krysanova, V., Muller-Wohlfeil, D.I., and A. Becker. 1998. Development and test of a spatially distributed hydrological water quality model for mesoscale watersheds. Ecol. Model. 106: 261–289.

Lee, K., Isenhart, T.M., Schultz, R.C., and S.K Mickelson. 2000. Multispecies riparian buffers trap sediment and nutrients during rainfall simulations. J. Environ. Qual. 29(4): 1200-1205.

Lyon, S.W., Gérard-Marchant, P., Walter, M.T., and T.S. Steenhuis. 2004. Using a topographic index to distribute variable source area runoff predicted with the SCS-Curve Number equation. Hydrological Processes 18(15): 2757–2771.

Lyon, S.W., Seibert, J., Lembo, A.J., Walter, M.T., and T.S. Steenhuis. 2006. Geostatistical investigation into the temporal evolution of spatial structure in a shallow water table. Hydrology and Earth System Sciences 10: 113–125.

McDonnell, J.J. 1990. A rationale for old water discharge through macropores in a steep, humid catchment. Water Resources Research 26: 2821–32.

McGlynn, B.L., McDonnell, J.J., Seibert, J., and C. Kendall. 2004. Scale effects on headwater catchment runoff timing, flow sources, and groundwater-streamflow relations, Water Resour. Res., 40, W07504,doi:10.1029/2003WR002494.

McHale, M., McDonnell, J.J., Mitchell, M.J., and C.P. Cirmo. 2002. A field based study of soil- and groundwater nitrate release in an Adirondack forested watershed. Water Resources Research 38(4): 1029/2000WR000102.

Michel, C., Andreassian, V., C. Perrin. 2005. Soil Conservation Service curve number method: How to mend a wrong soil moisture accounting procedure? Water Resour. Res., 41, W02011, doi:10.1029/ 2004WR003191.

Needelman, B.A., Gburek, W.J., Petersen. G.W., Sharpley, A.N., and P.J. Kleinman. 2004. Surface runoff along two agricultural hillslopes with contrasting soils. Soil Sci. Soc. Am. J. 68: 914-923.

Parlange, M.B., Steenhuis, T.S., Timlin, D.J., Stagnitti, F., and R.B. Bryant. 1989. Subsurface Flow Above a Fragipan Horizon. Soil Sciences 148: 77-86.

Pionke, H.B., Gburek, W.J., Sharpley, A.N., and R.R. Schnabel. 1996. Flow and nutrient export patterns for an agricultural hill-land watershed. Water Resour. Res. 32: 1795-1804.

Pionke, H.B., Gburek, W.J., Schnabel, R.R., Sharpley, A.N., and G.F. Elwinger. 1999. Seasonal flow, nutrient concentrations and loading patterns in stream flow draining an agricultural hill-land watershed. J. Hydrol. 220: 62–73.

Ponce, V.M., and R.H. Hawkins. 1996. Runoff curve number: Has it reached maturity? J. Hydrol. Eng., 1: 11 –19, doi:10.1061/(ASCE)1084-0699(1996)1:1(11).

Puckett, L.J. 1995. Identifying the major sources of nutrient water-pollution. Environ. Sci. Tech. 29: A408-A414.

Rao, N.S., Easton, Z.M., Schneiderman, E.M., Zion, M.S., Lee, D.R., and T.S. Steenhuis. 2009. Modeling Watershed-Scale Effectiveness of Agricultural Best Management Practices to Reduce Phosphorus Loading. Journal of Environmental Management 90: 1385-1395.

Sharpley, A.N., Chapra, S.C., Wedepohl, R., Sims, J.T., Daniel, T.C., and R.R. Reddy. 1994. Managing agricultural phosphorus for protection of surface waters: issues and options. Journal of Environmental Quality 23: 437–451.

Sharpley, A.N., McDowell, R.W., Weld, J.L., and P.J.A. Kleinman. 2001. Assessing site vulnerability to phosphorus loss in an agricultural watershed. J. Eviron. Qual. 30: 2026-357.

Shaw, S.B., and M.T. Walter. 2009. Formulating storm runoff risk using bivariate frequency analyses of rainfall and antecedent watershed wetness. Water Resour. Res. 45: W03404 DOI: 10.1029/2008WR006900.

Scherrer, S., Naef, F., Faeh, A.O., and I. Cordery. 2007. Formation of runoff at the hillslope scale during intense precipitation. Hydrology and Earth System Sciences 11: 907–922.

Schneiderman, E.M., Steenhuis, T.S., Thongs, D.J., Easton, Z.M., Zion, M.S., Mendoza, G.F., Walter, M.T., and A.L. Neal. 2007. Incorporating variable source area hydrology into the curve number based Generalized Watershed Loading Function model. Hydrological Processes 21: 3420–3430, DOI: 10.1002/hyp6556.

Sherlock, M.D., and J.J. McDonnell. 2003. A new tool for hillslope hydrologists: spatially distributed groundwater level and soilwater content measured using electromagnetic induction. Hydrol. Proces. 17: 1965-1977.

Srinivasan, M.S., Gerard-Marchant, P., Veith, T.L., Gburek, W.J., and T.S. Steenhuis. 2005. Watershed scale modeling of critical source areas of runoff generation and phosphorus transport. J. Am. Water Resour. Assoc. 41: 361–375.

Steenhuis, T.S., Richard, T.L., Parlange, M.B., Aburime, S.O., Geohring, L.D., and J.Y. Parlange. 1988. Preferential flow influences on drainage of shallow sloping soils. Agricultural Water Management, 14: 137-151.

Steenhuis, T.S., Winchell, M., Rossing, J., Zollweg, J.A., and M.F. Walter. 1995. SCS Runoff Equation Revisited for Variable-Source Runoff Areas. ASCE Journal of Irrigation and Drainage 121: 234–238.

Tromp-van Meerveld, H.J., and J.J. McDonnell. 2006b. Threshold relations in subsurface stormflow: A 147-storm analysis of the Panola hillslope. Water Resources Research, 42: W02410.

Tromp-van Meerveld, H.J., and J.J. McDonnell. 2006b. Threshold relations in subsurface stormflow: 2. The fill and spill hypothesis. Water Resources Research 42: W02411, Doi:10·1029/2004WR003800.

Tromp-van Meerveld, I., and J.J. McDonnell. 2009. Assessment of multi-frequency electromagnetic induction for determining soil moisture patterns at the hillslope scale. Journal of Hydrology, 368: 56-67.

Tromp-van Meerveld, I., M. Weiler. 2008. Hillslope dynamics modeled with increasing complexity. Journal of Hydrology 361: 24–40.

Tromp-van Meerveld, H.J., Peters, N.E., and J.J. McDonnell. 2007. Effect of bedrock permeability on subsurface stormflow and the water balance of a trenched hillslope at the Panola Mountain Research Watershed, Georgia, USA. Hydrological Processes 21: 750–769.

Uchida, T., Kosugi, K.I., and T. Mizuyama. 2002. Effects of pipe flow and bedrock groundwater on runoff generation in a steep headwater catchment in Ashiu, central Japan. Water Resources Research 38(7). doi:10.1029/2001WR00026.

USDA-SCS (Soil Conservation Service). 1972. National Engineering Handbook, Part 630 Hydrology, Section 4, Chapter 10.

Walter, M.T., Walter, M.F., Brooks, E.S., Steenhuis, T.S., Boll, J., and K.R. Weiler. 2000. Hydrologically sensitive areas: Variable Source Area hydrology implications for water quality risk assessment. Journal of Soil and Water Conservation 55(3): 277–284.

Walter, M.T., Brooks, E.S., Walter, M.F., Steenhuis, T.S., Scott, C.A., and J. Boll. 2001. Evaluation of soluble phosphorus transport from manure-applied fields under various spreading strategies. Journal of Soil and Water Conservation 56(4): 329–336.

Walter, M.T., Steenhuis, T.S., Mehta, V.K., Thongs, D., Zion, M., and E. Schneiderman. 2002. Refined conceptualization of TOPMODEL for shallow subsurface flows. Hydrolog. Process. 16(10): 2041– 2046.

Walter, M.T., Mehta ,V.K., Marrone, A.M., Boll, J., Steenhuis, T.S., and M.F. Walter. 2003. Simple estimation of prevalence of Hortonian flow in New York City watersheds. ASCE Journal of Hydrology and Engineering. 8(4): 214–218.

Walter, M.T., Brooks, E.S., McCool, D.K., King, L.G., Molnau, M., and J. Boll. 2005. Process-based snowmelt modeling: does it require more input data than temperature-index modeling? J. Hydrol. 300: 65–75.

APPENDIX A

ESTIMATION OF SOIL WATER CONTENT AND SOIL DEPTH IN A TRENCHED HILLSLOPE USING GROUND PENETRATING RADAR

A.1 Introduction

Soil water is a vital resource for natural ecosystems and human needs. Thus, variability of soil water content in space and time is important in many fields and reason for continuous research among hydrologists, soil scientists, ecologists, meteorologists and agronomists. Spatial and temporal variability of the soil water content, the water in the vadose zone, has impacts ranging from the field to the global scale. At the field scale spatiotemporal distribution of soil water is important for precision agriculture (Kennedy, 2002; Hubbard et al., 2006). Crops growing in areas with too much water can show adverse effects from water logging (e.g. reduced root respiration due to depletion of oxygen and increased availability of toxic ions under reduced soil conditions) leading to reduced crop quality. In contrast, drought stress can cause irreversible damage to crops growing in areas with too little water. Besides these extreme cases knowledge and monitoring of the water content at agricultural sites is generally critical for optimizing crop quality, achieving high irrigation efficiencies, and minimizing yield loss due to waterlogging or salinization of soils (Grote et al., 2003).

Near-surface water content is also an important input parameter for hydrological and atmospheric models. At the regional to continental scale, exchange of energy and moisture between the soil, vegetation, and the atmosphere impact the regional weather and climate. The soil water content largely influences the temperature and moisture of the lower atmosphere, which in turn regulate the relative magnitude of the sensible

and latent heat fluxes and the diurnal evolution of the atmospheric boundary layer (Callies et al, 1998). Recent studies of the impact of soil moisture availability on land-atmosphere coupling revealed that soil moisture availability can provide a critical constraint on the short and long-term memory of climatological forcing and surface evapotranspiration (e.g. Entin et al., 2000; Koster and Suarez, 1996, 2001; Koster et al., 2004). More specifically, the amount and depth of soil moisture available to plants can, in certain conditions, significantly control the timescale and rate of root water uptake and, hence, surface energy partitioning (Wang et al., 2006; Gochis et al., 2010). Similarly, simulated catchment-scale fluxes of energy and runoff have also been shown to be significantly impacted by spatial variations in soil depth and soil water content (Bertoldi et al., 2006; Tromp-van Meerveld and Weiler, 2008). Clearly there is demand for soil water content measurements across a range of spatial scales.

At the field scale point estimates of soil water content using traditional methods such as neutron probes (Holmes, 1956), gravimetric measurements of soil water content based on soil samples, or Time-domain reflectometry (TDR) (Topp et al., 1980) provide highly accurate and precise measurements. However, these methods are invasive, labor intensive, and represent most often integrated measurements of a particular depth or for very small areas or volumes, which have been problematic for carrying out repeated measurements over time and for scaling up soil moisture measurements to larger areas (e.g. hillslopes, watersheds) (Galagedara et al., 2003; Tromp-van Meerveld and McDonnell, 2009). Thus, during the past two decades hydrologists increasingly begun to discover non-invasive high-frequency electromagnetic techniques to estimate soil water content over larger areas. These techniques measure a soil water content proxy, namely dielectric permittivity, using either remotely sensed or ground-based passive microwave radiometry (reference) or active radar instruments (Jackson et al., 1996; Ulaby et al., 1996; Famiglietti et al.,

1999; van Oevelen, 2000). Due to the advances in image resolution (1 to several 1000 m^2) air-born or satellite-borne passive and active radar instruments play an increasingly important role in hydrological studies. However, water content estimates show limited penetration depth (approximately 0.05 m) in soils (Lakshmi, 2004) and require minimal vegetation cover to reduce interference of the radar signal (Jackson et al., 1996).

Ground penetrating radar (GPR), a non-intrusive geophysical method, has been cited in several studies as a potential alternative method to measure soil water variability at intermediate scales (Chanzy et al., 1996; Du and Rummel, 1994; Huisman et al., 2001; Huisman and Bouten, 2002). Soil water content measurements with surface GPR showed comparatively good agreement with TDR-measured water contents (Weiler et al., 1998; Huisman et al., 2001; Grote et al., 2003), gravimetrical water contents (Chanzy et al., 1996; Grote et al., 2003) and water contents measured with capacitance sensors (van Overmeeren et al., 1997). In addition GPR applied in boreholes allowed generation of soil water content profiles of the vadose zone (Gilson et al., 1996; Knoll and Clement, 1999; Parkin et al., 2000; Binley et al., 2001, 2002; Rucker and Ferré, 2003; Lunt et al., 2005). Soil water content can also be determined from air-launched surface reflectivity GPR systems (Redman et al., 2000; Davis and Annan, 2002), however, accuracy is highly impacted by the surface reflection coefficient, which is varying depending on the surface roughness of the ground and the soil water content (Huisman et al., 2003).

A.2 Principles of ground penetrating radar

Ground Penetrating Radar (GPR) is an active geophysical method that uses radio waves in the frequency range of 10 – 1000 MHz to map the presence and location of subsurface features at scales ranging from kilometers for geologic features to

centimeters for rebar in concrete structures (Davis and Annan, 1989). The GPR is in its most common setup a bistatic system with one antenna, the transmitter, radiating short pulses of electromagnetic waves (MHz or GHz), and the other antenna, the receiver, which measures the signal from the transmitter as a function of time. When the system is placed on the ground, spherical, electromagnetic waves are emitted upward into the air and downward into the soil as indicated in Figure 1. Beside the radar signal transmitted in the air, also known as the air wave, part of the radiated energy travels between the transmitter and receiver through the top of the soil, also known as the ground wave (Fig. A.1). In addition, energy transmitted into the ground will be (partly) reflected when contrasts in soil permittivity are encountered.

The successful application of GPR is dependent on soil texture and the electrical conductivity of the ground. The travel time of electromagnetic waves transmitted by the radar antenna depends on the relative dielectric permittivity (ε_r) (the permittivity relative to free space) and the relative magnetic permeability (μ_r) of the material through which it passes. In general the dielectric permittivity increases with the water content but decreases the penetration of the radar signal. Within the GPR frequency range (10 – 1000 MHz) the dielectric permittivity ranges between 80 (water) and 1 (air). For this frequency range the propagation velocity, v (m/s), of electromagnetic waves is only influenced by the relative dielectric permittivity and can be estimated in non-saline soils using the following equation (Wyseure et al., 1997):

$$v = \frac{c}{\sqrt{\varepsilon'}} \qquad \text{(A.1)}$$

where c is the free space electromagnetic propagation velocity (3×10^8 m/s) and ε' is the relative dielectric permittivity.

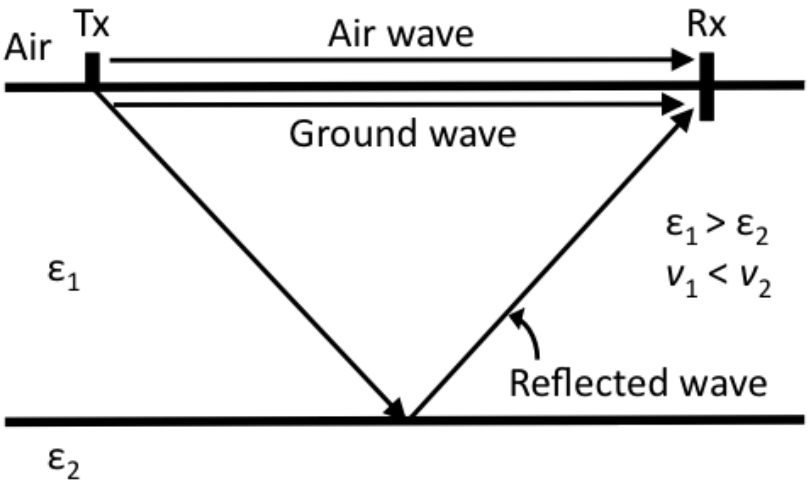

Figure A.1: Propagation paths of electromagnetic waves in a soil with two layers of contrasting dielectric permittivity (ε1 and ε2). T_x and R_x are the transmitter and receiver respectively.

Soil texture and electrical conductivity of the ground affect also the resolution and depth penetration of GPR. GPR resolution is determined by the wavelength of the emitted pulse, which is controlled by the frequency bandwidth of the GPR system. GPR resolution increases with increasing center frequency (Davis and Annan, 1989). Depth penetration of GPR measurements is controlled by both the center frequency and the soil electrical conductivity. Depth penetration is greatest in low conductive materials such as dry sand and gravel and can reach several tens of meters for low center frequencies (e.g. 50 – 100 MHz antennas) and between one to several meters for high-frequency system (e.g. 450-900 MHz). In silty sands or clay soils depth penetration is considerably lower, thus, successful application of GPR in this range of soils is limited.

A.3 Water content – permittivity relationships

The most common method to relate the apparent permittivity, ε, to volumetric soil water content, θ_v (m^3/m^3), is the empirical relationship developed by Topp et al. (1980):

$$\theta_v = -5.3 \times 10^{-2} + 2.92 \times 10^{-2}\varepsilon - 5.5 \times 10^{-4}\varepsilon^2 + 4.3 \times 10^{-6}\varepsilon^3 \qquad \text{(A.2)}$$

which was determined for mineral soils with various textures. The term *apparent* is used because the permittivity is estimated from the measured electromagnetic propagation velocity in the soil. The empirical equation from Topp et al. (1980) has an accuracy of 0.022 m^3/m^3 determined on mineral soils in an independent comparative study by Jacobsen and Schjønning (1994).

A more theoretical approach to relate soil water content and ε is based on dielectric mixing models, which use the volume fractions and the dielectric permittivity of each soil constituent (e.g. Dobson et al., 1985; Roth et al., 1990; Friedman, 1998; Jones and Friedman, 2000). Ledieu et al. (1986) and Herkelrath et al. (1991) suggested the following simplified equation to estimate soil water content based on permittivity, which is based on the assumption that water in the vapor phase and water bound to the soil particles are negligible:

$$\theta = a\sqrt{\varepsilon_b} - b \qquad \text{(A.3)}$$

where a and b are calibration parameters and $(\varepsilon_b)^{1/2}$ is the refractive index (Robinson et al., 2003). This semi-theoretical relationship has an accuracy of 0.0188 m^3/m^3 as determined by an independent validation on mineral soils performed by Jacobsen and Schjønning (1994).

It is important to note that most calibration equations that correlate soil water content with the dielectric permittivity were derived using TDR, which mainly operates in a frequency range of 500 to 1000 MHz (Robinson et al., 2003). In addition, it has long

been recognized that soils with high clay content exhibit significant permittivity dispersion at low frequencies (Olhoeft, 1987). Based on recent frequency-dependent permittivity measurements in differently textured media ranging from sandy soils to stone samples containing different amounts of montmorrillonite clay West et al. (2003) showed that significant frequency dispersion occurs at frequencies below 350 MHz. This implies that site-specific calibration may be required for accurate water content measurements with lower antenna frequencies, such as the commonly used 100 and 200 MHz antennas.

A.4 Estimation of soil water content with the ground wave

Measurement of soil water content with the ground wave is based on the principle that the ground wave is travelling between the transmitter and receiver through the top of the soil parallel to the soil surface. Thus, this method is independent of the presence of clearly reflecting soil layers (Du, 1996; Berktold et al., 1998; Sperl, 1999). The ground wave method for measuring soil water content can be performed using three major survey types, the common mid point (CMP), the wide-angle reflection and refraction (WARR), or the fixed offset method (FOM). In a CMP survey both transmitter and receiver are moved apart from each other at a constant spatial increment. In contrast, in WARR surveys the transmitter antenna is kept at a fixed location while the receiver antenna is moved away from the transmitter at a constant spatial increment. Both CMP and WARR surveys are used to estimate the propagation velocity of the emitted electromagnetic waves in the subsurface by analyzing the dependence of arrival time on antenna offset for events reflected from subsurface horizons. In both survey types the arrival time of the air wave and ground wave (Fig. A.2) is zero at the 0 m antenna offset and is linearly increasing with increasing antenna offset. While the air wave typically propagates at a velocity of approximately 0.3 m/ns, the lateral velocity of the

ground wave, is a function of the electrical conductivity and texture of the subsurface media, which can be estimated from the inverse of the slope of the time-offset relationship of the ground wave (Fig. A.2).

FOM surveys are conducted by keeping a fixed offset between the transmitter and receiver antenna while moving both antennas at a constant spatial increment over the survey area. This method is also called profiling. In contrast to CMP and WARR surveys where multiple traces are used to estimate the radar velocity (multiple trace analysis, MTA) in profiling surveys each single trace is used (single trace analysis, STA) to estimate the velocity (Galagedara et al., 2003).

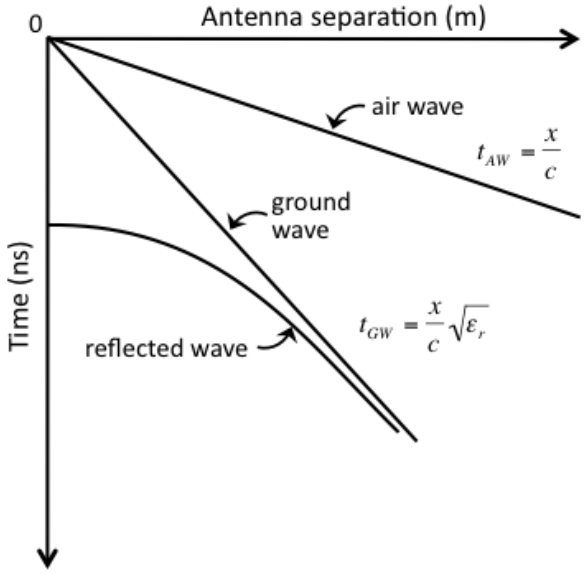

Figure A.2: Schematic layout of wave arrivals when performing a common-midpoint (CMP) or wide angle reflection and refraction (WARR) measurement. The ground wave can be identified as a wave with a linear move out starting from the origin of the x-t plot. In the slope equations, *c* is the electromagnetic velocity of air and *x* is the antenna separation.

Estimation of soil water content using multi-offset GPR measurements (CMP, WARR surveys) is cumbersome and time-consuming but of higher accuracy than the fixed offset profiling method (Huisman et al., 2001). Huisman et al. (2001) estimated an

accuracy of 0.024 m^3/m^3 by analyzing a set of 24 multi-offset measurements collected with 225 MHz antennas and the semi-theoretical soil water content–permittivity relationship of Herkelrath et al. (1991). Similarly Grote et al. (2003) compared 29 water content estimates obtained with a multi-offset GPR to gravimetric soil moisture measurements and estimated root-mean-squared-errors of 0.022 and 0.015 m^3/m^3 using 450 and 900 MHz antennas.

To estimate soil water content over larger areas the profiling or fixed offset method provides a much more time efficient approach. Given that the approximate arrival time of the ground wave is known, which can be estimated by completing one or more CMP profiles, Du (1996) and Sperl (1999) proposed the following procedure for water content mapping with the ground wave:

1. Identify an approximate ground wave arrival time for different antenna separations with a CMP or WARR measurement.
2. Choose an antenna separation where the ground wave is clearly separated from the air and reflected waves and,
3. Use this antenna separation for GPR profiling and relate changes in ground wave arrival time to changes in soil permittivity.

The soil permittivity can then be estimated using the approach of Sperl (1999) and the following relationship between ground wave arrival time t_{GW} (s), air wave arrival time t_{AW} (s), and antenna separation x (m):

$$\varepsilon = \left(\frac{c}{v}\right)^2 = \left[\frac{c\left(t_{GW} - t_{AW}\right) + x}{x}\right]^2 \qquad \text{(A.4)}$$

For soil water content measurements derived from ground wave travel time data both accurate zero time correction and accurate travel time determination are important

(Huisman et al., 2003). The zero time correction of the air wave, ground wave and reflected wave arrivals is required to correct for the additional travel time at the beginning of each measurement, which is mainly due to the travel time in the cables of the radar system. Huisman et al. (2003) proposed the following correction procedure consisting of (i) aligning the arrival times of the air wave to correct for drift in the zero time (e.g. caused by temperature changes affecting the radar system and the cables), (ii) estimating the average arrival time of the air wave, and (iii) calculating the zero time correction from the average arrival time and the known antenna separation. Instead of using an average arrival time of the air wave for the zero time correction many data processing software packages (e.g. ReflexW, Ekko viewer) support now automatic or semi-manual picks of the leading edge (onset) of the air and ground wave for each trace, which makes water content estimation easier.

Studies by Lesmes et al. (1999), Huisman et al. (2001, 2002, 2003), Hubbard et al. (2002), Garambois et al. (2001) and Galagedara et al. (2003) have confirmed that soil water content mapping using the ground wave method works well. Using comparative soil moisture measurements obtained with TDR, lysimeters, capacitance probes or electric resistivity accuracy of GPR estimated soil water contents ranged between 0.0026 and 0.03 m^3/m^3.

Although achieved accuracies of soil water content measurements with the ground wave are promising there still remains some debate about the effective measurement volume over which the ground wave averages (Galagedara et al., 2005a, b). Du (1996) suggested that the influence depth is approximately one-half of the wavelength [$\lambda=c/(f\varepsilon)^{1/2}$], which would for example result in an influence depth of 0.17m ($\varepsilon = 4.0$) to 0.07 m ($\varepsilon = 4.0$) using a center frequency of 200 MHz. Sperl (1999) showed that the influence depth is a function of the wavelength and suggested from a modeling experiment that the influence depth is approximately $0.145\lambda^{1/2}$, which results in a

depth ranging from 0.08 m (ε = 4.0) to 0.06 m (ε = 20.0) for the 200 MHz antennas. Irrigation experiments performed by Galagedara et al. (2005b) have shown that the influence depth is negatively correlated with GPR frequency and decreasing if moisture content in the topsoil layer is increasing. Grote et al. (2003) also concluded based on comparative soil water content measurements using 450 and 900 MHz GPR antennas and gravimetric measurements in soil depths ranging from 0-10 cm, 10-20 cm and 0-20 cm below the soil surface that values averaged across the 0-20 cm range showed best correlation with gravimetric measurements. Clearly further research is needed to better understand the ground wave zone of influence.

A.5 Soil water content and soil depth in the trenched hillslope

6.1.1 A.5.1 Soil depth

In the trenched hillslope addressed in this study soil moisture and depth to the fragipan was estimated from five GPR grids, each covering an approximate area of 31 m by 22 m and a line spacing of 0.74 m. A PulseEkko system (Sensors & Software Inc., Mississauga, ON, Canada) with 200 MHz antenna and 1 m fixed antenna offset was used. Data were stacked 32 times at each acquisition. Several common mid-point profiles were taken within these grids to estimate general ground wave, air wave, and reflected wave arrivals. GPR data were processed in ReflexW software (Sandmeier Software Inc., Karlsruhe, Germany), which included a manual correction of air-wave arrivals, application of a Dewow filter, subtraction of the DC-shift, calculation of a running average over three traces, and application of a gain function of 2 db/m before interpretation of the data (Fig. A.3).

To estimate the depth to the first reflector in the subsurface the following processing steps were performed:

1) Semi-automatic correction of the zero time through picking of the onset of the air wave using the phase follower.
2) Semi-automatic pick of the onset of the ground wave and reflected wave.
3) Estimation of the depth, D (m), of the reflector using an average ground wave velocity (v) and the two-way arrival time of the reflected wave (t_{RW}):

$$D = \frac{v \cdot t_{RW}}{2} \quad \text{(A.5)}$$

A general radar velocity of 0.063 m/ns was estimated based on a CMP profile (Fig. A.4) and from hyperbolas (Fig. A.5), which were fitted to several point reflectors in the recorded GPR profiles. Depth values estimated for each GPR profile were automatically assembled into X-Y grids, imported in ArcGIS (ESRI Inc.) and geo-referenced using differentially measured corner positions for each grid. GPR-based estimation of the depth to the flow-restricting fragipan averaged 0.66 m and ranged between 0.42 to 1.20 m (Fig. A.6). On-site validation of estimated soil depths was not performed.

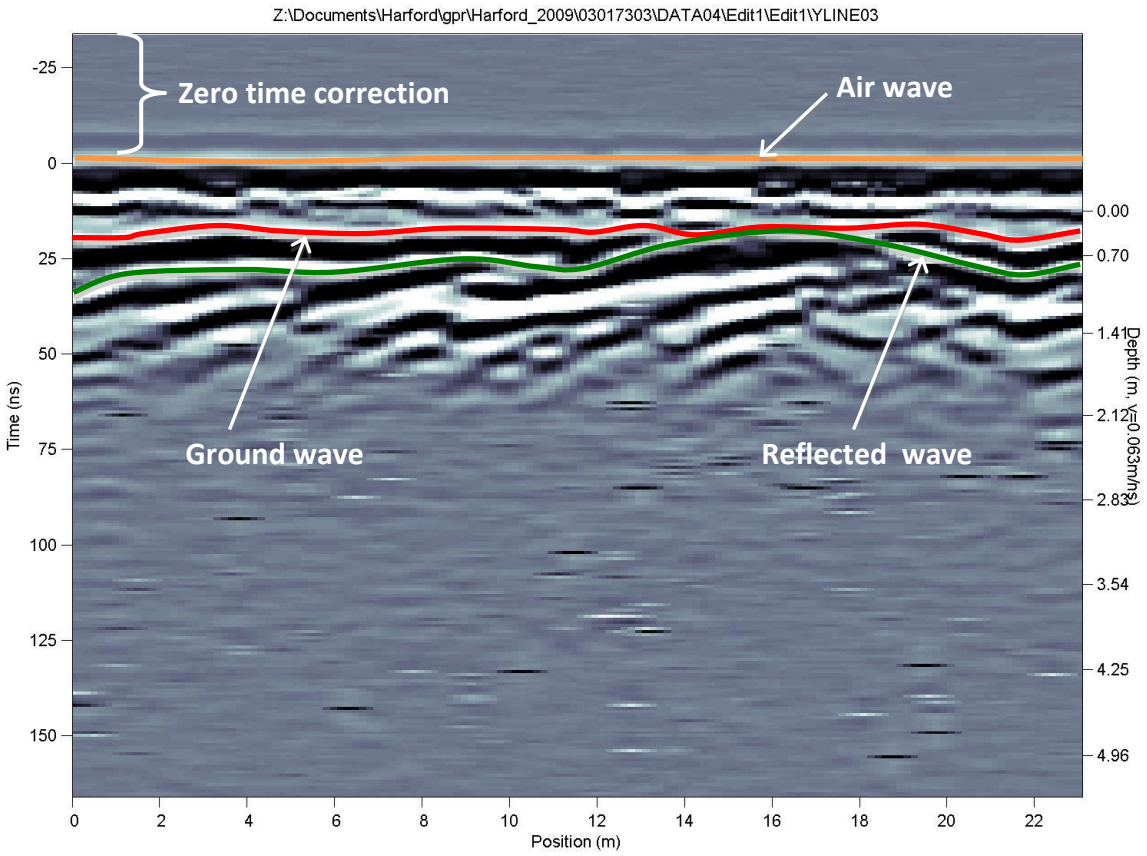

Figure A.3: GPR profile acquired in the trenched hillslope with a PulseEkko system, 200 MHz antennas in 1 m FO mode. The profile is shown after completion of data processing. The orange, red and green lines show the air wave, ground wave and reflected wave respectively.

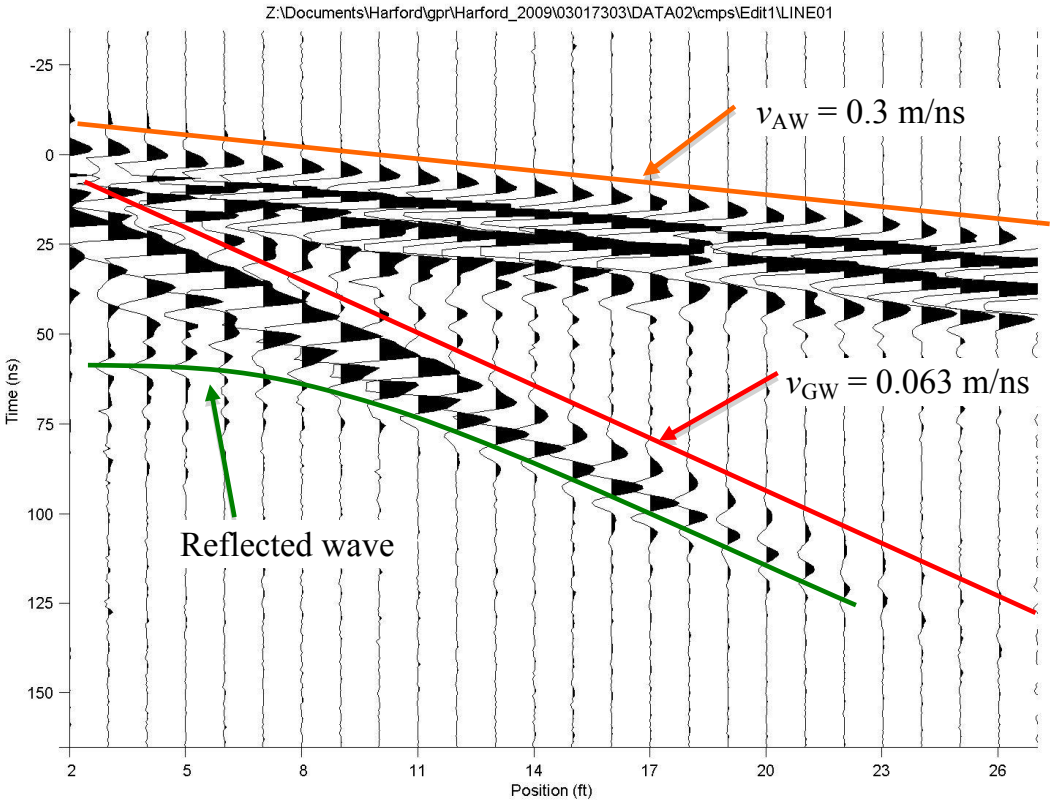

Figure A.4: CMP profile acquired in the trenched hillslope with a PulseEkko system, 200 MHz antennas. The orange, red and green lines indicate the air wave, ground wave and reflected wave respectively and associated velocities.

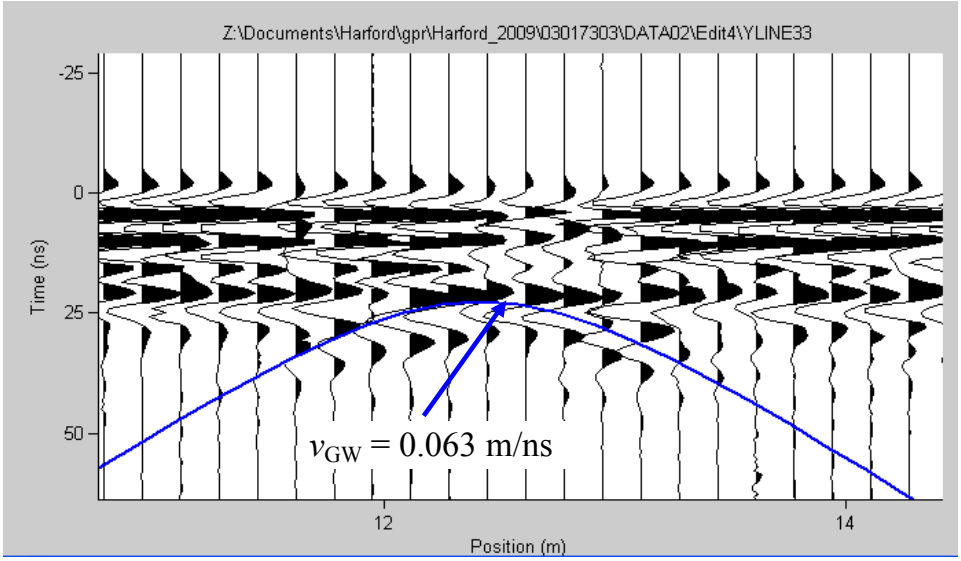

Figure A.5: Estimation of radar velocity by fitting a hyperbola to a point reflector in the subsurface. Depth to hyperbola is D = 0.6 m.

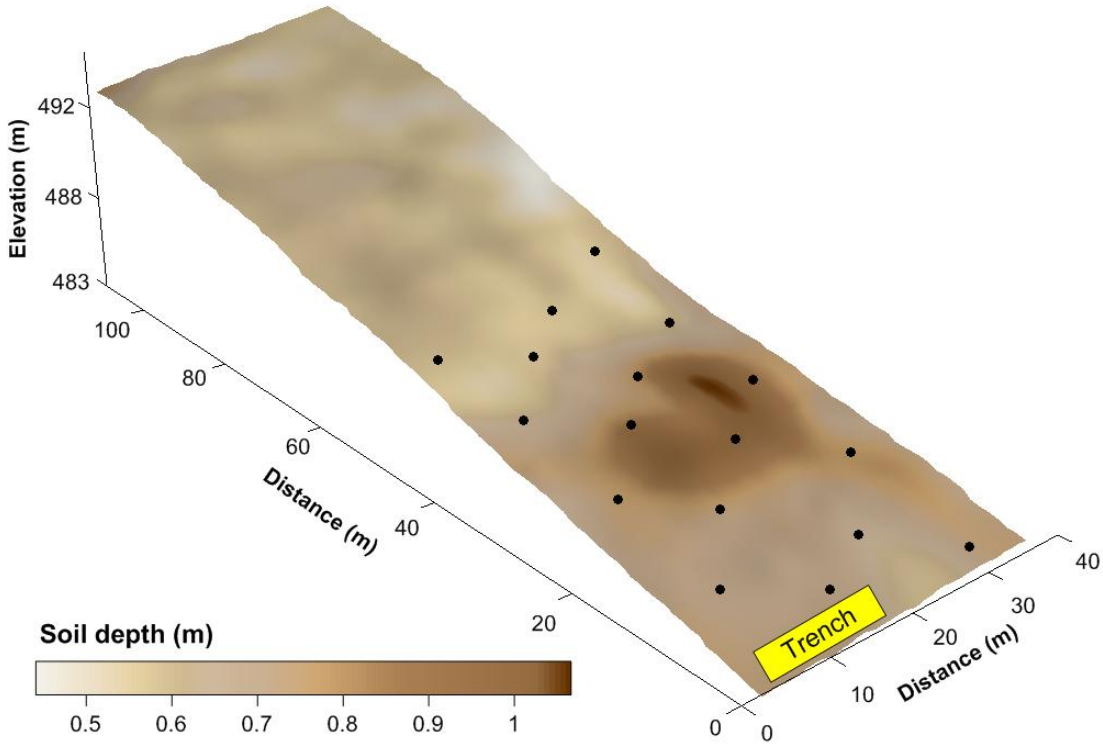

Figure A.6: Map of the soil depth in the trenched hillslope estimated from GPR profiles (PulseEkko system, 200 MHz antennas, 1 m FO) using the reflected wave. Black dots indicate the location of water level loggers.

6.1.2 A.5.2 Soil water content

Soil water content was derived from fixed offset GPR and the method outlined by Sperl (1999). First a time zero was estimated in each GPR profile by picking the leading edge (onset) of the direct air wave and then the leading edge of the direct ground wave. The difference in arrival times is attributed to differences in soil water content as shown in Fig. A.7. Greater differences between air wave and ground wave arrivals reflect a higher soil water content and a lower ground wave velocity in the subsurface.

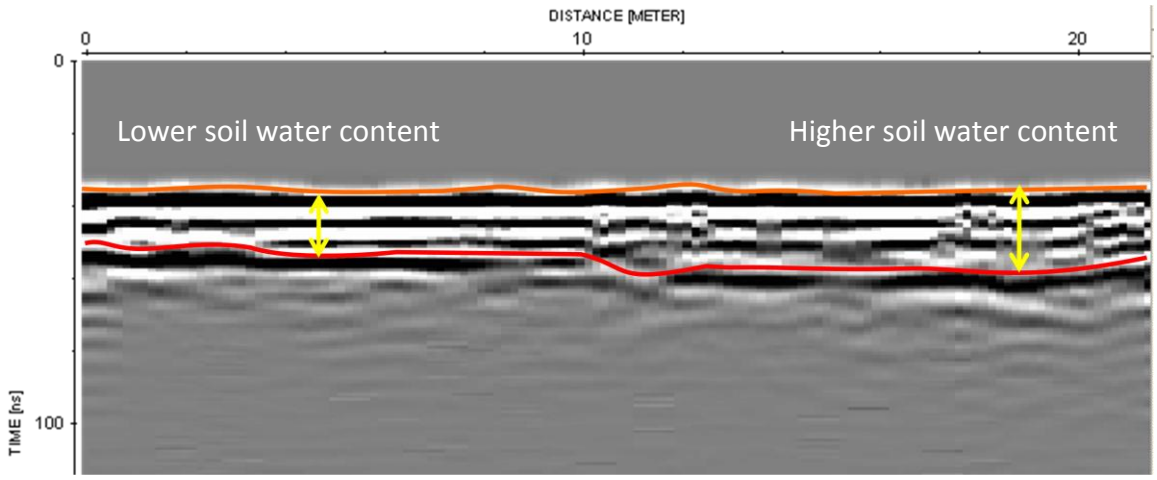

Fig. A.7: Influence of soil water content on arrival times of the air wave (orange) and ground wave (red).

Both the air wave and ground wave arrival reflect directly differences in the air wave and ground wave velocities. Thus, the general relationship between air wave arrival and ground wave arrival and how both relate to the air wave velocity and ground wave velocity can be derived as followed:

$$t_{AW} = \frac{x}{v_{AW}} \tag{A.6}$$

$$t_{GW} = \frac{x}{v_{GW}} \tag{A.7}$$

where t_{GW} (ns) is the picked ground wave arrival and t_{AW} (ns) is the picked air wave arrival, x (m) is the antenna separation and v_{GW} (m/ns) is the estimated ground wave velocity and v_{AW} (m/ns) is the air wave velocity (i.e. 0.3 m/ns). The difference (Δt) between the ground wave and air wave arrival is reflecting differences in soil water content, which can be estimated based on knowledge of the air wave and ground wave velocity and the antenna separation:

$$\Delta t = \frac{x}{v_{GW}} - \frac{x}{v_{AW}} \tag{A.8}$$

Equation A.8 can be simplified using picked arrival times of the air wave (t_{AW}) and ground wave (t_{GW}) only as well as the calculated travel time of the air wave at x (m) antenna separation:

$$\Delta t = t_{GW} - t_{air} - t_{AW} \tag{A.9}$$

In a next step the ground wave velocity v_{GW} (m/ns) is estimated based on the antenna distance x (m) and the difference of picked arrival times Δt (ns).

$$v_{GW} = \frac{x \times v_{AW}}{\Delta t \times v_{AW} - x} \tag{A.10}$$

Since the air wave velocity is typically a magnitude higher than the ground wave velocity this term becomes very small and can be neglected for a quick approximation of the ground wave velocity.

$$v_{GW} \approx \frac{x}{\Delta t} \tag{A.11}$$

Based on the ground wave velocity the apparent permittivity ε is calculated for each recorded trace:

$$\varepsilon = \left(\frac{c}{v_{GW}} \right)^2 \tag{A.12}$$

Finally the volumetric soil water content θ_v can be estimated using the empirical equation of Topp et al. (1980) (Eq. A.2).

The soil water content in the field site estimated with the ground wave method and the empirical relationship of Topp et al. (1980) a ranged between 0.2 and 0.5 m^3/m^3 (Fig. A.8). For validation of soil water contents gravimetric and volumetric soil moisture was measured in 17 locations in the hillslope by taking soil samples from 10 cm below soil surface. Samples were taken with a 7.2-cm-diameter stainless steel ring (V_0=276.9 cm^3) and were stored in sealed plastic bags until further analysis in the lab. The samples were weighed before and after drying them for 48 hours at 105 °C in a drying

oven. Volumetric soil water content θ_v of the soil samples was estimated using the following relationship:

$$\theta_v = \frac{m_w - m_d}{\rho_w \cdot V_b} \tag{A.13}$$

where m_w and m_d (g) are the masses of the soil sample before and after drying them in the oven, ρ_w (g/cm^3) is the density of water and V_b is the volume of the sample before drying the sample. In addition volumetric soil moisture was measured using the HydroSense time-domain reflectometer (TDR) (Campbell Scientific, Logan UT) with two 12 cm probe rods. The HydroSense water content sensor measures soil moisture in the range between 0 (air dried soil) and 100% (in water or fully saturated soil).

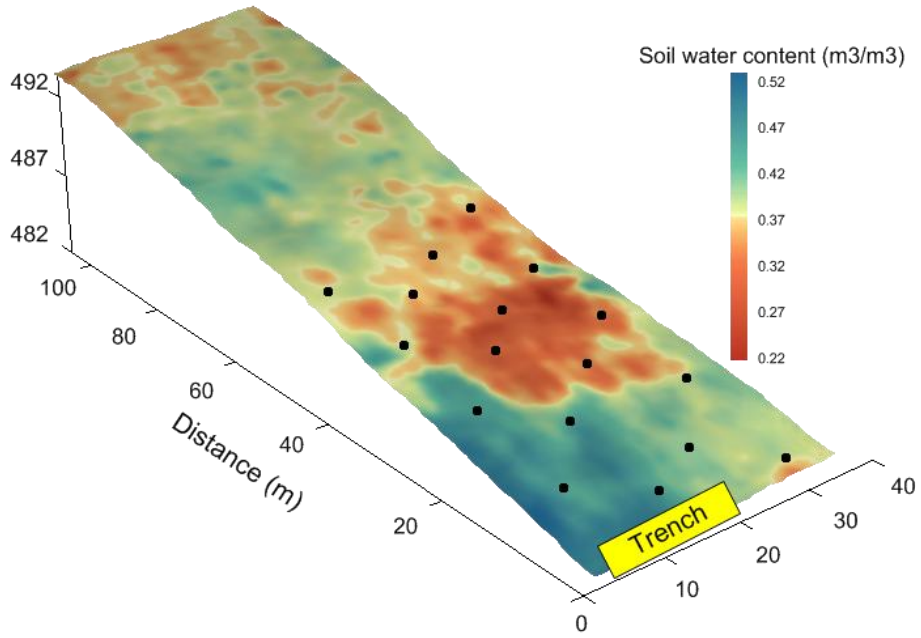

Figure A.8: Map of the soil water content in the trenched hillslope estimated from GPR profiles (PulseEkko system, 200 MHz antennas, 1 m FO) using the ground wave method and the empirical equation of Topp et al. (1980). Black dots indicate the location of water level loggers.

For direct comparison of θ_v estimated with TDR and GPR and the θ_v of the soil samples the apparent relative permittivity, ε_a, was calculated by solving Eq. A.2 for ε. Both methods showed a good linear relationship of r^2=0.76 (θ_v-$_{GPR}$) and r^2=0.79 (θ_v-

$_{TDR}$) with the gravimetrically estimated soil water content ($\theta_{v\text{-}soil}$) (Fig. A.9b). Linear regression of θ_v-$_{GPR}$ and $\theta_{v\text{-}TDR}$ shows a moderate fit with r^2=0.58. Soil water contents estimated with the TDR probe underpredicted $\theta_{v\text{-}soil}$, while the GPR ground wave method over predicted $\theta_{v\text{-}soil}$. Similar results were also reflected by the root-mean-squared error between $\theta_{v\text{-}soil}$ and θ_v estimated using TDR (RMSE = 0.05 m^3/m^3) or the ground wave method (RMSE = 0.16 m^3/m^3). The RMSE between θ_v-$_{GPR}$ and $\theta_{v\text{-}TDR}$ equals RMSE=0.2 m^3/m^3. The regression line between $\theta_{v\text{-}soil}$ and $\theta_{v\text{-}GPR}$ shows a linear offset of 0.17 m^3/m^3 but a slope close to 1. This linear offset might result from the fact that the GPR profile measurements were taken five days prior to the simultaneously performed TDR measurements and the soil sampling and indicate that soils further decreased in soil water content during that period. In addition the higher soil water contents estimated with the ground wave method represent average values for the Fresnel zone (the effective measurement volume over which the ground wave averages), which could have a greater influence depth than sampled with the TDR probe or the soil samples. Fig. A.9a shows linear regressions between the volumetric water content estimated from soil samples and the square root of the apparent relative permittivity estimated with the ground wave method from FOM GPR profiles and from TDR point measurements. Both regressions can be used to calibrate soil water content measurements based on field estimates of the apparent relative permittivity.

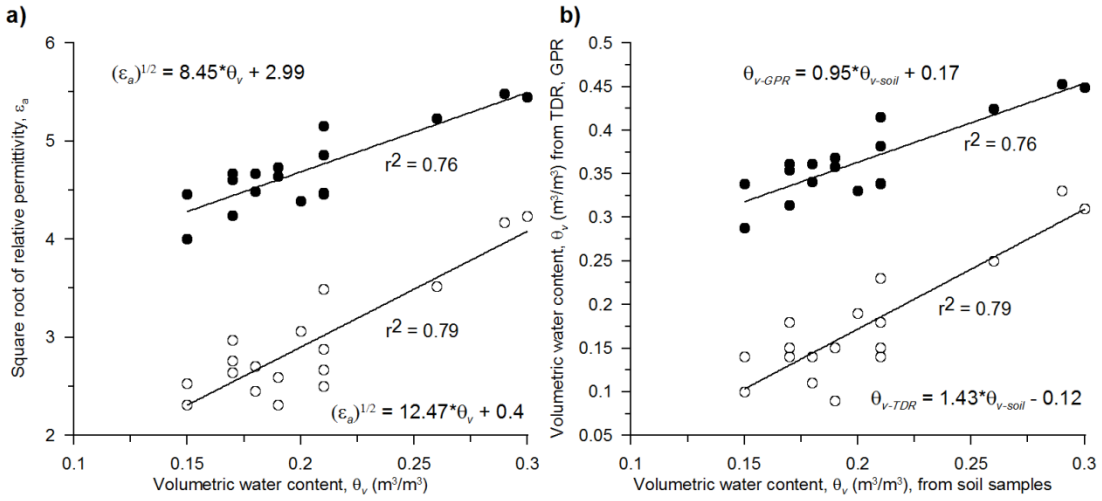

Figure A.9: (a) Regressions of gravimetrically estimated soil water contents versus the square root of the apparent relative permittivity (ε_a) estimated with TDR (open circles) and the GPR ground wave method (solid circles) respectively. (b) Regressions of volumetric soil water content (θ_v) determined from soil samples versus θ_v estimated with TDR (open circles) and the GPR ground wave method (solid circles). $\theta_{v\text{-}GPR}$, $\theta_{v\text{-}TDR}$, and $\theta_{v\text{-}soil}$ are soil water contents estimated with the GPR ground wave method, TDR and from soil samples respectively.

A.6 Conclusions

The soil moisture distribution was estimated in a trenched hillslope using the ground wave method and a ground penetrating system (GPR) with 200 MHz antennas. Fixed-offset GPR traces were collected with 1.0 m antenna separation in 5 grids covering a total area of 0.4 ha in the hillslope. Soil water contents estimated with the ground wave method were compared to soil water contents estimated from 17 undisturbed soil samples as well as point measurements taken with a time-domain reflectometer (TDR-probe). Soil water contents estimated with the ground wave method generally agreed well with soil water contents obtained from soil samples but showed a linear positive offset of 0.17 m^3/m^3. This overprediction could either result from the time difference between soil sampling and GPR profiling (5 days) or could indicate that the sampling depth (ground wave influence depth) is higher than assessed with the TDR probe or the soil sampling. These results show that the empirical equation of Topp et al. (1980)

provides a universally applicable approach to relate field-estimated differences in the relative permittivity to soil water content, but suggest that on-site calibration of GPR data using soil samples or TDR measurements should be performed to increase measurement accuracy.

REFERENCES

Berktold, A., Wollny, K.G., and H. Alstetter. 1998. Subsurface moisture determination with the ground wave of GPR. p. 675–680. In Proc. Int. Conf. on Ground-Penetrating Radar, 7th, Lawrence, KS, May 1998, Univ. of Kansas, Lawrence.

Bertoldi, G., Rigon, R., and T.M. Over. 2006. Impact of watershed geomorphic characteristics on the energy and water budgets. Journal of Hydrometeorology 7: 389–403.

Binley, A., Winship, P., Middleton, R., Pokar, M., and J. West. 2001. High-resolution characterization of vadose zone dynamics using cross-borehole radar. Water Resour. Res. 37: 2639–2652.

Binley, A., Winship, P., West, L.J., Pokar, M., and R. Middleton. 2002. Seasonal variation of moisture content in unsaturated sandstone inferred from borehole radar and resistivity profiles. J. Hydrol. 267: 160–172.

Callies, U., Rhodin, A., and D.P. Eppel. 1998. A case study on variational soil moisture analysis from atmospheric observations. J. Hydrol. 212–213: 95–108.

Chanzy, A., Tarussov, A., Judge, A., and F. Bonn. 1996. Soil water content determination using a digital ground-penetrating radar. Soil Sci. Soc. Am. J. 60: 1318–1326.

Davis, J.L., and A.P. Annan. 1989. Ground-penetrating radar for high resolution mapping of soil and rock stratigraphy. Geophys. Prospect. 37: 531–551.

Dobson, M.C., Ulaby, F.T., Hallikainen, M.T., and M.A. El-Rayes. 1985. Microwave dielectric behaviour of wet soil. Part II. Dielectric mixing models. IEEE Trans. Geosci. Remote Sens. 23: 35–46.

Du, S. 1996. Determination of water content in the subsurface with the ground wave of ground penetrating radar. Ph.D. thesis. Ludwig-Maximilians-Universität, Munich, Germany.

Du, S., and P. Rummel. 1994. Reconnaissance studies of moisture in the subsurface with GPR. Proc. of 5th International Conference on Ground-Penetrating Radar, Univ. of Waterloo, Kitchener, Ontario, Canada.

Entin, J., Robock, A., Vinnikov, K.Y., Hollinger, S.E., Liu, S., and A. Namkai. 2000. Temporal and spatial scales of observed soil moisture variations in the extratropics. Journal of Geophysical Research 105: 11 865–11 877.

Famiglietti, J.S., Deveraux, J.A., Laymon, C.A., Tsegaye, T., Houser, P.R., Jackson, T.J., Graham, S.T., Rodell, M., and P.J. van Oevelen. 1999. Ground-based investigation of soil moisture variability within remote sensing footprints during the Southern Great Plains 1997 (SGP97) hydrology experiment. Wat. Resour. Res. 35: 1839–1851.

Friedman, S.P. 1998. A saturation degree-dependent composite spheres model for describing the effective dielectric constant of unsaturated porous media. Wat. Resour. Res. 34: 2949–2961.

Galagedara, L.W., Parkin, G.W., and J.D. Redman. 2003. An analysis of the ground-penetrating radar direct ground wave method for soil water content measurement, Hydrological Processes 17: 3615–3628.

Galagedara, L.W., Parkin, G.W., Redman, J.D., von Bertoldi, P., and A.L. Endres. 2005a. Field studies of the GPR ground wave method for estimating soil water content during irrigation and drainage, Journal of Hydrology 301: 182-197.

Galagedara, L.W., Parkin, G.W., and J.D. Redman. 2005b. Measuring and modeling of direct ground wave depth penetration under transient soil moisture conditions, Subsurface Sensing Technologies and Applications 6(2): 193-205.

Garambois, S., Senechal, P., and H. Perroud. 2002. On the use of combined geophysical methods to assess water content and water conductivity of near-surface formations. J. Hydrol. 259: 32–48.

Gilson, E.W., Redman, J.D., Pilon, J., and A.P. Annan. 1996. Near surface applications of borehole radar. In Proc. of the Symp. on the Application of Geophysics to Engineering and Environmental Problems, Keystone, CO. Environ. Eng. and Geophys. Soc., Denver, CO, p. 545–553.

Gochis, D.J., Vivoni, E.R., and C.J. Watts. 2010. The impact of soil depth on land surface energy and water fluxes in the North American Monsoon region. Journal of Arid Environments, 74: 564-571.

Grote, K., Hubbard, S., and Y. Rubin. 2003. Field-scale estimation of volumetric water content using ground-penetrating radar ground wave techniques. Water Resour. Res. 39(11): 1321, doi:10.1029/2003WR002045, 2003.

Holmes, J.W. 1956. Calibration and field use of the neutron scattering method of measuring soil water content. Australian Journal of Applied Science 7: 45–58.

Herkelrath, W.N., Hamburg, S.P., and F. Murphy. 1991. Automatic, real-time monitoring of soil moisture in a remote field area with time domain reflectometry. Water Resour. Res. 27: 857–864.

Hubbard, S.S., Grote, K., and Y. Rubin. 2002. Mapping the volumetric soil water content of a California vineyard using high-frequency GPR ground wave data. Leading Edge Explor. 21: 552–559.

Hubbard, S., Lunt, I., Grote, K., and Y. Rubin. 2006. Vineyard soil water content: Mapping small scale variability using ground penetrating radar. Geoscience Canada Reprint Series: 193-202.

Huisman, J.A., and W. Bouten. 2003. Accuracy and reproducibility of measuring soil water content with the ground wave of ground penetrating radar. J. Environ. Eng. Geophys. 8: 65–73.

Huisman, J.A., Hubbard, S.S., Redman, J.D., and A.P. Annan. 2003. Measuring soil water content with ground penetrating radar: a review. Vadose Zone Journal 2: 476-491.

Huisman, J.A., Snepvangers, J.J.J.C., Bouten, W., and G.B.M. Heuvelink. 2002. Mapping spatial variation in surface soil water content: Comparison of ground-penetrating radar and time domain reflectometry. J. Hydrol. 269: 194–207.

Huisman, J.A., Sperl, C., Bouten, W., and J.M. Verstraten. 2001. Soil water content measurements at different scales: Accuracy of time domain reflectometry and ground-penetrating radar. J. Hydrol. 245: 48–58.

Jackson, T.J., Schmugge, J., and E.T. Engman. 1996. Remote sensing applications to hydrology: Soil moisture. Hydrol. Sci. J. 41: 517–530.

Jacobsen, O.H., and P. Schjønning. 1994. Comparison of TDR calibra- tion functions for soil water determination. In Proc. Time Domain Reflectometry, Applications in Soil Science, Research Centre Foulum, Denmark. 16 Sept. 1994. SP-Report 25-33. Danish Inst. of Plant and Soil Sci., Tjele, Denmark, p. 9–23.

Jones, S.B., and S.P. Friedman. 2000. Particle shape effect on the effective permittivity of anisotropic or isotropic media consisting of aligned or randomly oriented ellipsoidal particles. Water Resour. Res. 36: 2821–2833.

Kennedy, J. 2002. Understanding grape berry development. Practical Winery and Vineyard, July/August: 14-23.

Knoll, M.D., and W.P. Clement. 1999. Vertical radar profiling to determine dielectric constant, water content and porosity values at well locations. In Proc. of SAGEEP'99, Oakland, CA. Environ. Eng. and Geophys. Soc., Denver, CO, p. 821–830.

Koster, R., and M. Suarez 1996. The influence of land surface moisture retention on precipitation statistics. Journal of Climate 9: 2551–2567.

Koster, R., and M. Suarez. 2001. Soil moisture memory in climate models. Journal of Hydrometeorology 2: 558–570.

Koster, R.D., Dirmeyer, P.A., Guo, Z.C., Bonan, G., Chan, E., Cox, P., Gordon, C.T., Kanae, S., Kowalczyk, E., Lawrence, D., Liu, P., Lu, C.H., Malyshev, S., McAvaney, B., Mitchell, K., Mocko, D., Oki, T., Oleson, K., Pitman, A., Sud, Y.C., Taylor, C.M., Verseghy, D., Vasic, R., Xue, Y.K., and T. Yamada. 2004. Regions of strong coupling between soil moisture and precipitation. Science 305: 1138–1140.

Lakshmi, V. 2004. The role of satellite remote sensing in the prediction of ungauged basins. Hydrological Processes 18: 1029–1034.

Ledieu, J., De Ridder, P., De Clerck, P., and S. Dautrebande. 1986. A method of measuring soil moisture by time domain reflectometry. J. Hydrol. 88: 319–328.

Lesmes, D.P., Herbstzuber, R., and D. Wertz. 1999. Terrain permittivity mapping: GPR measurements of near-surface soil moisture. In Proc. SAGEEP'99, Oakland, CA. Environ. Eng. and Geophys. Soc., Denver, CO, p. 575–582.

Lunt, I.A., Hubbard, S.S., and Y. Rubin. 2005. Soil moisture content estimation using ground- penetrating radar reflection data, Journal of Hydrology 307: 254-269.

Olhoeft, G.R. 1987. Electrical properties from 10.3 to 10.9 Hz: Physics and chemistry. Proc. Phys. Chem. Porous Media II 154: 281–298.

Parkin, G., Redman, D., von Bertoldi, P., and Z. Zhang. 2000. Measurement of soil water content below a wastewater trench using ground-penetrating radar. Water Resour. Res. 36: 2147–2154.

Robinson, D.A., Jones, S.B., Wraith, J.M., Or, D., and S.P. Friedman. 2003. A review of advances in dielelectric and electric conductivity measurements using time domain reflectometry. Vadose Zone J. 2: 444–475.

Roth, K., Schulin, R., Flühler, H., and W. Attinger. 1990. Calibration of time domain reflectometry for water content measurement using a composite dielectric approach. Water Resour. Res. 26: 2267–2273.

Rucker, D.F., and P.A. Ferré. 2003. Near-surface water content estimation with borehole ground penetrating radar using critically refracted waves. Vadose Zone J. 2: 247–252.

Sperl, C. 1999. Determination of spatial and temporal variation of the soil water content in an agro-ecosystem with ground-penetrating radar. (In German.) Ph.D. thesis. Technische Universitat München, Munich, Germany.

Topp, G.C., Davis, J.L., and A.P. Annan. 1980. Electromagnetic determination of soil water content: Measurements in coaxial transmission lines. Water Resour. Res. 16: 574–582.

Tromp-van Meerveld, I., and M. Weiler. 2008. Hillslope dynamics modeled with increasing complexity. Journal of Hydrology 361: 24–40.

Tromp-van Meerveld, I., and J.J. McDonnell. 2009. Assessment of multi-frequency electromagnetic induction for determining soil moisture patterns at the hillslope scale. Journal of Hydrology, 368: 56-67.

Ulaby, F.T., Dubois, P.C., and J. van Zyl. 1996. Radar mapping of surface soil moisture. J. Hydrol. 184: 57–84.

van Oevelen, P.J. 2000. Estimation of areal soil water content through microwave remote sensing. Ph.D. thesis. Wageningen University, The Netherlands.

van Overmeeren, R.A., Sariowan, S.V., and J.C. Gehrels. 1997. Ground penetrating radar for determining volumetric soil water content; results of comparative measurements at two sites. J. Hydrol. 197: 316–338.

Wang, A., Zeng, X., Shen, S.S.P., Zeng, Q.C., and R.E. Dickinson. 2006. Timescales of land surface hydrology. Journal of Hydrometeorology 7: 868–879.

Weiler, K.W., Steenhuis, T.S., Boll, J., and K.-J.S. Kung. 1998. Comparison of ground penetrating radar and time domain reflectometry as soil water sensors. Soil Sci. Soc. of Am. J. 62: 1237–1239.

West, L.J., Handley, K., Huang, Y., and M. Pokar. 2003. Radar frequency dielectric dispersion in sandstone: Implications for determination of moisture and clay content. Water Resour. Res. 39. DOI:10.1029/2001WR000923.

Wyseure, G.C.L., Mojid, M.A., and M.A. Malik. 1997. Measurement of volumetric water content by TDR in saline soils. Eur. J. Soil Sci. 48: 347–354.